MSc Environomical Pathways for Sustainable Energy Systems - SELECT

MSc Thesis

Modelling laminar flame using simple chemical reacting system

Author: ZEIN ELDIN MOHAMED ELSERFY

Supervisor:

Principal supervisor: ASSENSI OLIVA

Session: August 2015

Escola d'Enginyeria de Terrassa

UNIVERSITAT POLITÈCNICA DE CATALUNYA

MSc SELECT is a cooperation between

KTH-Royal Institute of Technology, Sweden | Aalto University, Finland | Universitat Politècnica de Catalunya, Spain | Eindhoven University of Technology, Netherlands | Politecnico di Torino, Italy | AGH University of Science and Technology, Poland | Instituto Superior Técnico, Portugal

Abstract

The objective of my thesis work is to model laminar diffusion flame using simple chemical reacting system (SCRS) combustion model. This combustion model assumes that the chemical reactions are infinitely fast and take place via a global one-step without intermediate reactions. The detailed kinetics is considered unimportant as this model is concerned with the global nature of the combustion process and with the final major species concentration. The model is developed using C++ computer language. The algorithm used for solving Navier-stokes and mixture fraction equations is the fractional step method for compressible flow with low Mach number. Low Mach number approximation is used in simplifying the flow equations as flow speed is very low compared to speed of sound. By modelling diffusion flame through an SCRS, flame temperature and species concentration are retrieved from mixture fraction field.

The thesis is divided into six chapters. Chapter 1 is an introductory chapter about objective, scope and justification of the work. In Chapter 2 the conservation laws of fluid motion are explained. In chapter 3, the discretization of the computational domain and discretization of different terms in the transport equations are explained. The fractional step method algorithm for incompressible flow and compressible flow with low Mach number are illustrated in chapter 4.In chapter 5, the code is verified for incompressible flow by the method of manufactured solution (MMS) and by comparing code results with benchmark solutions of driven cavity and differentially heated cavity for incompressible flow, while for compressible flow code result is compared with benchmark solution of differentially heated cavity with high temperature difference. In chapter 6 SCRS model is discussed and the simulation results for diluted methane diffusion flame are presented.

The simulation results for the laminar diffusion flame show that the flame reaches its maximum temperature at the stoichiometric mixture fraction contour line where oxygen and fuel are completely consumed. The flame length is changed by altering fuel or oxidant streams velocities. Also changing the percentage of nitrogen gas in the fuel and oxidant stream affect both flame length and flame maximum temperature.

Acknowledgment

In full gratitude I would like to acknowledge the following individuals who encouraged, inspired, supported and assisted me in carrying out my master thesis work.

- I would like to thank my supervisor Prof. Dr. Asssi Oliva for his support and guidance in conducting my master thesis and giving me the opportunity to do my research in Heat and Mass Transfer Technological lab in UPC
- Special thanks to Prof Dr. David Carlos Segarra ,Dr. Hamdi Kessentini and Jordi Ventosa for their support and help in learning computational fluid dynamics basics.
- Thanks to Jordi Chiva for his support and guidance in learning C++ language.
- My gratitude to KIC InnoEnergy for awarding me Scholarship that allows me to do my master degree in highly ranked universities
- Thanks to teaching staff of Alexandria faculty of Engineering, Mechanical department for their support during my undergraduate studies`.
- My family and friends for their support and encouragement during my study

Contents

List of figures

List of Tables

List of Abbreviation

CFD	Computational fluid dynamics
UD	Upwind Differencing
CD	Central Differencing
TDMA	Tri-diagonal matrix algorithm
MMS	Method of manufactured solutions
SCRS	Simple chemical reacting system
GS	Gauss–Seidel

1 Introduction

1.1 Objective

The object of my work is to study the modelling of diffusion laminar flames using simple chemical reacting system (SCRS) combustion model. This model assumes that the chemical reactions are infinitely fast and take place in a single step process neglecting the detailed kinetics involved in the combustion process and concerned only with the global nature of the combustion process and the final major species concentrations. In this model low Mach number approximation is used in Navier stokes and mixture faction equations as flow velocity is very low compared to speed of sound. The aim of modelling laminar flame is to calculate temperature, mixture fraction and species mass fraction distribution and to study the influence of some parameters like fuel jet velocity on flame length.

1.2 Justification

Computational fluid dynamics (CFD) is nowadays used for simulating combustion process which is important for many industries like automotive, aerospace, chemical process, energy and home appliances. CFD tool is used for modelling combustion process using basic transport equation for fluid flow and heat transfer with additional models for combustion chemistry. Modelling combustion process using CFD help in optimizing combustion process and studying different parameters influence on combustion. It also reduces cost and save time compared to experimental testing that consumes a lot of money and time as it requires expensive temperature resistant measurement probes, laser measurements or atomization particle analysis. It can provide detailed insights for different scenarios that are difficult to be obtained through experimental testing and measurement.

1.3 Scope

The scope of the work is modelling laminar diffusion flame using simple chemical reacting system model that assumes that the chemical reaction is fast and takes place in one step concerned only with the final major species concentration. The flow is considered compressible flowing with low speed compared to the speed of sound

therefore low Mach number approximation is used in simplifying Navier Stokes and Energy transport equations. The specific heat (C_P) is assumed to be constant in the simulation. The computational domain is 2D due to geometric configuration of the case of study. The code is verified for incompressible flow cases using method of manufactured solutions (MMS) and by analysing two benchmark cases: driven cavity and differentially heated thermal cavity. After that, the code is verified for compressible flow case by comparing its results with benchmark solution for differentially heated thermal cavity with large temperature difference. The unsteady numerical simulations are performed with a finite volume code based on the fractional step method algorithm in a staggered grid system.

2 Governing equations

2.1 Introduction

In this chapter we will develop the mathematical formulation for general purpose model of fluid flow and heat transfer based on conservation of mass, momentum and energy. The governing equations of fluid flow represent mathematical statements of the conservation laws of physics:

- The mass of a fluid is conserved as mass can neither be created nor destroyed.
- The rate of change of momentum equals the sum of the forces on a fluid particle (Newton's second law)
- The rate of change of energy is equal to the sum of the rate of heat addition to and the rate of work done on a fluid particle (first law of thermodynamics)

2.2 Hypotheses

1. Newtonian fluid
2. compressible flow
3. single phase flow
4. negligible radiation energy
5. low Mach number flow

2.3 Conservation of mass equation

For the derivation of mass conservation equation, we should first write down mass balance for a fluid element.

Rate of increase of mass = Net influx of mass

The conservation of mass can be written in integral form, considering density (ρ) as function of space coordinates and time (ρ = ρ(x, y, z, t)) and velocity vector of the flow

(U) function of space coordinates and time and has three components u, v and w aligned to the coordinate axes x, y and z respectively. The fluid element has volume (dV) and elemental surface area (ds).

$$\int_{dV} \frac{\partial}{\partial t}(\rho\, dV) + \int_{dV} \nabla.(\rho\, U)dV = 0 \qquad \textbf{(2.1)}$$

Using Gauss's theorem states that volume integral of the divergence of a vector field in a region inside a volume, is equal to the surface integral of the outward flux normal to the closed surface that bounds the volume. For a vector a, the Gauss theorem is given by,

$$\int_{dV} \nabla.a\, dV = \int_{dS} a\,.\boldsymbol{n}\, ds \qquad \textbf{(2.2)}$$

The volume integration can be converted to surface integration and the mass conservation can be written as follows, where n is unit vector normal to surface.

$$\int_{dV} \frac{\partial}{\partial t}(\rho\, dV) + \int_{dS} (\rho\, U).\boldsymbol{n}\, ds = 0 \qquad \textbf{(2.3)}$$

For incompressible flow, the density is considered constant $\left(\frac{\partial \rho}{\partial t}\right) = 0$, so mass conservation equation can be reduced to the following form

$$\int_{dS} U.n\, ds = 0 \qquad \textbf{(2.4)}$$

Mass conservation can be written in differential form for compressible and incompressible flow as shown in equation (2.5) & (2.6) respectively.

$$\frac{\partial \rho}{\partial t} + \nabla.(\rho\, U) = 0 \qquad \textbf{(2.5)}$$

$$\nabla.U = 0 \qquad \textbf{(2.6)}$$

2.4 Momentum equation

Newton's second law states that the rate of change of momentum of a fluid particle equals the sum of the forces on the particle:

Rate of increase in momentum=Net influx of momentum + body force + surface force

The surface forces include pressure force and viscous force, while body force includes gravity force, centrifugal force and Coriolis force and electromagnetic force.

The momentum equation can be written as shown in the following equation

$$\frac{\partial}{\partial t}\int_{dV} \rho\, U\, dV = -\int_{dS} \rho U\, U.n\, ds - \int_{dS} P\, n.\, dS + \int_{dS} \tau : n\, dS + \int_{dV} \rho\, g\, dV \qquad \textbf{(2.7)}$$

Where,

U: Velocity vector

τ : Viscous Stress tensor

g: Acceleration due to gravity

For Newtonian fluid, viscous stresses are linearly related to the rates of strain arising from shear and dilatation and must be symmetric so that $\tau_{ij} = \tau_{ji}$ .The viscous stress tensor is shown in equation (2.8).

$$\tau = (\lambda \nabla . U) I + 2\mu D \qquad \textbf{(2.8)}$$

Where,

λ : Dilatational viscosity ((λ =- 2/3 μ) for gases)

I: Identity matrix

μ : Dynamic viscosity

D : Deformation tensor

The deformation tensor for Newtonian fluid are shown in the following equation

$$D = \frac{1}{2} (\nabla . U + \nabla . U^T) \quad \textbf{(2.9)}$$

The momentum equation in i - direction can be written as shown in equation (2.10)

$$\frac{\partial}{\partial t}\int_{dV} \rho\, u_i dV = -\int_{dS} \rho u_i\, (U.n) ds - \int_{dS} P\, n_i\, dS + \int_{dS} n_j\, \tau_{ij}\, dS + \int_{dV} \rho\, g_i\, dV \quad \textbf{(2.10)}$$

And the viscous stress can be written in the following form

$$\tau_{ij} = \lambda\, \delta_{ij}\, \nabla . U + \mu(\frac{\partial u_i}{\partial x_j} + \frac{\partial u_j}{\partial x_i}) \quad \textbf{(2.11)}$$

For incompressible flow with constant viscosity, the momentum equation can be simplified as shown in equation (2.13).In this equation, Boussinesq approximation is used for simplifying the gravity force term, in which density is related to density at reference temperature and thermal expansion coefficient as shown in equation (2.12).

$$\rho = \rho_0\, [1 - \beta_o\, (T - T_0)] \quad \textbf{(2.12)}$$

Where,

ρ_0 : Density at reference temperature

β_0 : Thermal expansion coefficient at reference temperature

$$\frac{\partial}{\partial t}\int_{dV} \rho\, u_i dV = -\int_{dS} u_i\, (\rho U.n) ds - \int_{dS} P\, n_i\, dS + \int_{dS} \mu\, \nabla u_i\, .n\, dS - \int_{dV} \rho_0\, \beta_0 g_i (T - T_0)\, dV \quad \textbf{(2.13)}$$

Momentum equation can be written in differential form for compressible and incompressible flow as shown in equation (2.14) & (2.15).

$$\frac{\partial \rho u_i}{\partial t} = -\frac{\partial \rho u_i u_j}{\partial x_j} - \frac{\partial p}{\partial x_i} + \frac{\partial \tau_{ij}}{\partial x_j} + \rho g_i \qquad \textbf{(2.14)}$$

$$\rho \frac{\partial u_i}{\partial t} = -\frac{\rho \partial u_i u_j}{\partial x_j} - \frac{\partial p}{\partial x_i} + \mu \Delta u_i - \rho_0 \, \beta_0 g_i (T - T_0) \qquad \textbf{(2.15)}$$

2.5 Conservation of energy

The energy equation is a mathematical statement which is based on the physical law that states

Rate of change of energy in particle =	Rate of energy received by heat and work transfers by that particle.

Using Reynolds transport theorem we can put the energy conservation in integral form as shown below

$$\frac{D}{Dt}\int_{dV} \rho \left[e + \frac{1}{2}\, u_i u_i\right] dV = \int_{dv} \rho g_i u_i dv + \int_{dS} n_i \left[-p u_i + \tau_{ij} u_j - q_i\right] dS$$

$$= \int_{dV} \left[\rho g_i u_i + \frac{\partial}{\partial x_i}(-p u_i + \tau_{ij} u_j - q_i)\right] dV \qquad \textbf{(2.16)}$$

Where,

e : Internal energy

q_i : Heat flux vector

From the integral energy equation we obtain the total energy equation in differential form by the observation that the volume is arbitrary and thus that the integration itself has to be zero as shown in equation (2.17)

$$\rho \frac{D}{Dt}\left[e + \frac{1}{2}\, u_i u_i\right] = \rho g_i u_i + \frac{\partial}{\partial x_i}\tau_{ij} u_j - \frac{\partial q_i}{\partial x_i} - \frac{\partial}{\partial x_i}(p u_i) \qquad \textbf{(2.17)}$$

The mechanical energy equation is found by taking the dot product between the momentum equation and u as shown below

$$\rho \frac{D}{Dt}\left(\frac{1}{2}u_i u_i\right) = \rho g_i u_i - u_i \frac{\partial p}{\partial x_i} + u_i \frac{\partial \tau_{ij}}{\partial x_i} \quad \textbf{(2.18)}$$

The thermal energy equation can be obtained by subtracting mechanical energy equation form total energy equation

$$\rho \frac{De}{Dt} = -p \frac{\partial u_i}{\partial x_i} + \tau_{ij} \frac{\partial u_i}{\partial x_j} - \frac{\partial q_i}{\partial x_i} \quad \textbf{(2.19)}$$

Alternative form for writing thermal energy equation using enthalpy definition

$$h = e + p/\rho \quad \textbf{(2.20)}$$

By taking derivative to the previous equation, we get the following equation

$$\frac{Dh}{Dt} = \frac{De}{Dt} + \frac{1}{\rho}\frac{Dp}{Dt} - \frac{p}{\rho^2}\frac{D\rho}{Dt} \quad \textbf{(2.21)}$$

From conservation of mass equation, $\frac{D\rho}{Dt}$ can be replaced by $-\rho \frac{\partial u_i}{\partial x_i}$, so we get the following equation

$$\frac{De}{Dt} = \frac{Dh}{Dt} - \frac{1}{\rho}\frac{Dp}{Dt} - \frac{p}{\rho}\frac{\partial u_i}{\partial x_i} \quad \textbf{(2.22)}$$

By substituting equation **(2.22)** into equation **(2.19)** , the thermal energy equation can be written in the following form

$$\rho \frac{Dh}{Dt} = \frac{Dp}{Dt} + \tau_{ij} \frac{\partial u_i}{\partial x_j} - \frac{\partial q_i}{\partial x_i} \quad \textbf{(2.23)}$$

The heat flux is related to the temperature gradients using Fourier's law

$$q_i = -k\frac{\partial T}{\partial x_i} \quad \textbf{(2.24)}$$

Where, K is the thermal conductivity

Using Fourier's law, the thermal energy can be written as shown in equation **(2.25)**

$$\rho\frac{Dh}{Dt} = \frac{Dp}{Dt} + \tau_{ij}\frac{\partial u_i}{\partial x_j} + \frac{\partial}{\partial x_i}(k\frac{\partial T}{\partial x_i}) \quad \textbf{(2.25)}$$

For flow with variable density and low Mach number, the thermal energy equation can be modified to the following form neglecting viscous heating term $\tau_{ij}\frac{\partial u_i}{\partial x_j}$ and $u_i\frac{\partial p}{\partial x_i}$ and assuming that total pressure will be equal thermodynamics part as hydrodynamic part (P) is negligible, so that p can be replaced by P_0 ,which is the thermodynamic pressure that is spatially uniform.

$$\rho\frac{Dh}{Dt} = \frac{dP_0}{dt} + \frac{\partial}{\partial x_i}(k\frac{\partial T}{\partial x_i}) \quad \textbf{(2.26)}$$

For incompressible flow, the thermal energy equation can be written as shown below using equation **(2.19)** in which the viscous heating term $\tau_{ij}\frac{\partial u_i}{\partial x_j}$ is neglected and $p\frac{\partial u_i}{\partial x_i}$ is equal to zero.

$$\rho\frac{De}{Dt} = -\frac{\partial q_i}{\partial x_i} \quad \textbf{(2.27)}$$

As for incompressible flow e=cT, where c is the specific heat. The thermal energy equation for incompressible flow can be written as follow

$$\rho c\ \frac{DT}{Dt} = -\frac{\partial}{\partial x_i}(k\frac{\partial T}{\partial x_i}) \quad \textbf{(2.28)}$$

2.6 Differential and integral forms of the general transport equations

There are significant commonalities between different conservation equations, so a general variable ∅ can be used for writing the different conservation equations in one general form as shown below in which ∅ can represent any scalar quantity like T or u or v:

$$\frac{\partial(\rho\emptyset)}{\partial t} + div(\rho U\emptyset) = div(\Gamma\ grad\emptyset) + S_\emptyset \qquad \textbf{(2.29)}$$

This equation is called transport equation for property ∅, which includes different transport process: the rate of change term and the convective term on the left hand side and the diffusive term (Γ = diffusion coefficient) and the source term respectively on the right hand side. The equation can be also written in integral form as shown below

$$\int_V \frac{\partial(\rho\emptyset)}{\partial t} dV + \int_V div(\rho U\emptyset)\ dV = \int_V div(\Gamma\ grad\emptyset)\, dV + \int_V S_\emptyset\ dV \qquad \textbf{(2.30)}$$

Using the Gauss divergence theorem, the integration over the volume can be rewritten as integration over the entire bounding surface of the control volume

$$\int_V \frac{\partial(\rho\emptyset)}{\partial t} dV + \int_s n.(\rho U\emptyset)\ dS = \int_s n.(\Gamma\ grad\emptyset)\, dS + \int_V S_\emptyset\ dV \qquad \textbf{(2.31)}$$

The different values of property($\emptyset$) , diffusion coefficient (Γ) and source term ($S_\emptyset$) for various conservation equations are listed in Table 2.1, Where φ is thermal energy source term

Conservation equation	∅	$\boldsymbol{\Gamma}$	$\boldsymbol{S_\emptyset}$
Mass	1	0	0
Momentum - x direction for incompressible flow	u	μ	$-\frac{\partial P}{\partial x}$
Momentum - x direction for compressible flow	u	μ	$-\frac{\partial p}{\partial x} + \frac{\partial}{\partial x}\left(\lambda\ divU + \mu\frac{\partial u}{\partial x}\right) + \frac{\partial}{\partial y}\left(\mu\frac{\partial v}{\partial x}\right)$

Momentum - y direction for incompressible flow	v	μ	$-\frac{\partial p}{\partial y} - \rho_0 \beta_0 g_i (T - T_0)$
Momentum - y direction for compressible flow	v	μ	$-\frac{\partial p}{\partial y} + \frac{\partial}{\partial y}\left(\lambda\, div U + \mu \frac{\partial v}{\partial y}\right) + \frac{\partial}{\partial x}\left(\mu \frac{\partial u}{\partial y}\right) + \rho g_y$
Thermal energy for incompressible flow (constant c_p)	T	$\frac{k}{c_p}$	$\frac{\varphi}{C_p}$
Thermal energy for compressible flow (constant c_p with low Mach no.)	T	$\frac{k}{c_p}$	$\frac{\varphi}{C_p} + \frac{1}{C_p}\frac{dP_0}{dt}$

Table 2.1: Parameter to be replaced in general transport equation to reproduce conservation equations

3 Discretization of governing equation

3.1 Domain discretization

The process of domain discretization is the first step in finite volume analysis. In order to solve physical problem numerically the computational domain has to be discretised into elemental volumes. The network of discrete volume is called grid. The governing equations are solved numerically over these control volumes to give a solution over the domain. Computational grids are classified according to their type of construction into structured and non-structured mesh.

3.1.1 Unstructured mesh

Unstructured meshes contain cells having triangle in 2D mesh or tetrahedral shape in 3D mesh as shown in (Figure 3.1). The number of corner nodal points surrounding each cell is not necessarily constant. It is characterized by irregular connectivity which makes it more suitable for complex geometries.

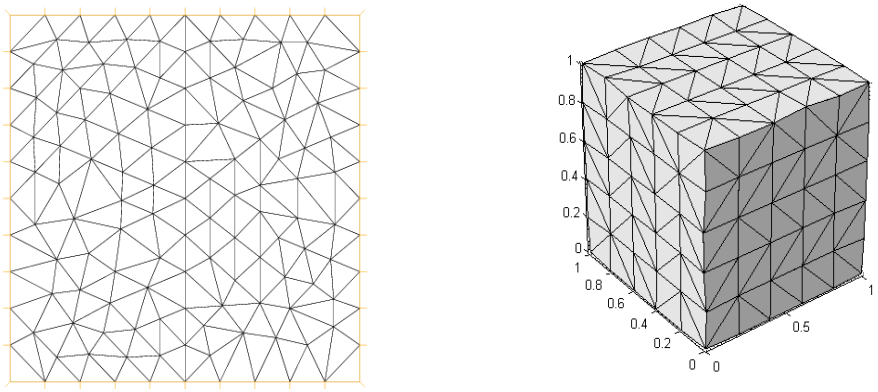

(a) (b)

Figure 3.1: unstructured mesh in 2 D (a) and 3D (b).[1]

3.1.2 Structured mesh

Structured mesh contains cells having either regular quadrilateral shape element with four nodal corner points in 2D mesh or hexahedral shape with 8 nodal points in 3D mesh. It is characterized by regular connectivity and its orthogonal mesh in Cartesian system.

This means that it is more suitable for geometries with orthogonal shapes. It can be uniform or non-uniform structured mesh. For uniform mesh cell spacing is equal in all directions, while non-uniform mesh the spacing can take any values as shown in Figure 3.2 (b).

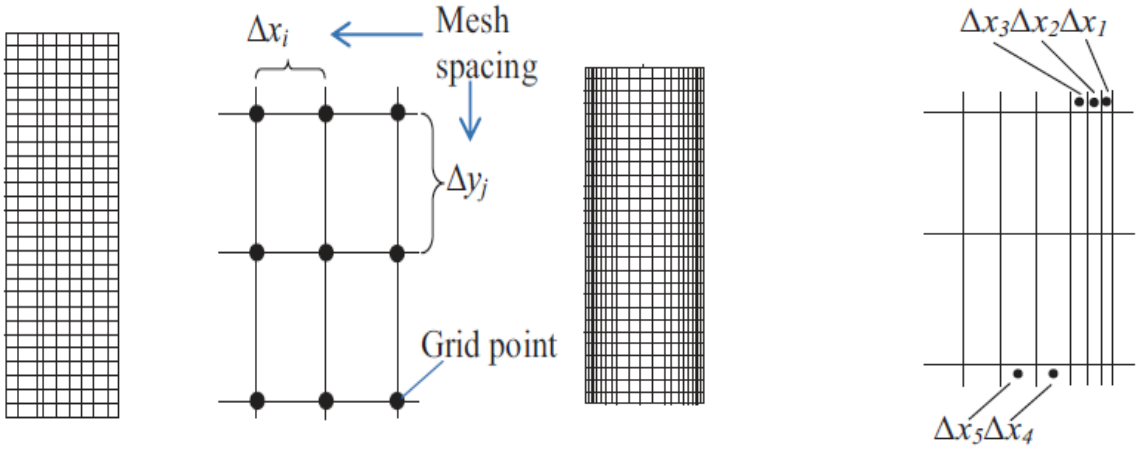

Figure 3.2: Types of structure mesh in 2D mesh:(a) uniform mesh,(b) non-uniform mesh[2]

3.1.2.1 Collocated grid system

In collocated grids, the velocities (u, v) and the pressure and other scalars are stored at the at cell centre as shown in Figure 3.3. The volume fluxes are calculated at cell faces by interpolating for cell cantered velocity to the faces and multiplying them by cell face area. Collocated mesh has one major difficulty as cell face velocity are linearly interpolated between neighbouring momentum cell velocities and pressure gradient present in the momentum equation is represented by central differencing, so if the pressure field has a checkboard pattern, it would be seen by momentum equation as uniform field. One way to solve this problem is to use staggered mesh. It has some advantages compared to staggered grid in which all variables are stored in the same control volume so that convection coefficients in the discretised equations are the same for all variables.

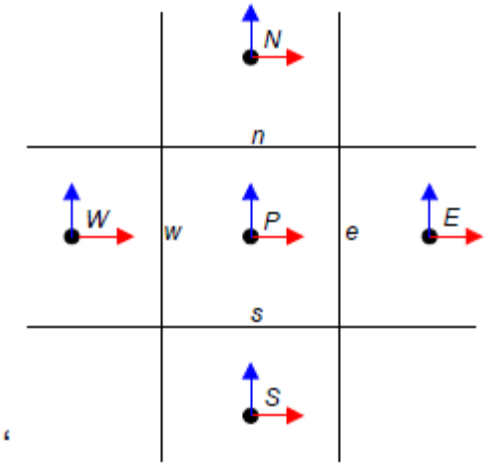

Figure 3.3: collocated structured mesh[3]

3.1.2.2 Staggered grid mesh

On staggered grid the scalar variables (pressure, density, temperature etc.) are stored in the cell centre of the control volumes, while velocity (u, v) are located at the cell faces as shown in Figure 3.4 , this is different from collocated grid in which velocity was stored in cell centre. The staggered grid is mainly used for structured meshes. The advantage of staggered grid is avoiding odd-even coupling between pressure and velocity that occur in collocated grid and leads to checkerboard pattern, while it disadvantage is that different variable are stored at different places and this makes it difficult to work with different control volume for different variable.

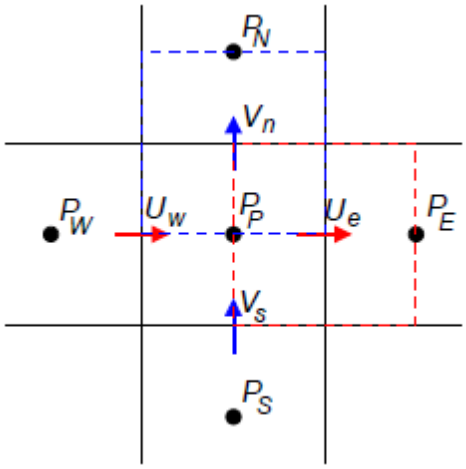

Figure 3.4: staggered structured grid[3]

3.2 Discretization of the Transport Equation

In this section, different term of the general transport equation will be discretised. The equation is written in the form of general transport equation over control volume v as shown below

$$\int_V \underbrace{\frac{\partial(\rho\emptyset)}{\partial t}}_{\substack{Temporal \\ derivative}} dV + \int_V \underbrace{\nabla.(\rho U\emptyset)dV}_{convective\ term} = \int_V \underbrace{\nabla.(\Gamma\,\nabla\emptyset)dV}_{Diffusion\ term} + \int_V \underbrace{S_\emptyset\, dV}_{source\ term} \qquad \textbf{(3.1)}$$

It can be seen from previous equation that general transport equation is second order as the diffusion term includes as second order derivative of ∅ in space. To represent this equation with acceptable accuracy, the different terms must be discretised with order equal to or higher than the order of discretised equation.

As mentioned before that by using Gauss theorem, the volume integration of vector divergence field for region inside volume is equal to surface integration of outward flux normal to closed surface that surround the volume, so that general transport equation can be modified to the following form

$$\int_V \frac{\partial(\rho\emptyset)}{\partial t} dV + \int_s \underbrace{n.(\rho U\emptyset)dS}_{convection\ flux} = \int_s \underbrace{n.(\Gamma\,\nabla\emptyset)dS}_{Diffusion\ flux} + \int_V S_\emptyset\ dV \qquad \textbf{(3.2)}$$

3.2.1 Approximation of Surface Integrals and Volume Integrals

In equation (3.2), there are a series of surface and volume integration need to be calculated over the control volume. These integration need to be approximated to at least second order accuracy to confirm same level of accuracy.

To calculate the surface integration for convective and diffusion flux term, we need the value of the transported property ∅ on the faces of the control volume. This information is not available as these variables are calculated at control volume centroid, so some approximations need to be introduced:

1- ∅ Varies linearly over the face over each face of the control volume, so the surface integration can be approximated in terms of variable values for ∅ at one or more location on the cell face. The integral can be evaluated using different rules (a) midpoint, (b) trapezoid, or (c) Simpson's rule. By using midpoint rule which is of second order accuracy, ∅ can be represented by its mean value at

face centroid, so the surface integral can be approximated as the product of the mean value of ∅ over the surface and surface area.

2- Approximate the cell face values in terms of the CV central value.

Using these approximations and assumptions the surface integral for convection and diffusion fluxes can be approximated as follows:

$$\int_s \mathrm{n}.(\rho \mathrm{U}\emptyset)\mathrm{dS} = \sum_f \int_s \mathrm{n}.(\rho \mathrm{U}\emptyset)_f \, \mathrm{ds} \approx \sum_f \mathrm{n}.\left(\overline{\rho \mathrm{U}\emptyset}\right)_f \mathrm{S_f} = \sum_f \mathrm{n}.(\rho \mathrm{U}\emptyset)_f \, \mathrm{S_f} \qquad \textbf{(3.3)}$$

$$\int_s n.(\Gamma \nabla\emptyset)dS = \sum_f \int_s \mathrm{n}.(\Gamma \nabla\emptyset)_f \, \mathrm{ds} \approx \sum_f \mathrm{n}.\left(\overline{\Gamma \nabla\emptyset}\right)_f \mathrm{S_f} = \sum_f \mathrm{n}.(\Gamma \nabla\emptyset)_f \, \mathrm{S_f} \qquad \textbf{(3.4)}$$

To approximate volume integrals in equation (3.2), similar approximation used in surface integral is utilised. $S_\emptyset$ varies linearly over the control volume and $S_\emptyset$ can be represented by mean value at control volume centroid S_p using midpoint rule.

$$\int_V S_\emptyset \; dV = \overline{S_\emptyset} \, V = S_p \, V \qquad \textbf{(3.5)}$$

Introducing equation (3.3) , (3.4) & (3.5) into equation (3.2), we get the following equation

$$\frac{\partial}{\partial \mathrm{t}} \rho \emptyset \mathrm{V} + \sum_f \mathrm{n}.(\rho \mathrm{U}\emptyset)_f \, \mathrm{S_f} = \sum_f \mathrm{n}.(\Gamma \nabla\emptyset)_f \, \mathrm{S_f} + \mathrm{S_p} \, \mathrm{V} \qquad \textbf{(3.6)}$$

3.2.2 Convective Term Spatial Discretization

The convective term in equation (3.1) is discretised using equation (3.3)

$$\begin{aligned} \int_v \nabla.(\rho U\emptyset)dV &= \sum_f \mathrm{n}.(\rho \mathrm{U}\emptyset)_f \, \mathrm{S_f} \\ &= \sum_f \mathrm{n}.(\rho U)_f \, \emptyset_f \;\; \mathrm{S_f} \\ &= \sum_f F \, \emptyset_f \end{aligned} \qquad \textbf{(3.7)}$$

Where, F in equation (3.7) represents mass flux through control volume faces

$$F = \mathrm{n}.(\rho U)_f \;\; \mathrm{S_f} \qquad \textbf{(3.8)}$$

From the previous equation, it can be seen that values of F depend on face values of ρ and U.For momentum equation in x-direction, the mass flux terms across different control volume faces are calculated as shown below

$$F_n = (\rho v)_A A_{AN} + (\rho v)_B A_{BN} \quad \textbf{(3.9)}$$

$$F_s = (\rho v)_c A_{AN} + (\rho v)_D A_{BN} \quad \textbf{(3.10)}$$

$$F_e = \rho_e \frac{u_E + u_P}{2} A_e \quad \textbf{(3.11)}$$

$$F_e = \rho_w \frac{u_W + u_P}{2} A_w \quad \textbf{(3.12)}$$

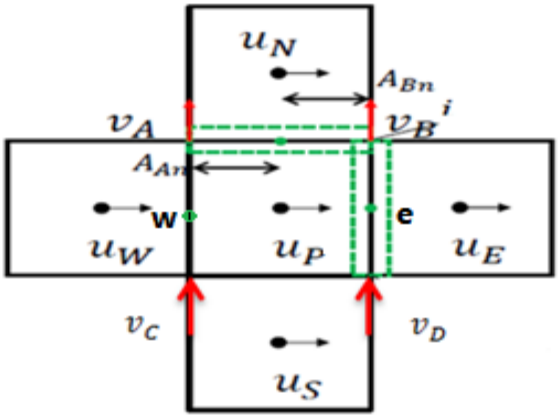

Figure 3.5: Mass fluxes across u control volume

The mass fluxes across v control volume are calculated in similar way like u control volume shown above. For temperature control volume, the mass fluxes are calculated using values of ρ , u and v already computed at the faces of the control volume.

While the face value of transported quantity (∅) is calculated using convection differencing scheme.

3.2.2.1 Convection Interpolation Schemes

The role of convection interpolation schemes is to determine the value of transported quantity (∅) at the face of the control volume, so that $\emptyset_f$ is determined using the values of ∅ at neighbouring control volumes

- **Upwind Differencing (UD) scheme.**

The face value is determined according to the direction of the flow as shown in Figure 3.6.

$$\emptyset_f = \begin{cases} \emptyset_P & F \geq 0 \\ \emptyset_N & F < 0 \end{cases} \quad \textbf{(3.13)}$$

The upwind scheme guarantees the Conservativeness, boundedness and transportiveness as it account for the direction of the flow [4],but it has low accuracy as it is a first order accurate based on backward differencing that leads to introducing numerical diffusion error.

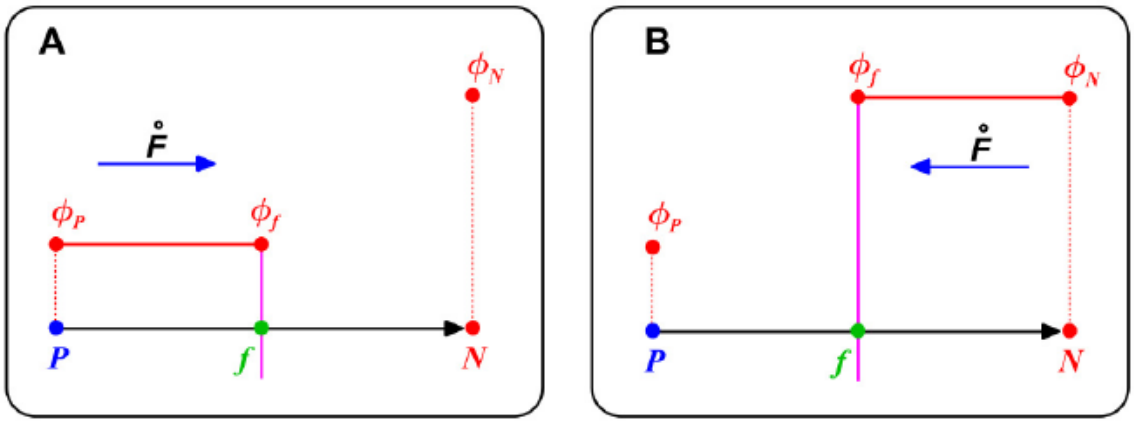

Figure 3.6: upwind interpolation scheme A) F≥0, B) F<0 [5]

- **Central Differencing (CD) scheme**

This scheme is also known as linear interpolation scheme in which the face centred value of the transported quantity is calculated from simple weighted linear interpolation between the values of the control volumes $\emptyset_P$ and $\emptyset_N$ as shown in Figure 3.7.

$$\emptyset_f = \emptyset_P \left(\frac{x_N - x_f}{x_N - x_P} \right) + \emptyset_N \left(\frac{x_f - x_P}{x_N - x_P} \right) \quad \textbf{(3.14)}$$

In case of using uniform mesh, the face is located at the midway between two neighbouring control volumes of node P and N, so the value at face can be calculated using arithmetic average.

$$\emptyset_f = \frac{\emptyset_P + \emptyset_N}{2} \quad \textbf{(3.15)}$$

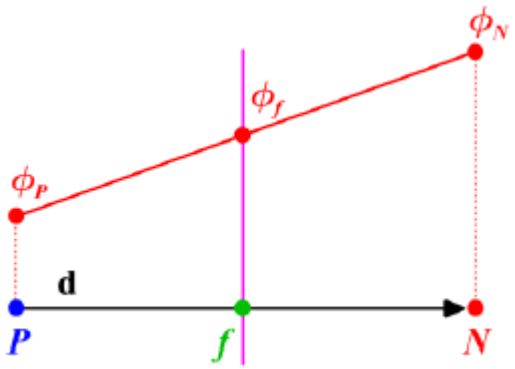

Figure 3.7: Central Differencing (CD) scheme [5]

The central scheme satisfies conservativeness and it is a second order accuracy, but it does not possess the transportiveness property at high peclet number because central scheme does not recognize the direction of the flow or the strength of the convection relative to diffusion. Also the boundedness property is not guaranteed at high peclet number which might cause non-physical oscillation in the solution.

- **QUICK scheme**

QUICK stands for Quadratic Upwind Interpolation for Convective Kinetics, which is a quadratic curve fitting using two nodes upstream (U,C) and one node downstream (D) in order to calculate the transported quantity (∅) at face center as shown in Figure 3.8.The formula of quick scheme is shown below using the notation of Darwish [6]

$$\overline{\emptyset}_f = \overline{x}_f + \frac{\overline{x}_f(\overline{x}_f - 1)}{\overline{x}_c(\overline{x}_c - 1)}(\overline{\emptyset}_f - \overline{x}_c) \quad \textbf{(3.16)}$$

Where, $\overline{x}$ and $\overline{\emptyset}$ are the normalized distance and transported property respectively given by equation (2.15) & (3.18)

$$\overline{x} = \frac{x - x_U}{x_D - x_U} \quad \textbf{(3.17)}$$

$$\overline{\emptyset} = \frac{\emptyset - \emptyset_U}{\emptyset_D - \emptyset_U} \quad \textbf{(3.18)}$$

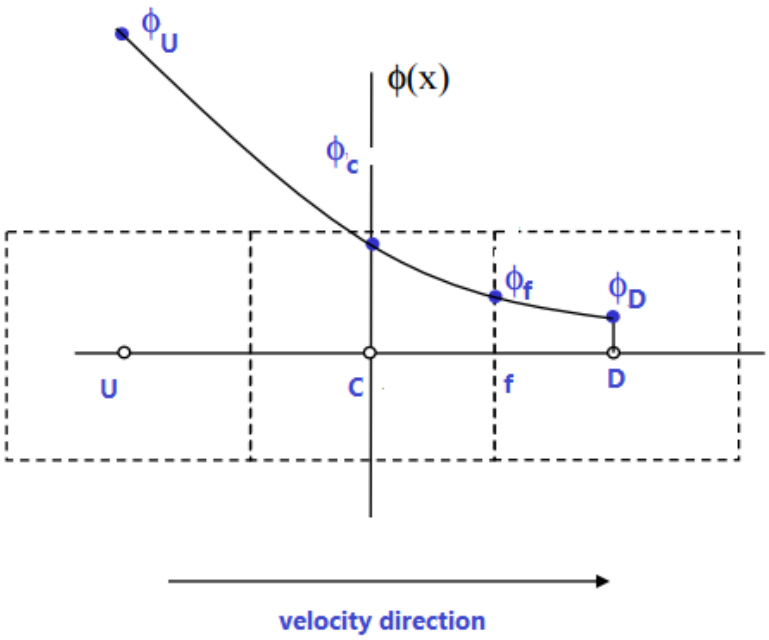

Figure 3.8: quick scheme

This scheme is third order accuracy, but it may leads to stability problems in regions with strong gradients, overshoot and undershoot.

- **Smart scheme**

  Smart stands for Sharp and Monotonic Algorithm for Realistic Transport, this scheme employ a composite approach as it combined a high resolution schemes with low order scheme. This scheme is bounded and prevents the spatial oscillation while maintain a high order of accuracy [7],but its disadvantage is that it requires more computational time compared to other conventional schemes. The accuracy of smart scheme is between second and fourth order. The formula is shown below

$$\overline{\emptyset}_f = \begin{cases} \dfrac{\overline{x}_f(1-3\overline{x}_c+2\overline{x}_f)}{\overline{x}_c(1-\overline{x}_c)}\,\emptyset_c & if \quad 0 < \emptyset_c \le \dfrac{\overline{x}_c}{3} \\ \dfrac{\overline{x}_f(\overline{x}_f-\overline{x}_c)}{1-\overline{x}_c}+\dfrac{\overline{x}_f(\overline{x}_f-1)}{\overline{x}_c(\overline{x}_c-1)}\,\emptyset_c & if \quad \dfrac{\overline{x}_c}{3} < \emptyset_c \le \dfrac{(1+\overline{x}_f-\overline{x}_c)\overline{x}_c}{\overline{x}_f} \\ 1 & if \quad \dfrac{(1+\overline{x}_f-\overline{x}_c)\overline{x}_c}{\overline{x}_f} < \emptyset_c \le 1 \\ \emptyset_c & otherwise \end{cases} \tag{3.19}$$

3.2.3 Diffusion Term Spatial Discretization

The diffusion term in equation (3.1) is discretised using equation (3.4)

$$\int_v \nabla.(\Gamma\,\nabla\emptyset)dV = \sum_{\mathrm{f}} \mathrm{n}.(\Gamma\,\nabla\emptyset)_{\mathrm{f}}\,\mathrm{S_f} = \sum_{\mathrm{f}} \Gamma_f\,\mathrm{n}.(\nabla\emptyset)_{\mathrm{f}}\;\mathrm{S_f} \tag{3.20}$$

The diffusion coefficient at the control volume faces (Γ_f) is calculated by taking harmonic mean for diffusion coefficient values at control volume centre. The diffusion coefficient at the east face is calculated in equation (3.21). $(\nabla\emptyset)_f$ is calculated at the face centre using central differencing scheme. $(\nabla\emptyset)_e$ at the east face is calculated as shown in equation (3.22)

$$\Gamma_e = \frac{d_{PE}}{\dfrac{\Gamma_E}{d_{eE}}+\dfrac{\Gamma_p}{d_{Pe}}} \tag{3.21}$$

$$(\nabla\emptyset)_e = \frac{\emptyset_E - \emptyset_p}{X_E - X_p} \tag{3.22}$$

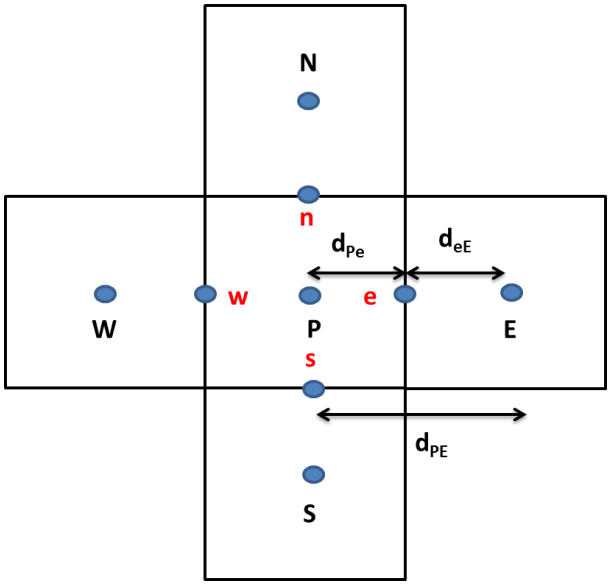

Figure 3.9: calculating diffusion term

3.2.4 Source Term Spatial Discretization

For discretizing the source term in momentum equation in x-direction shown in Table 2.1.The source term is shown in integral form in equation (3.23)

$$\int_v S_\emptyset \, dV = \int_v \left[-\frac{\partial p}{\partial x} + \frac{\partial}{\partial x}\left(\lambda \, div U + \mu \frac{\partial u}{\partial x}\right) + \frac{\partial}{\partial y}\left(\mu \frac{\partial v}{\partial x}\right) \right] dV \qquad \textbf{(3.23)}$$

By using Gauss theorem, equation (3.23) is modified to the following form

$$\int_v S_\emptyset \, dV = -\int_s p \, n_x ds + \int_s \left(\lambda \, div U + \mu \frac{\partial u}{\partial x}\right) n_x \, ds + \int_s \mu \frac{\partial v}{\partial x} \, n_y \, ds \qquad \textbf{(3.24)}$$

The term $\frac{\partial u}{\partial x}$ at east and west surface and term $\frac{\partial v}{\partial x}$ at north and south surface are discretised using central differencing scheme

$$\left.\frac{\partial u}{\partial x}\right|_{s_e} = \frac{u_E - u_P}{\Delta x} \qquad \textbf{(3.25)}$$

$$\left.\frac{\partial u}{\partial x}\right|_{s_w} = \frac{u_p - u_w}{\Delta x} \qquad \textbf{(3.26)}$$

$$\left.\frac{\partial v}{\partial x}\right|_{s_n} = \frac{v_B - v_A}{\Delta x_u} \quad \textbf{(3.27)}$$

$$\left.\frac{\partial v}{\partial x}\right|_{s_s} = \frac{v_D - v_C}{\Delta x_u} \quad \textbf{(3.28)}$$

Where,

Δx: Distance between two consecutive control volume centres

Δx_u: Distance between control volume faces

S_e, S_w , S_n , S_s : East, west, north and south faces of control volume

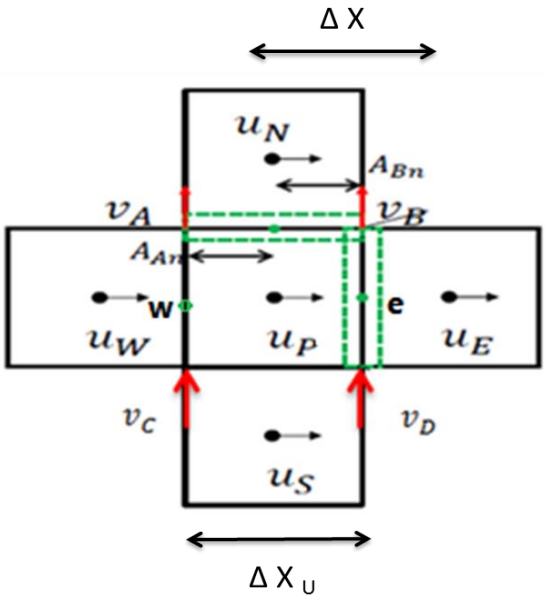

Figure 3.10: u control volume

The source terms of momentum equation in y-direction is discretised by the same method described above.

3.2.5 Temporal Discretization

The fractional step method will be used for solving the momentum and energy equations and this method will be explained in detail in the following chapter. For carrying out the time integration for these equations, a fully explicit time scheme is proposed. In order to simplify the notation, momentum in x-direction, momentum in y-direction and thermal energy equations can be rewritten in the following forms:

$$\rho \frac{\partial u}{\partial t} = R(u) - \frac{\partial \mathrm{P}}{\partial \mathrm{x}} \quad \textbf{(3.29)}$$

$$\rho \frac{\partial v}{\partial t} = R(v) - \frac{\partial \mathrm{P}}{\partial \mathrm{y}} \quad \textbf{(3.30)}$$

$$\rho \frac{\partial T}{\partial t} = R(T) \quad \textbf{(3.31)}$$

Where, R(u) ,R(v) and R(T) stands for convection, diffusion and source terms in momentum in x-direction, momentum in y-direction and thermal energy equations respectively. These terms are listed in Table 2.1.

$$R(u) = -\nabla.(\rho U u) - \nabla.(\mu \nabla u) + S_u \quad \textbf{(3.32)}$$

$$R(v) = -\nabla.(\rho U v) - \nabla.(\mu \nabla v) + S_v \quad \textbf{(3.33)}$$

$$R(T) = -\nabla.(\rho U T) - \nabla.\left(\frac{k}{c_p}\nabla T\right) + S_T + \frac{1}{c_p}\frac{dp_o}{dt} \quad \textbf{(3.34)}$$

For the time derivative term, a central difference scheme is used. The time derivative term of momentum equation in x-direction is shown in the following equation

$$\rho \frac{\partial u}{\partial t}\bigg|^{t=n+\frac{1}{2}} \approx \frac{\rho^{n+1}u^{n+1} - \rho^n u^n}{\Delta t} \quad \textbf{(3.35)}$$

A fully explicit second order Adams-Bashforth scheme is used for R(u)

$$R(u)^{t=n+\frac{1}{2}} \approx \frac{3}{2} R(u^n) - \frac{1}{2} R(u^{n-1}) \quad \textbf{(3.36)}$$

For the pressure gradient term, a first order backward Euler scheme is used, so the momentum equation in x-direction can be written in the following form

$$\frac{\rho^{n+1}u^{n+1} - \rho^n u^n}{\Delta t} = \frac{3}{2} R(u^n) - \frac{1}{2} R(u^{n-1}) - \frac{\partial \mathrm{P}^{n+1}}{\partial \mathrm{x}} \quad \textbf{(3.37)}$$

The same step can be done for temporal discretization of momentum equation in y-direction and thermal energy equations as they can be written as shown in equation (3.38) & (3.39) respectively.

$$\frac{\rho^{n+1}v^{n+1} - \rho^n v^n}{\Delta t} = \frac{3}{2} R(v^n) - \frac{1}{2} R(v^{n-1}) - \frac{\partial \mathrm{P}^{n+1}}{\partial \mathrm{y}} \quad \textbf{(3.38)}$$

$$\frac{\rho^{n+1}T^{n+1} - \rho^{n}T^{n}}{\Delta t} = \frac{3}{2}\,R(T^{n}) - \frac{1}{2}\,R(T^{n-1}) \qquad \textbf{(3.39)}$$

4 Fractional step method algorithm

4.1 Fractional step method for incompressible flow

The time integration of Navier-Stokes equation is carried out by the fractional step method which is a projection method. The solution of Navier-stokes equation is carried out in two steps. In the first step, an incomplete form of momentum equation that does not include the pressure gradients term is integrated at each time step to yield an approximate velocity field that is called predictor velocity. This predictor velocity is not divergence free, then Poisson equation is solved using the predictor velocity and the yield pressure field is used to correct the predictor velocity to produce divergence free velocity field that satisfies the incompressibility constraint[8].

As mentioned before in the previous chapter in section (2.5) that a fully explicit time integration scheme is used for the momentum equation.

$$\rho \frac{\partial U}{\partial t} = R(u) - \nabla \mathrm{P} \tag{4.1}$$

After using a central differencing scheme for time derivative term $\left(\frac{\partial U}{\partial t}\right)$ and fully explicit second order Adams-Bashforth scheme for R (u) and first order backward Euler scheme for pressure gradient term, the momentum equation can be modified to the following form:

$$\frac{\rho^{n+1}U^{n+1} - \rho^{n}U^{n}}{\Delta t} = \frac{3}{2}\,R(U^{n}) - \frac{1}{2}\,R(U^{n-1}) - \nabla \mathrm{P}^{n+1} \tag{4.2}$$

As the density is constant for incompressible flow, so equation (4.2) can be written in the following form

$$U^{n+1} = U^{n} + \frac{\Delta t}{\rho}\left(\frac{3}{2}\,R(U^{n}) - \frac{1}{2}\,R(U^{n-1})\right) - \nabla \mathrm{P}^{n+1} \tag{4.3}$$

Equation (4.3) can be modified to the following form using the predictor velocity vector (U_p).From this equation it can be seen that velocity field (U^P) can be decomposed into divergence free part (U^{n+1}) and scalar part (p).This decomposition sometimes called Helmholtz-Hodge theorem.

$$U^{P} = U^{n+1} + \frac{\Delta t}{\rho}\nabla \mathrm{P}^{n+1} \tag{4.4}$$

The Predictor velocity (U^P) is that is given by the following equation

$$U^P = U^n + \frac{\Delta t}{\rho}\left(\frac{3}{2}\,R(U^n) - \frac{1}{2}\,R(U^{n-1})\right) \tag{4.5}$$

Poisson equation for determining the pressure is derived from velocity decomposition equation (4.4) by applying divergence operator

$$\nabla . U^P = \nabla . U^{n+1} + \nabla . \left(\frac{\Delta t}{\rho}\nabla \mathrm{P}^{n+1}\right) \tag{4.6}$$

As $\nabla . U^{n+1} = 0$, the final form of Poisson equation for the pressure is shown in equation(4.7)

$$\Delta P^{n+1} = \frac{\rho}{\Delta t}\nabla . U^P \tag{4.7}$$

After solving Poisson equation, the pressure is used for correcting the predictor velocity to get velocity at new time step

$$U^{n+1} = U_p - \frac{\Delta t}{\rho}\nabla \mathrm{P}^{n+1} \tag{4.8}$$

4.1.1 Discretization of Poisson equation

Poisson equation can be written in integral form as shown in equation (4.9)

$$\int_v \Delta P^{n+1}\, dV = \int_v \frac{\rho}{\Delta t}\nabla . U^P\, dV \tag{4.9}$$

By using Gauss divergence theorem, Poisson equation is modified to the following form

$$\int_s \nabla {P_f}^{n+1}\, ds = \int_s \frac{\rho}{\Delta t}\nabla . {U^P}_f\, ds \tag{4.10}$$

Poisson equation is discretised as shown in equation (4.11)

$$\begin{aligned}\frac{{p_E}^{n+1} - {p_p}^{n+1}}{d_{EP}}A_e - \frac{{p_p}^{n+1} - {p_W}^{n+1}}{d_{PW}}A_w + \frac{{p_N}^{n+1} - {p_p}^{n+1}}{d_{NP}}A_N - \frac{{p_P}^{n+1} - {p_S}^{n+1}}{d_{PS}}A_s \\ = \frac{1}{\Delta t}\left[(\rho u^p A)_e - (\rho u^p A)_w + (\rho v^p A)_n - (\rho u^p A)_s\right]\end{aligned} \tag{4.11}$$

Poisson equation can be written in the following form

$$a_p {p_p}^{n+1} = a_E {p_E}^{n+1} + a_W {p_W}^{n+1} + a_N {p_N}^{n+1} + a_S {p_S}^{n+1} + b_p \quad \textbf{(4.12)}$$

Where, coefficients are determined from the following equations

$$a_E = \frac{A_e}{d_{EP}} \quad \textbf{(4.13)}$$

$$a_W = \frac{A_w}{d_{PW}} \quad \textbf{(4.14)}$$

$$a_N = \frac{A_n}{d_{NP}} \quad \textbf{(4.15)}$$

$$a_S = \frac{A_s}{d_{PS}} \quad \textbf{(4.16)}$$

$$a_p = a_E + a_W + a_N + a_S \quad \textbf{(4.17)}$$

$$b_p = -\frac{1}{\Delta t}[(\rho u^p A)_e - (\rho u^p A)_w + (\rho v^p A)_n - (\rho u^p A)_s] \quad \textbf{(4.18)}$$

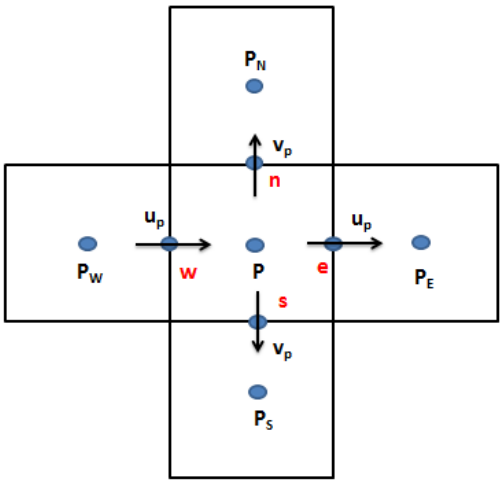

Figure 4.1: Poisson equation discretization

After writing Poisson equation in the discretised form, a system of linear algebraic will need to be solved. The complexity and size of the set of equations depend on the problem dimensions and number of grid nodes and the way of discretising the equations.

4.1.2 Solver

For solving set of algebraic equations two technique are used: direct and iterative methods. Iterative methods are based on repeated application of relatively simple algorithm after a number of repetitions convergences to exact solution is reached. The number of operations to solve a system of N equations with N unknowns is of the order of N per iteration. Iterative methods have the advantages of simplicity and easy to be implemented. Examples of iterative methods are Jacobi and Gauss–Seidel point .One other hand; in direct methods the number of operations is of N^3. Examples of direct methods are Cramer's rule matrix inversion and Gaussian elimination.

- **Gauss-Seidel algorithm**

  Gauss-Seidel method is applied to any matrix with non-zero elements on the diagonals. Convergence is guaranteed if one of these criteria is achieved[9], the first one is that the matrix should be diagonally dominant. Diagonally dominant means that coefficient on the diagonal for every row in the matrix must be equal to or larger than the sum of the other coefficient in the row and at least one row with a diagonal coefficient greater than the sum of other coefficients. The second criteria is that the matrix must be symmetric and positive definite. The solution procedures start by assuming initial guess solution, then the new values for ∅ are calculated from equation (4.19) using values calculated at current iteration and values stored form previous iteration. After that the approximate relative error is calculated using equation (4.20) and checked with the pre-specified tolerance. If the error is less than pre-specified tolerance, iterative process is stopped if not the solution at the current iteration is used as initial guess for the next iteration and iterative process is continued until convergence is reached.

$$a_P \emptyset_P = a_E \emptyset_E + a_W \emptyset_W + a_N \emptyset_N + a_S \emptyset_S + b_p \quad \textbf{(4.19)}$$

$$\epsilon = \frac{\sqrt{\sum(\emptyset_p{}^k - \emptyset_p{}^{k-1})^2}}{\sqrt{\sum(\emptyset_p{}^{k-1})^2}} \quad \textbf{(4.20)}$$

Where,

K: current iteration

K-1: previous iteration

- **Tri-diagonal matrix algorithm**

It is also known as Thomas algorithm as it was developed by Thomas (1949)[4].It is a simplified form of Gaussian elimination that can be used for solving tri-diagonal system of equation. The TDMA is considered direct method for one dimensional matrix, but applied iteratively in a line by line for solving multi-dimensional matrix. Its advantages are computationally inexpensive and a minimum amount of storage is required.

Consider a system of equations has a tri-diagonal form as shown below

$$\begin{bmatrix} 1 & -\alpha_1 & 0 & 0 & 0 & 0 & 0 \\ -\beta_2 & D_2 & -\alpha_2 & 0 & 0 & 0 & 0 \\ 0 & -\beta_3 & D_3 & -\alpha_3 & 0 & 0 & 0 \\ 0 & 0 & -\beta_4 & D_4 & -\alpha_4 & 0 & 0 \\ . & . & . & . & . & . & . \\ 0 & 0 & 0 & 0 & -\beta_n & D_n & -\alpha_n \\ 0 & 0 & 0 & 0 & 0 & -\beta_{n+1} & D_{n+1} \end{bmatrix} \begin{bmatrix} \emptyset_1 \\ \emptyset_2 \\ \emptyset_3 \\ \emptyset_4 \\ . \\ \emptyset_n \\ \emptyset_{n+1} \end{bmatrix} = \begin{bmatrix} c_1 \\ c_1 \\ c_1 \\ c_1 \\ . \\ c_n \\ c_{n+1} \end{bmatrix} \quad \textbf{(4.21)}$$

In the above set of equations $\emptyset_1$ and $\emptyset_{n+1}$ are known boundary values, so equations can be written in general form

$$-\beta_j \emptyset_{j-1} + D_j \emptyset_j - \alpha_j \emptyset_{j+1} = c_j \quad \textbf{(4.22)}$$

Using forward elimination, equation **(4.22)** can be modified to the following form

$$\emptyset_j = A_j \emptyset_{j+1} + c_j' \quad \textbf{(4.23)}$$

Where,

$$A_j = \frac{\alpha_j}{D_j - \beta_j A_{j-1}} \quad \textbf{(4.24)}$$

$$c_j' = \frac{\beta_j c_{j-1}' + c_j}{D_j - \beta_j A_{j-1}} \quad \textbf{(4.25)}$$

After getting the values of A_j and c_j' for all unknown $\emptyset$ using forward elimination from j=2 to j=n-1, backward substitution is used. As the value of $\emptyset$

is known at boundary location $(n+1)$, so the value of $\emptyset_j$ can be obtained in reverse order ($\emptyset_n$, $\emptyset_{n-1}$, $\emptyset_{n-2}$,……., $\emptyset_2$) using equation (4.23)**.**

TDMA can be applied iteratively to solve system of equations for two-dimensional problems. The general form of system of equation in 2-dimensional system is shown in equation

$$a_P\emptyset_P = a_E\emptyset_E + a_W\emptyset_W + a_N\emptyset_N + a_S\emptyset_S + b_p \quad \textbf{(4.26)}$$

If TDMA is used for solving (n-s) lines as shown in Figure 3.1 , equation (4.26) can be written in the following form:

$$-a_S\emptyset_S + a_P\emptyset_P - a_N\emptyset_N = a_E\emptyset_E + a_W\emptyset_W + b_p \quad \textbf{(4.27)}$$

Comparing equation (4.27) to equation (4.22), we can deduce the following relations

$$\beta_j = a_S \quad \textbf{(4.28)}$$

$$D_j = a_p \quad \textbf{(4.29)}$$

$$\alpha_j = a_N \quad \textbf{(4.30)}$$

$$c_j = a_E\emptyset_E + a_W\emptyset_W + b_p \quad \textbf{(4.31)}$$

The right hand side of equation (4.27) is assumed to be temporary known, so that equation along n-s line can be solved for j =2, 3… n as shown in Figure 4.2.After that calculation is moved to the next n-s line. The sequence in which n-s lines are calculated is called swept direction. If the swept direction is from west to east the values of $\emptyset_W$ are known from previous line calculations, while the values of $\emptyset_E$ are unknown so they are assumed equal to their values at previous iteration. This makes solution process iterative and this process is repeated until convergence is reached.

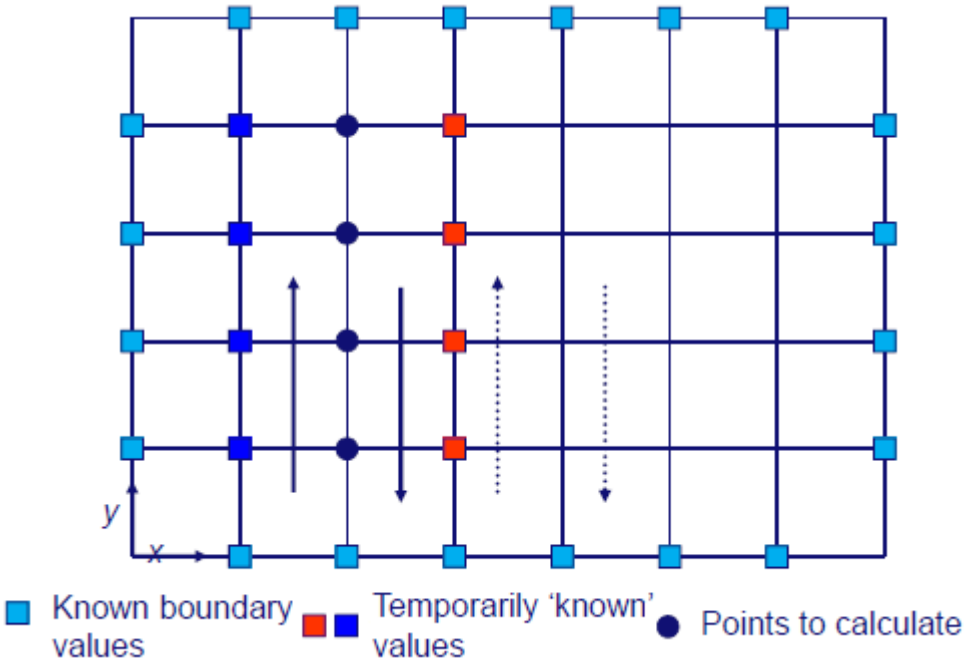

Figure 4.2: using TDMA for solving n-s lines (line by line)

4.1.3 Boundary Conditions and Initial Conditions

Each control volume provides one algebraic equation. Volume integrals are calculated in the same manner for all interior control volumes, but fluxes through control volume face coincident with problem domain boundary need special treatment. These fluxes must be known or expressed as function of interior control volume values. Since these nodes are located on the domain boundary and no nodes located outside the boundary, their values can be only calculated based on one-side differences (forward or backward differences) or extrapolations.

Common types of boundary conditions are constant gradient, fixed value and symmetry boundary condition.

- **Constant gradient boundary conditions**, this condition is also known as Neumann boundary condition, where the gradient of the variable in direction normal to domain boundary is equal constant.

$$\frac{\partial \emptyset}{\partial \eta} = constant \qquad \textbf{(4.32)}$$

Where,

η: Normal direction

This condition is implemented for Poisson equation by setting the equation coefficient as shown below for north boundary condition with zero pressure gradient as an example.

$$\begin{aligned} a_E &= 0 \\ a_W &= 0 \\ a_P &= 1 \\ a_N &= 0 \\ a_s &= 1 \\ b_p &= 0 \end{aligned} \qquad \textbf{(4.33)}$$

For velocity boundary condition, zero gradient boundary condition is implemented as shown below for north boundary as an example

$$u_P = u_S \qquad \textbf{(4.34)}$$

- **Fixed value boundary condition**, that is also known as Dirichlet, which is implemented by setting the value of variable of the nodes at domain boundary to fixed value.

$$\emptyset = constant \qquad \textbf{(4.35)}$$

This condition is implemented for Poisson equation by setting all equation as shown below

$$\begin{aligned} a_E &= 0 \\ a_W &= 0 \\ a_P &= 1 \\ a_N &= 0 \\ a_s &= 1 \\ b_p &= constant \end{aligned} \qquad \textbf{(4.36)}$$

While, for velocity equation, it is implement by setting velocity value to fixed value

$$u = constant \tag{4.37}$$

Symmetry boundary condition, which treats the variables as if the boundary is a mirror plane. This condition sets the component of the variables normal to symmetry plane to zero; while parallel components and scalar quantity are calculated by setting their gradient in direction normal to the plane to zero. An example of symmetry boundary condition if it is applied on the west boundary is shown below

$$u = 0 \tag{4.38}$$

$$\frac{\partial v}{\partial x} = 0 \tag{4.39}$$

$$\frac{\partial \emptyset}{\partial x} = 0 \tag{4.40}$$

4.1.4 Determination of Δt

As explicit temporal scheme is used in the fractional step method, so some time restrictions on the time step will be introduce to guarantee solution stability and obtain converged solution. Courant-Friedrichs-Lewy Condition for the numerical stability of difference schemes is used for determining the time step which states that for given a space discretization, a time step bigger than some computable quantity should not be taken, so that time step must be kept small to allow information to have sufficient time to travel through space discretization[10] and it is mathematically expressed as shown:

$$\Delta t \left(\frac{|u_i|}{\Delta x_i}\right)_{max} \leq C_{conv} \tag{4.41}$$

$$\Delta t \left(\frac{\frac{\Gamma}{\rho}}{{\Delta x_i}^2}\right)_{max} \leq C_{visc} \tag{4.42}$$

Where, the bounding values C_{conv} and C_{visc} must be smaller than unity. In our case, we use values recommended by [11] using values of $C_{conv} = 0.35$ and $C_{visc} = 0.2$.

4.1.5 Algorithm flow chart

In the previous sections, we have discussed different procedures of fractional step method for incompressible flow. Now we will show how they work together as one unit as shown below.

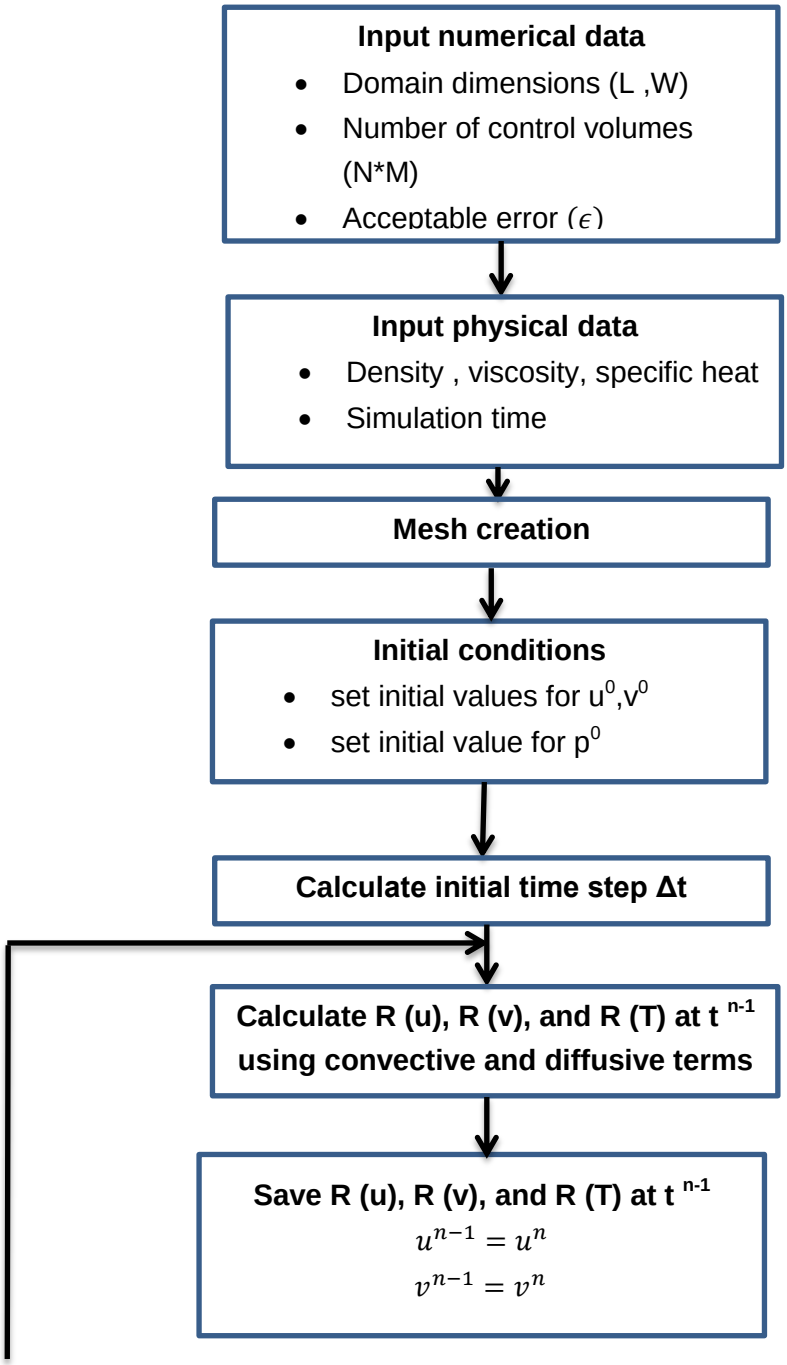

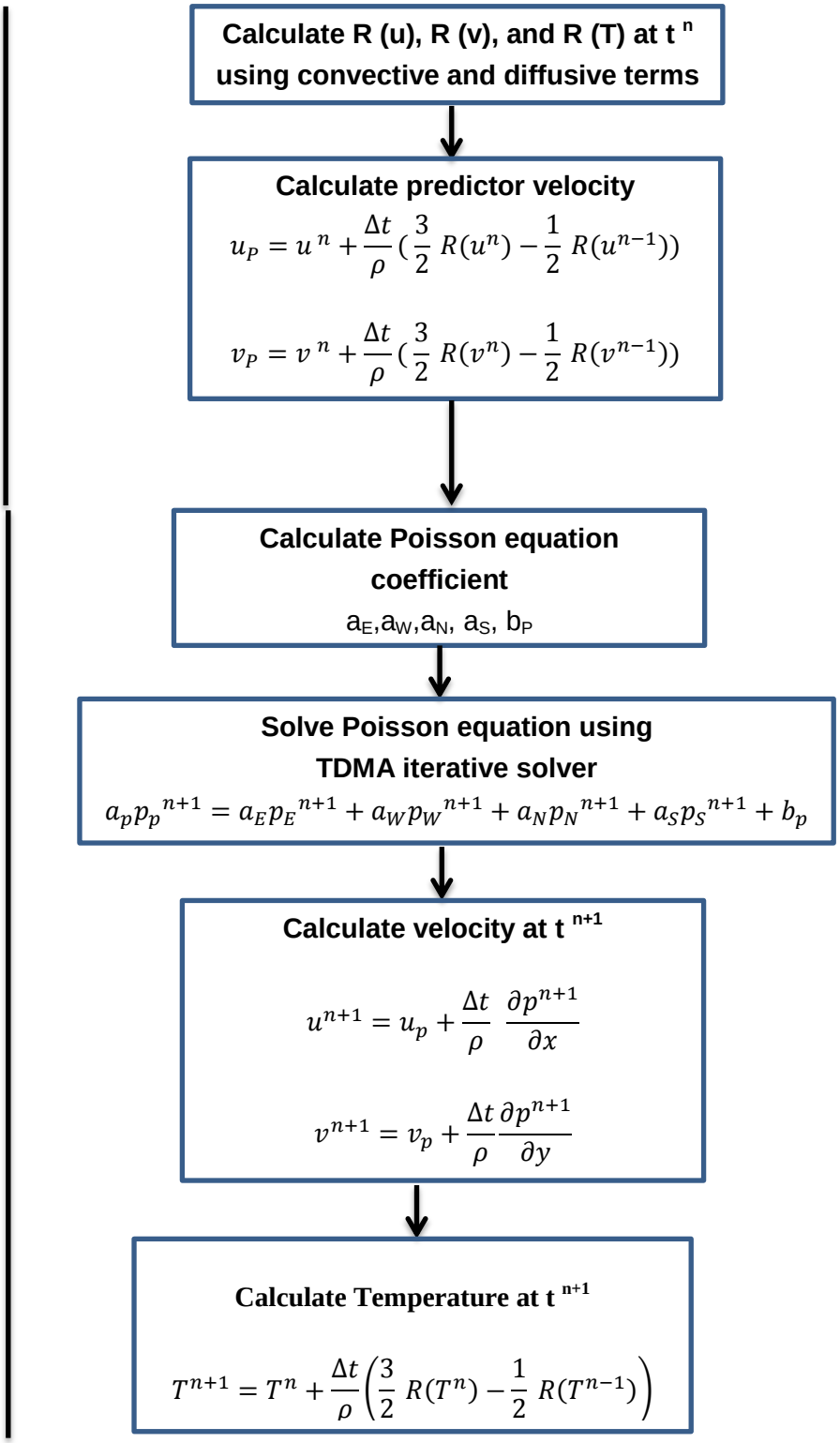
Calculate R (u), R (v), and R (T) at t n using convective and diffusive terms
Calculate predictor velocity
$u_P = u^n + \frac{\Delta t}{\rho}(\frac{3}{2} R(u^n) - \frac{1}{2} R(u^{n-1}))$
$v_P = v^n + \frac{\Delta t}{\rho}(\frac{3}{2} R(v^n) - \frac{1}{2} R(v^{n-1}))$
Calculate Poisson equation coefficient
a_E, a_W, a_N, a_S, b_P
Solve Poisson equation using TDMA iterative solver
$a_p p_p{}^{n+1} = a_E p_E{}^{n+1} + a_W p_W{}^{n+1} + a_N p_N{}^{n+1} + a_S p_S{}^{n+1} + b_p$
Calculate velocity at t n+1
$u^{n+1} = u_p + \frac{\Delta t}{\rho} \frac{\partial p^{n+1}}{\partial x}$
$v^{n+1} = v_p + \frac{\Delta t}{\rho} \frac{\partial p^{n+1}}{\partial y}$
Calculate Temperature at t n+1
$T^{n+1} = T^n + \frac{\Delta t}{\rho}\left(\frac{3}{2} R(T^n) - \frac{1}{2} R(T^{n-1})\right)$

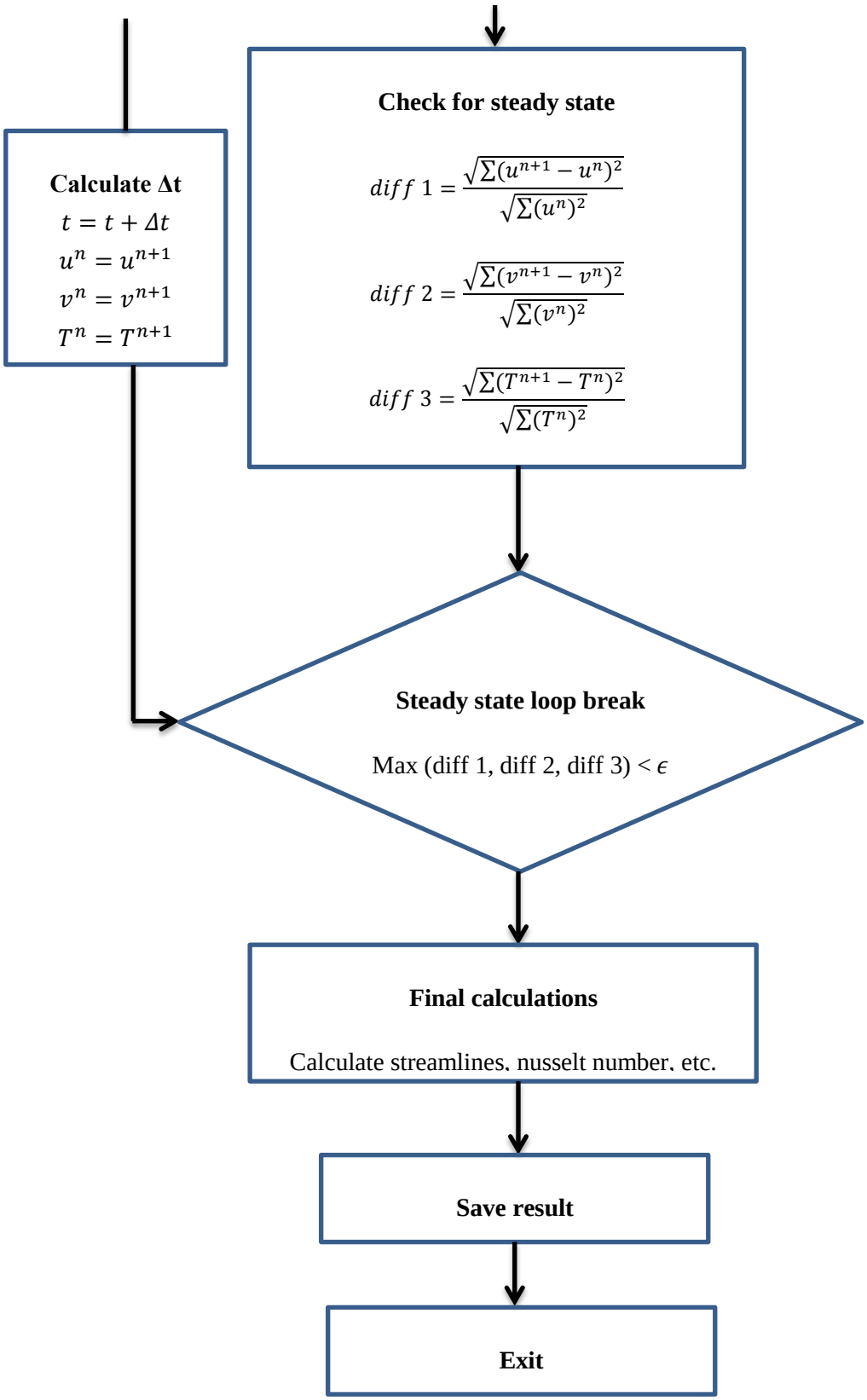
Calculate Δt
$t = t + \Delta t$
$u^n = u^{n+1}$
$v^n = v^{n+1}$
$T^n = T^{n+1}$
Check for steady state
$diff\ 1 = \frac{\sqrt{\sum(u^{n+1} - u^n)^2}}{\sqrt{\sum(u^n)^2}}$
$diff\ 2 = \frac{\sqrt{\sum(v^{n+1} - v^n)^2}}{\sqrt{\sum(v^n)^2}}$
$diff\ 3 = \frac{\sqrt{\sum(T^{n+1} - T^n)^2}}{\sqrt{\sum(T^n)^2}}$
Steady state loop break
Max (diff 1, diff 2, diff 3) < ϵ
Final calculations
Calculate streamlines, nusselt number, etc.
Save result
Exit

4.2 Fractional step method for compressible flow with low Mach number

Fractional step for incompressible flow can be extended using Adams-Bashforth and Crank-Nicolson time integration schemes to simulate compressible flow with low Mach number and high density variations[12, 13].In this case Bossinesq approximation that neglect density variation cannot be used in describing fluxes with high density variation. In low Mach number Navier-stokes equation the velocity divergence is not zero and acoustic waves are neglected and high order terms that depend on Mach number are removed.The pressure is split into dynamic pressure and thermodynamic pressure. The thermodynamic pressure is used to calculate the density using ideal gas state law.

4.2.1 Numerical algorithm

The fractional step method for compressible flow with low Mach number is done in predictor-corrector sub-steps. In the predictor step a second order Adams-Bashforth time integration scheme is used to calculate the predicted scalar fields and predictor velocity is calculated after correcting the pseudo velocity in the pressure correction step to satisfy the continuity equation. While in the corrector step a Crank-Nicolson time integration scheme is used to calculate scalar field at the new time step and velocity is calculated after the pressure correction step. In both steps pressure correction requires solving Poisson equation using TDMA solver.

The algorithm scheme will be discussed in the following sub sections and it will be divided into two parts: predictor step and corrector step. Before discussing the algorithm, we will summarize flow equations which are continuity, Navier-Stokes and energy equation shown in equation (4.43) , (4.44) & (4.45).

$$\frac{\partial \rho}{\partial t} + \frac{\partial \rho u_j}{\partial x_j} = 0 \qquad \textbf{(4.43)}$$

$$\frac{\partial \rho u_i}{\partial t} = -\frac{\partial \rho u_i u_j}{\partial x_j} - \frac{\partial p}{\partial x_i} + \frac{\partial \tau_{ij}}{\partial x_j} + \rho g_i \qquad \textbf{(4.44)}$$

$$\rho \frac{\partial h}{\partial t} = -\rho u_j \frac{\partial h}{\partial x_j} + \frac{dp_0}{dt} - \frac{\partial q_j}{\partial x_j} \qquad \textbf{(4.45)}$$

4.2.1.1 Predictor

1. Predicted scalar fields are calculated using second order Adams-Bashforth time integration scheme, so that Predicted enthalpy is calculated by applying Adams-Bashforth time integration scheme on energy transport equation as shown in equation (4.46) .This scheme is fully explicit time scheme that depend on scalar fields and density at current time step (t^n) and previous time step (t^{n-1}).

$$\rho^n \frac{h^* - h^n}{\Delta t} = \frac{3}{2}\left(\rho^n \frac{\partial h}{\partial t}\Big|^n\right) - \frac{1}{2}\left(\rho^{n-1} \frac{\partial h}{\partial t}\Big|^{n-1}\right) \quad \textbf{(4.46)}$$

2. The temperature at each control volume can be calculated using equation of the enthalpy of non-reacting flows which is equal to the sensible enthalpy.

$$h = \int_{T_0}^{T} C_P \, dT \quad \textbf{(4.47)}$$

3. Evaluate thermodynamic pressure which is constant and equal to ambient pressure for open system but for closed system, the pressure at given time is calculated using the total mass in the enclosure and temperature field.

$$M_0 = \frac{p_0}{R_i} \int_V \frac{1}{T} dV \quad \textbf{(4.48)}$$

$$p_0 = \frac{M_0 \, R_i}{\int_V \frac{1}{T} dV} \quad \textbf{(4.49)}$$

Where,

p_0: Thermodynamic pressure

M_0: Total mass in the closure

R_i : Universal gas constant

4. Calculate predicted density from equation of state as shown in equation

$$\rho^* = \frac{p_0}{R_i T} \quad \textbf{(4.50)}$$

5. The intermediate velocity field $\hat{u}_i$ that is calculated by integrating pressure-split momentum equation.

$$\frac{\rho^* \hat{u}_i - \rho^n {u_i}^n}{\Delta t} = \frac{3}{2} {R_i}^n - \frac{1}{2} {R_i}^{n-1} \quad \textbf{(4.51)}$$

Where,

$$R_i = -\frac{\partial \rho u_i u_j}{\partial x_j} - \frac{\partial p}{\partial x_i} + \frac{\partial \tau_{ij}}{\partial x_j} + \rho g_i \quad \textbf{(4.52)}$$

6. The predicted hydrodynamic pressure p^* is determined by solving Poisson equation

$$\nabla^2 p^* = \frac{1}{\Delta t} [\nabla . (\rho^* \hat{u}_i) - \nabla . (\rho^* {u_i}^*)] \quad \textbf{(4.53)}$$

Where, $\nabla . (\rho^* {u_i}^*)$ can be replaced by $-\frac{\partial \rho}{\partial t}\Big|^*$ from continuity equation

$$\nabla . (\rho^* {u_i}^*) = -\frac{\partial \rho}{\partial t}\Big|^* \quad \textbf{(4.54)}$$

and $\frac{\partial \rho}{\partial t}\Big|^*$ is given by second order discretization

$$\frac{\partial \rho}{\partial t}\Big|^* = \frac{1}{2\,\Delta t} (3\rho^* - 4\rho^n + \rho^{n-1}) \quad \textbf{(4.55)}$$

7. Finally , the predicted velocity field ${u_i}^*$ is determined using the projection step

$$\frac{\rho^* {u_i}^* - \rho^* \hat{u}_i}{\Delta t} = -\frac{\partial p^*}{\partial x_i} \quad \textbf{(4.56)}$$

4.2.1.2 Corrector

1. The temporal derivative of scalar fields at new time step are calculated based on predicted values and values at old time step (t^n). Enthalpy at the new time step is calculated using second order Crank-Nicolson time integration scheme.

$$\rho^n \frac{h^{n+1} - h^n}{\Delta t} = \frac{1}{2} \left(\rho^n \frac{\partial h}{\partial t}\Big|^n + \rho^* \frac{\partial h}{\partial t}\Big|^{**} \right) \quad \textbf{(4.57)}$$

Where, time derivative of predicted enthalpy $\frac{\partial h}{\partial t}\Big|^{**}$ is calculated from equation (4.45) using predicted values.

2. Calculate thermodynamic pressure p_o if it is not constant from equation (4.49).

3. evaluate gas density at the new tine step using ideal gas law

$$\rho = \frac{p_0}{R_i T} \tag{4.58}$$

4. Determine second intermediate velocity u_i' from pressure split momentum equation.

$$\frac{\rho^{n+1} u_i' - \rho^n {u_i}^n}{\Delta t} = \frac{3}{2} {R_i}^n - \frac{1}{2} {R_i}^{n-1} \tag{4.59}$$

5. the pressure at the new time step is calculated from Poisson equation

$$\nabla^2 p^{n+1} = \frac{1}{\Delta t} [\nabla . (\rho^{n+1} u_i') - \nabla . (\rho^{n+1} {u_i}^{n+1})] \tag{4.60}$$

Where, $\nabla . (\rho^{n+1} {u_i}^{n+1})$ can be replaced by $-\frac{\partial \rho}{\partial t}\Big|^{n+1}$ from continuity equation

$$\nabla . (\rho^{n+1} {u_i}^{n+1}) = -\frac{\partial \rho}{\partial t}\Big|^{n+1} \tag{4.61}$$

and $\frac{\partial \rho}{\partial t}\Big|^{n+1}$ is given by second order discretization

$$\frac{\partial \rho}{\partial t}\Big|^{n+1} = \frac{1}{2\,\Delta t} (3\rho^{n+1} - 4\rho^n + \rho^{n-1}) \tag{4.62}$$

6. finally , calculate the velocity at the new time step

$$\frac{\rho^{n+1} {u_i}^{n+1} - \rho^{n+1} u_i'}{\Delta t} = -\frac{\partial p^{n+1}}{\partial x_i} \tag{4.63}$$

4.2.2 Algorithm flow chart

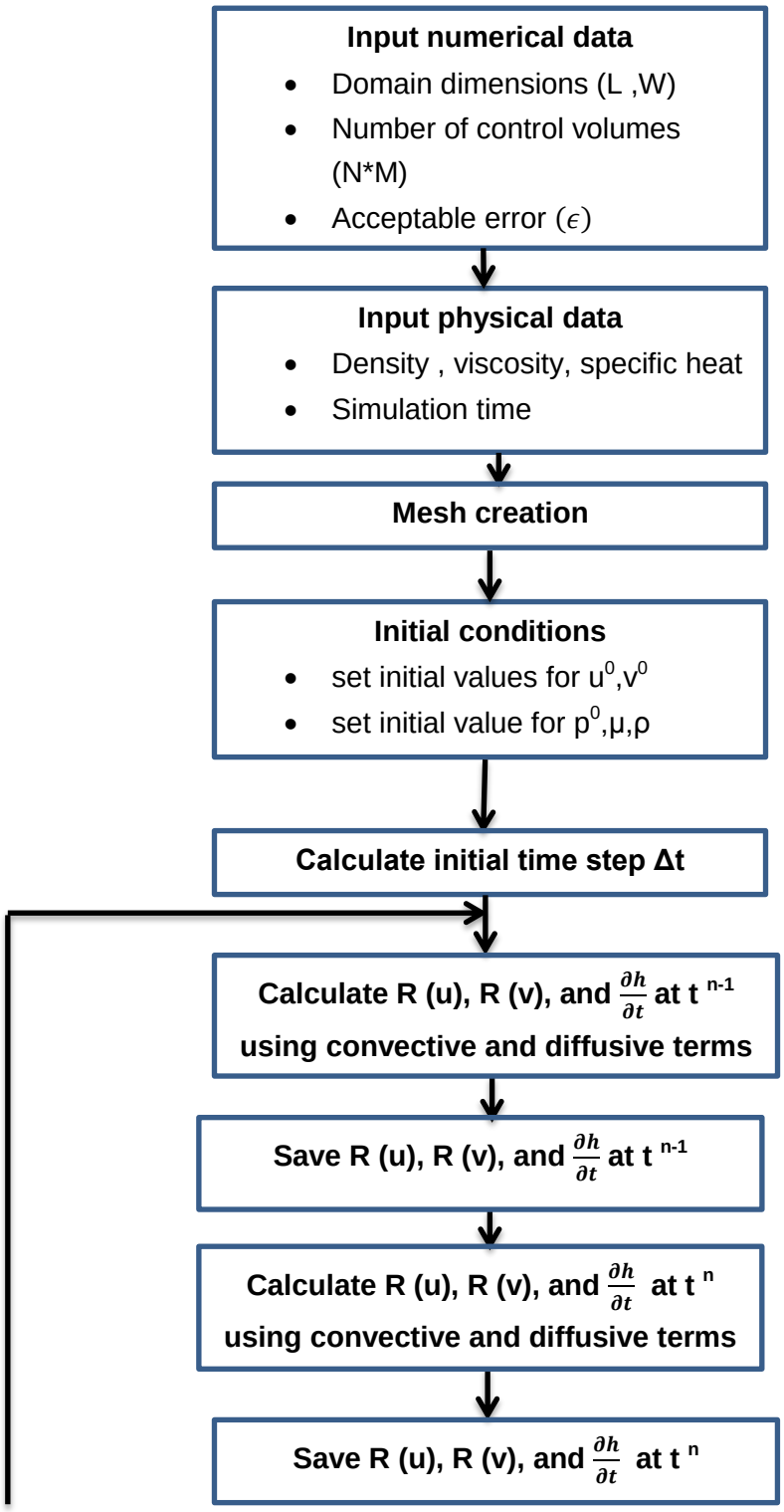
Input numerical data
Domain dimensions (L ,W)
Number of control volumes (N*M)
Acceptable error (ϵ)
Input physical data
Density , viscosity, specific heat
Simulation time
Mesh creation
Initial conditions
set initial values for u^0,v^0
set initial value for p^0,μ,ρ
Calculate initial time step Δt
Calculate R (u), R (v), and $\frac{\partial h}{\partial t}$ at t $^{n-1}$ using convective and diffusive terms
Save R (u), R (v), and $\frac{\partial h}{\partial t}$ at t $^{n-1}$
Calculate R (u), R (v), and $\frac{\partial h}{\partial t}$ at t ^{n} using convective and diffusive terms
Save R (u), R (v), and $\frac{\partial h}{\partial t}$ at t ^{n}

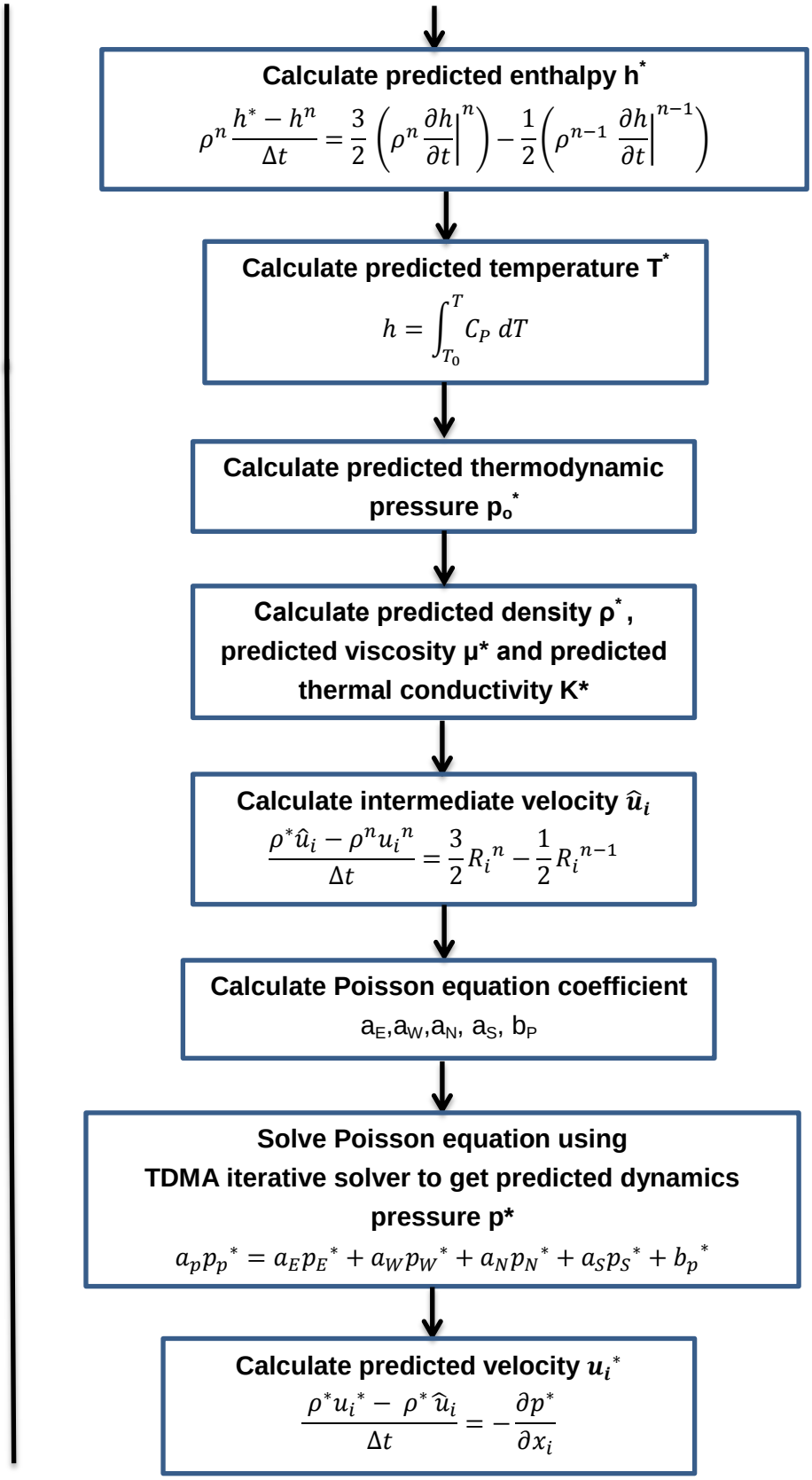
Calculate predicted enthalpy h*
$\rho^n \frac{h^* - h^n}{\Delta t} = \frac{3}{2}\left(\rho^n \frac{\partial h}{\partial t}\Big|^n\right) - \frac{1}{2}\left(\rho^{n-1} \frac{\partial h}{\partial t}\Big|^{n-1}\right)$
Calculate predicted temperature T*
$h = \int_{T_0}^{T} C_P \, dT$
Calculate predicted thermodynamic pressure p₀*
Calculate predicted density ρ*, predicted viscosity μ* and predicted thermal conductivity K*
Calculate intermediate velocity $\hat{u}_i$
$\frac{\rho^* \hat{u}_i - \rho^n {u_i}^n}{\Delta t} = \frac{3}{2} {R_i}^n - \frac{1}{2} {R_i}^{n-1}$
Calculate Poisson equation coefficient
a_E, a_W, a_N, a_S, b_P
Solve Poisson equation using TDMA iterative solver to get predicted dynamics pressure p*
$a_p {p_p}^* = a_E {p_E}^* + a_W {p_W}^* + a_N {p_N}^* + a_S {p_S}^* + {b_p}^*$
Calculate predicted velocity ${u_i}^*$
$\frac{\rho^* {u_i}^* - \rho^* \hat{u}_i}{\Delta t} = -\frac{\partial p^*}{\partial x_i}$

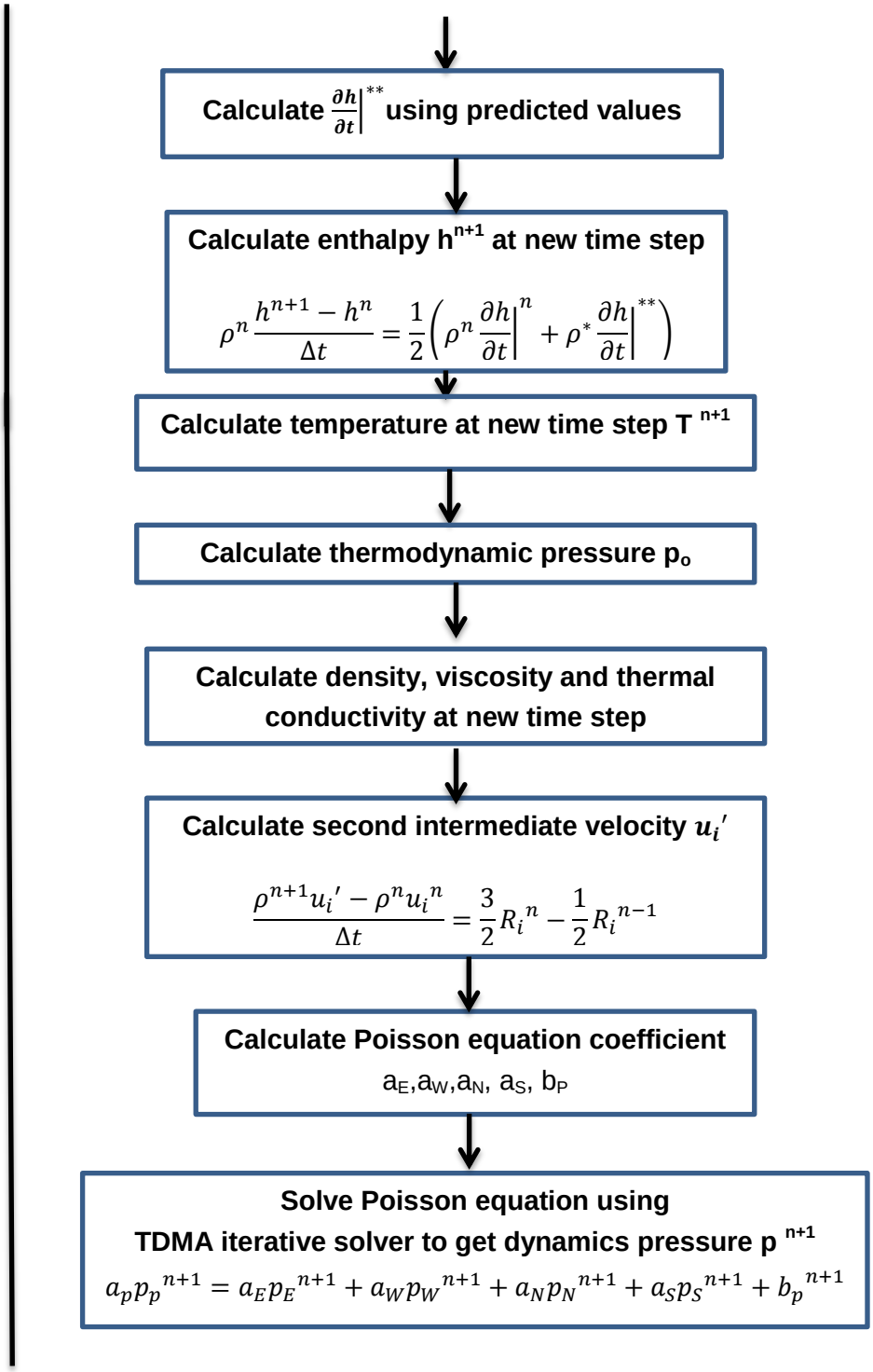
Calculate $\frac{\partial h}{\partial t}\Big|^{**}$ using predicted values
Calculate enthalpy h^{n+1} at new time step
$\rho^n \frac{h^{n+1}-h^n}{\Delta t} = \frac{1}{2}\left(\rho^n \frac{\partial h}{\partial t}\Big|^n + \rho^* \frac{\partial h}{\partial t}\Big|^{**}\right)$
Calculate temperature at new time step T^{n+1}
Calculate thermodynamic pressure p_o
Calculate density, viscosity and thermal conductivity at new time step
Calculate second intermediate velocity u_i'
$\frac{\rho^{n+1}u_i' - \rho^n {u_i}^n}{\Delta t} = \frac{3}{2}{R_i}^n - \frac{1}{2}{R_i}^{n-1}$
Calculate Poisson equation coefficient
a_E, a_W, a_N, a_S, b_P
Solve Poisson equation using
TDMA iterative solver to get dynamics pressure p^{n+1}
$a_p {p_p}^{n+1} = a_E {p_E}^{n+1} + a_W {p_W}^{n+1} + a_N {p_N}^{n+1} + a_S {p_S}^{n+1} + {b_p}^{n+1}$

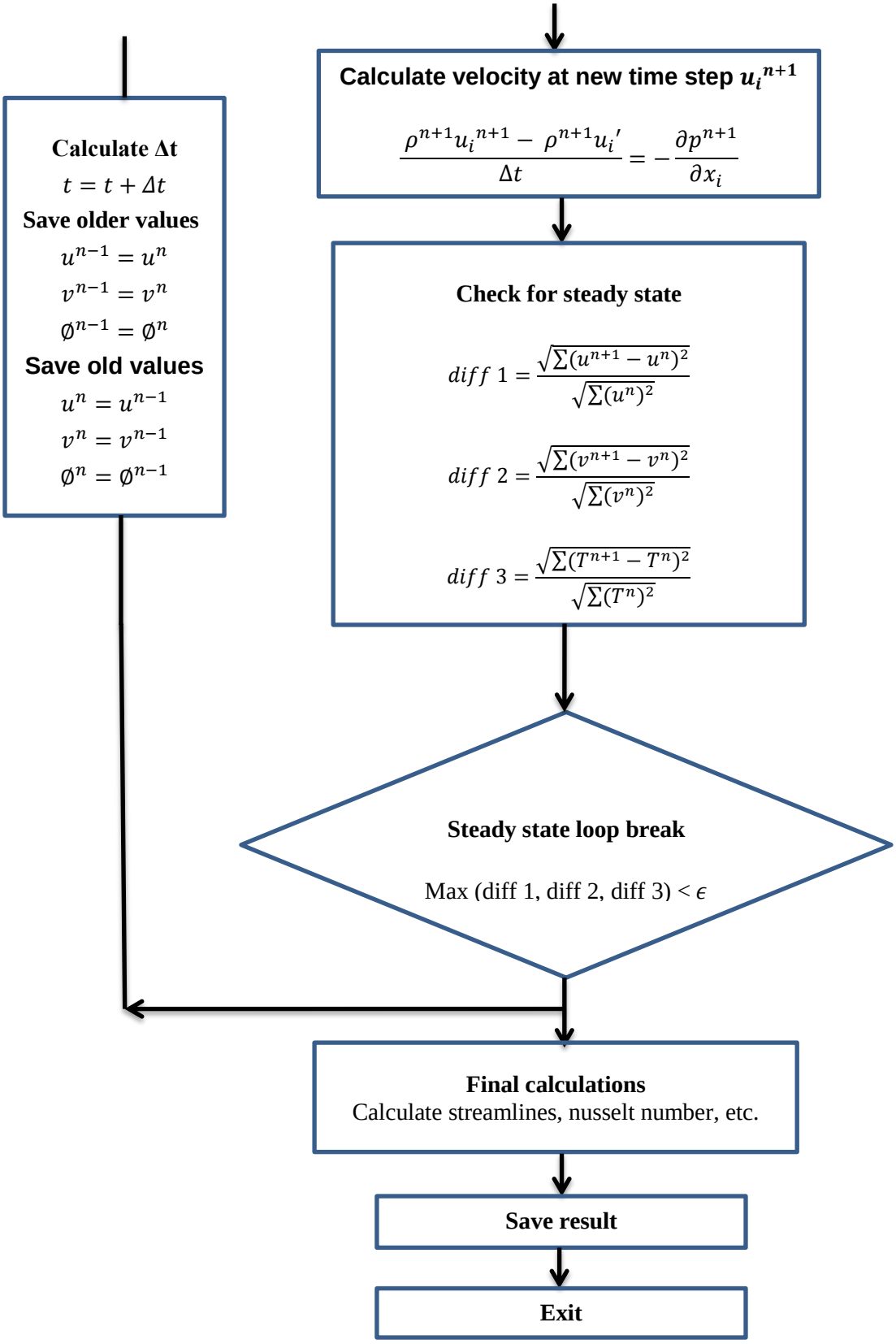
Calculate velocity at new time step u_i^{n+1}
$\frac{\rho^{n+1}u_i^{n+1} - \rho^{n+1}u_i'}{\Delta t} = -\frac{\partial p^{n+1}}{\partial x_i}$
Check for steady state
$diff\ 1 = \frac{\sqrt{\sum(u^{n+1} - u^n)^2}}{\sqrt{\sum(u^n)^2}}$
$diff\ 2 = \frac{\sqrt{\sum(v^{n+1} - v^n)^2}}{\sqrt{\sum(v^n)^2}}$
$diff\ 3 = \frac{\sqrt{\sum(T^{n+1} - T^n)^2}}{\sqrt{\sum(T^n)^2}}$
Steady state loop break
Max (diff 1, diff 2, diff 3) < ϵ
Calculate Δt
$t = t + \Delta t$
Save older values
$u^{n-1} = u^n$
$v^{n-1} = v^n$
$\emptyset^{n-1} = \emptyset^n$
Save old values
$u^n = u^{n-1}$
$v^n = v^{n-1}$
$\emptyset^n = \emptyset^{n-1}$
Final calculations
Calculate streamlines, nusselt number, etc.
Save result
Exit

5 Code verification

In this chapter, we will verify and assesses our code to make sure that it is correctly implemented. In verification process the accuracy of the solution provided by our computational simulation code is compared with known solution or experimental data. Verification is defined as the process of testing how far the model implementation accurately represents the developer's conceptual description of the model and the solution to the model. This process strategy is based on identification, quantification and reduction of error in the model and its solution. To measure numerical solution error, model solution should be compared to highly accurate analytical or numerical solution (benchmark solution),so that verification can provides an evidence that the conceptual model is correctly solved using discretized mathematical equations implemented in simulation code.

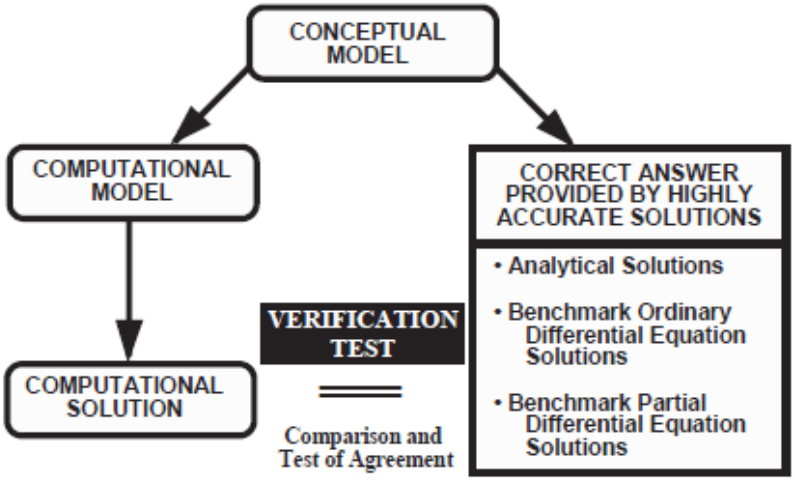

Figure 5.1: Verification process[14]

The five major sources of errors in CFD are[14]:

1. insufficient spatial discretization convergence
2. insufficient temporal discretization convergence
3. insufficient convergence of an iterative procedure
4. computer round-off
5. computer programming errors

The first three errors are considered to be within the realm of CFD as the first two errors depend mainly on the way of discretizing different terms in flow governing equations and the third one depend on convergence criteria set for the iterative process. The fourth

error source is of minor importance and rarely dealt within CFD. The fifth source of error belongs to computer science field as it dealt with programming errors.

5.1 Incompressible flow

The incompressible flow program code will be firstly checked by method of manufactured solutions (MMS) in the next subsection which is considered to be in the category of analytical solution and after that results of code will be compared with benchmark solution for driven cavity and thermal differential heated cavity.

5.1.1 The Method of manufactured solutions (MMS)

The MMS method provides a straight forward technique for verifying code accuracy by generating an analytical solution that can be compared with numerical solution. The idea of MMS method is to simply manufacture an exact solution for a system of equations without being concerned with physical realism as the verification is a purely mathematical exercise[15].Suppose we need to solve a differential equation for quantity ∅ in the following form:

$$\frac{\partial \emptyset}{\partial t} = F(\emptyset) \tag{5.1}$$

After that a source term S is added to the previous equation

$$\frac{\partial \emptyset}{\partial t} = F(\emptyset) + S \tag{5.2}$$

And the source term is calculated for a manufactured solution $\emptyset^M$ as shown in equation (5.3)

$$S = \frac{\partial \emptyset^M}{\partial t} - F(\emptyset^M) \tag{5.3}$$

The source term is calculated analytically and added to equation need to be tested. After that modified equation is solved numerically and compared to analytical solution and the error is calculated for different mesh sizes.

To make the verification process using the MMS easier, it will be divided into three steps:

1. The velocity component in x-direction u(x,y) is considered unknown while the rest of functions and parameters are known and the numerical solution of u(x,y) is compared with known analytical solution.
2. The velocity component in y-direction v(x,y) is considered unknown while the rest of functions and parameters are known and the numerical solution of v(x,y) is compared with known analytical solution.
3. The resolution of coupling of continuity and momentum equations is tested. In this step, both u(x,y) and v(x,y) are assumed unknown and their numerical solutions are compared to known analytical solutions.

The analytical known velocity and pressure fields that will be used in our testing our code are listed below:

$$\mathrm{u}(\mathrm{x},\mathrm{y}) = \mathrm{x}^2\mathrm{y} \tag{5.4}$$

$$\mathrm{v}(\mathrm{x},\mathrm{y}) = -\mathrm{x}\mathrm{y}^2 \tag{5.5}$$

$$\mathrm{P}(\mathrm{x},\mathrm{y}) = \mathrm{x}^3 + \mathrm{y}^3 \tag{5.6}$$

The velocity field (u,v) satisfies the continuity equation and the divergence of the velocity vector is zero (div U=0) as the flow is incompressible.

1. **First step:**

   The velocity component in x-direction is unknown and the other functions v(x,y) and p(x,y) are known. The analytical velocity field u_a is compared with the numerical one u_n. A source term F_{x,u_a} should be added to the momentum equation in x-direction as shown below and it is calculated using partial derivatives that are substituted in the momentum equation. The expression is shown in equation

$$\rho u\frac{\partial u}{\partial x} + \rho v\frac{\partial u}{\partial y} = -\frac{\partial p}{\partial x} + \mu\left(\frac{\partial^2 u}{\partial x^2} + \frac{\partial^2 u}{\partial y^2}\right) + F_{x,u_a} \tag{5.7}$$

$$F_{x,u_a} = \rho x^3 y^2 + 3x^2 - 2\mu y \tag{5.8}$$

   The equations are solved considering:

   - Density: $\rho = 1\ kg/m^3$
   - viscosity: $\mu = 0.5\ kg/m^2 s$

- domain:$\Omega = X * Y$,on L_x=1.5 , L_y=1
- criteria to stop execution: $|\emptyset^n - \emptyset^{n-1}| < 10^{-10}$

The numerical solution of u is calculated for different number of control volumes and the results are compared to the analytical solution. The error is calculated as shown below:

$$E_D(u) = \frac{\max(|u_a - u_n|)}{\max(|u_a|)} \quad \textbf{(5.9)}$$

The goal of this test is to check the coincidence between the order of the used numerical scheme and the order of the calculated error convergence obtained with our code. The results are shown in Table 2.1.

Number of control volumes	$\boldsymbol{E_D(u)}$	$\boldsymbol{log_2\left(\frac{E_D(u)_{n-1}}{E_D(u)_n}\right)}$
15,10	1.0306*10^{-2}	
30,20	5.4349*10^{-3}	0.924
60,40	2.7487*10^{-3}	0.982
120,80	1.3865*10^{-3}	0.984
240,160	6.6385*10^{-4}	1.062

Table 5.1: Error convergence for u variable

2. second step

a similar procedures carried in the first step will be applied, but in this case velocity component in y-direction v will be unknown and other functions u(x,y) and p(x,y) will be known. The source term F_{y,v_a} that will be added to momentum equation in y-direction is calculated:

$$\rho u\frac{\partial v}{\partial x} + \rho v\frac{\partial v}{\partial y} = -\frac{\partial p}{\partial y} + \mu\left(\frac{\partial^2 v}{\partial x^2} + \frac{\partial^2 v}{\partial y^2}\right) + F_{y,v_a} \quad \textbf{(5.10)}$$

$$F_{y,v_a} = \rho x^2 y^3 + 3y^2 + 2\mu x \quad \textbf{(5.11)}$$

The numerical solution of velocity in y direction v_n is compared to analytical solution v_a and the convergence error are calculated as shown in Table 5.2

Number of control volumes	$E_D(v)$	$log_2\left(\frac{E_D(v)_{n-1}}{E_D(v)_n}\right)$
15,10	$1.96*10^{-2}$	
30,20	$8.62*10^{-3}$	1.182234
60,40	$4.08*10^{-3}$	1.07876
120,80	$1.99*10^{-3}$	1.038502
240,160	$9.78*10^{-4}$	1.023605

Table 5.2: Error convergence for v variable

3. Third step:

Once momentum equations in both x and y directions are correctly checked, the resolution of the coupling needs to be verified. The same analytical velocity and pressure are used and the same source term in equation (5.8) and (5.11) are added to momentum equation in x and y direction respectively.

The unknown variable will be u(x,y),v(x,y) and p(x,y).The numerical solutions for these variable u_n, v_n and p_n are compared to the analytical solution.

The equations are solved considering:

- Density:$\rho = 2\ kg/m^3$
- viscosity:$\mu = 0.8\ kg/m^2 s$
- domain:$\Omega = X * Y$,on L_x=1 , L_y=1.5
- criteria to stop solver: $\in < 10^{-10}$ where $\in$ simulation result error
- criteria to stop iterative loop of Poisson equation: $|p_i - p_{i-1}| < 10^{-6}$

The convergence error for u and v variable are listed in Table 5.3 and convergence error for p is listed in Table 5.4.

Number of control volumes	$E_D(u)$	$log_2\left(\frac{E_D(u)_{n-1}}{E_D(u)_n}\right)$	$E_D(v)$	$log_2\left(\frac{E_D(v)_{n-1}}{E_D(v)_n}\right)$
10,15	$4.80*10^{-3}$		$6.64*10^{-3}$	
20,30	$2.41*10^{-3}$	0.9958	$2.53*10^{-3}$	1.387863
40,60	$1.21*10^{-3}$	0.9953	$1.11*10^{-3}$	1.183043
80,120	$6.02*10^{-4}$	1.0045	$5.23*10^{-4}$	1.094013
160,240	$3.01*10^{-4}$	0.9983	$2.53*10^{-4}$	1.046203

Table 5.3: Error convergence for u and v variable

Number of control volumes	$E_D(p)$	$log_2\left(\frac{E_D(p)_{n-1}}{E_D(p)_n}\right)$
10,15	$6.954*10^{-2}$	
20,30	$3.521*10^{-2}$	0.981896
40,60	$1.767*10^{-2}$	0.994408
80,120	$8.958*10^{-3}$	0.980314
160,240	$4.564*10^{-3}$	0.972842

Table 5.4: Error convergence for p variable

It can be concluded from the results of error convergence in Table 5.1, Table 5.2, Table 5.3 and Table 5.4 that the logarithms of the quotients of consecutive error $log_2\left(\frac{E_D(\Delta)_{n-1}}{E_D(\Delta)_n}\right)$ is nearly equal to 1.The momentum and Poisson equation are discretized using numerical schemes of different orders . The diffusive terms are discretized using second order central differencing scheme, while the convective terms are discretized according to the convective numerical scheme used. In this case upwind scheme is used for discretizing convective terms which are of order 1.From the results, we can deduce that the error in the convective terms predominate over the others as the logarithms of the quotients of consecutive error is approaching 1 which is equal to the order of upwind scheme.

5.1.2 Lid Driven cavity

The objective of comparing our results with the benchmark solution of the driven cavity case is to ensure that continuity and Navier-Stokes equations for incompressible flow have been modelled correctly in our code.

5.1.2.1 Problem description

The problem considers incompressible flow in square cavity with upper wall moving with velocity u while other walls have no-slip tangential and zero normal velocity boundary condition as shown in Figure 3.1.

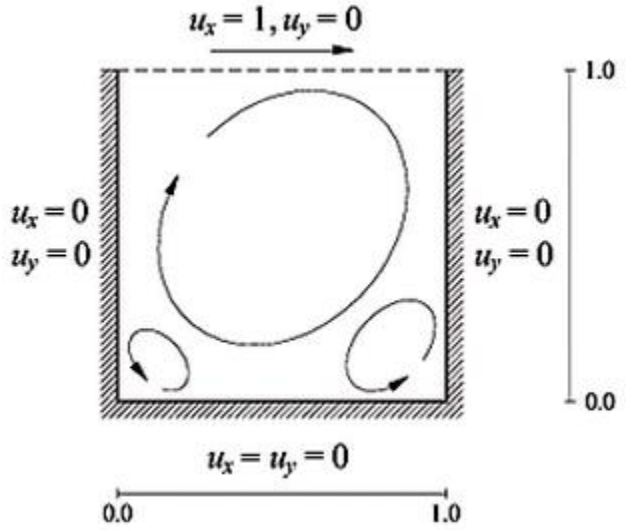

Table 5.5: Driven cavity problem description [16]

5.1.2.2 Boundary conditions

The upper wall has a uniform velocity in x-direction (u =1 m/s) and zero velocity component in the normal direction (v =0 m/s), while the other walls has zero tangential and normal velocity components (u=0 m/s & v=0 m/s).

For pressure boundary conditions, zero pressure gradients in the normal direction are assumed for all the walls $\left(\frac{\partial p}{\partial n} = 0\right)$. As the Poisson equation is solved by TDMA solver, so it will have infinite number of solutions with the zero gradients boundary condition for all

the walls. In order to avoid this problem, the pressure is set to fixed value at one control volume in the problem domain.

5.1.2.3 Results

In this section, we will compare our numerical results with the benchmark solution [17] for different Reynold numbers (100,400,3200,5000,7200). The benchmark solution is presented by the values of horizontal velocity component (u) along vertical axis passing through geometric center of cavity and vertical velocity component (v) along horizontal axis passing through the geometric center of the cavity.

First, we will compare our numerical result at Reynold number 400 using different numerical schemes for the convective terms to benchmark solution. The numerical schemes used for convective terms are upwind, hybrid, central and smart scheme. The results using different scheme are compared to the benchmark solution as shown in Figure 5.2 and Figure 5.3.The mesh size used in our simulation is 50*50 control volume. From the figures we can conclude that both central and smart schemes give quite identical results to benchmark solution. If we compare smart and central scheme results, we can deduce that smart is better and the reason is that its accuracy is between second and fourth order compared to central scheme which is of second order.

As smart scheme provides results with the smallest error compared to benchmark solution, so smart scheme will be used for comparing our results for different Reynold numbers .A mesh size of 150*150 control volume is used. The results are compared with reference solution from Figure 5.2 to Figure 5.13.The streamlines for different Reynold numbers are shown in Figure 5.14 to Figure 5.18.

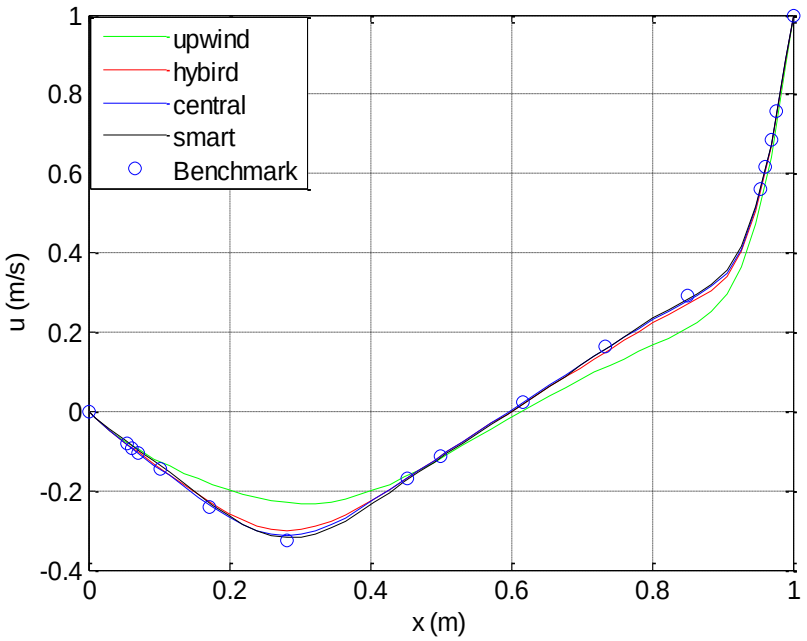

Figure 5.2: Results of u-velocity along the vertical axis passing through geometric centre of cavity Re=400 (50*50 CV)

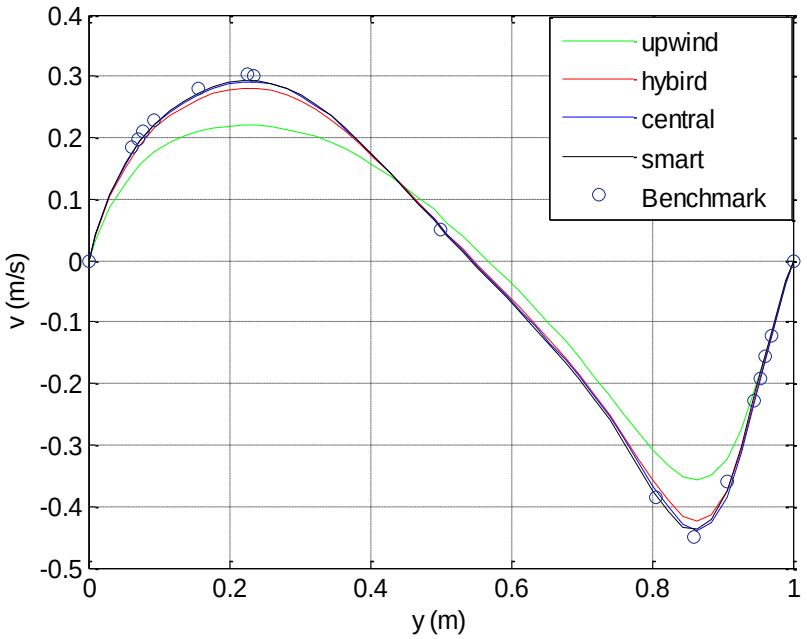

Figure 5.3: Results of v-velocity along the horizontal axis passing through geometric centre of cavity Re=400 (50*50 CV)

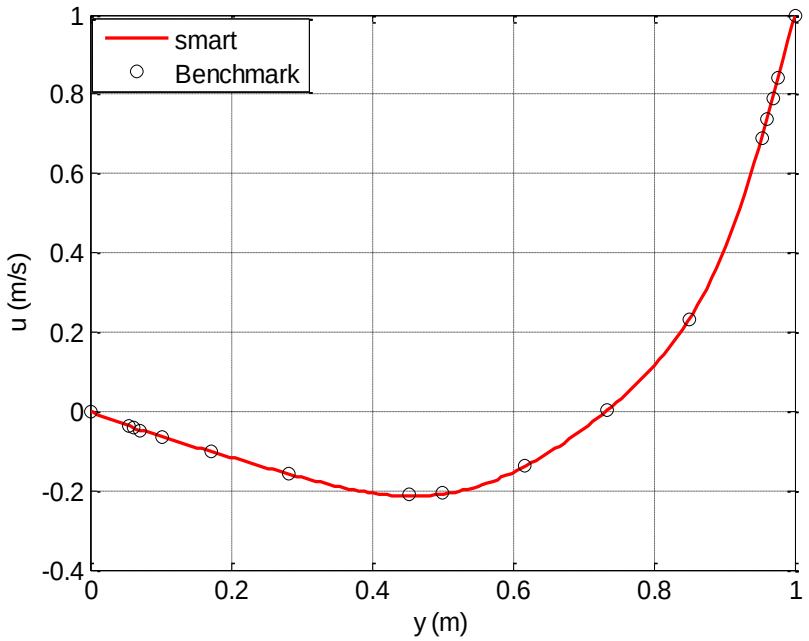

Figure 5.4: Results of u-velocity along the horizontal axis passing through geometric centre of cavity Re=100 (150*150 CV)

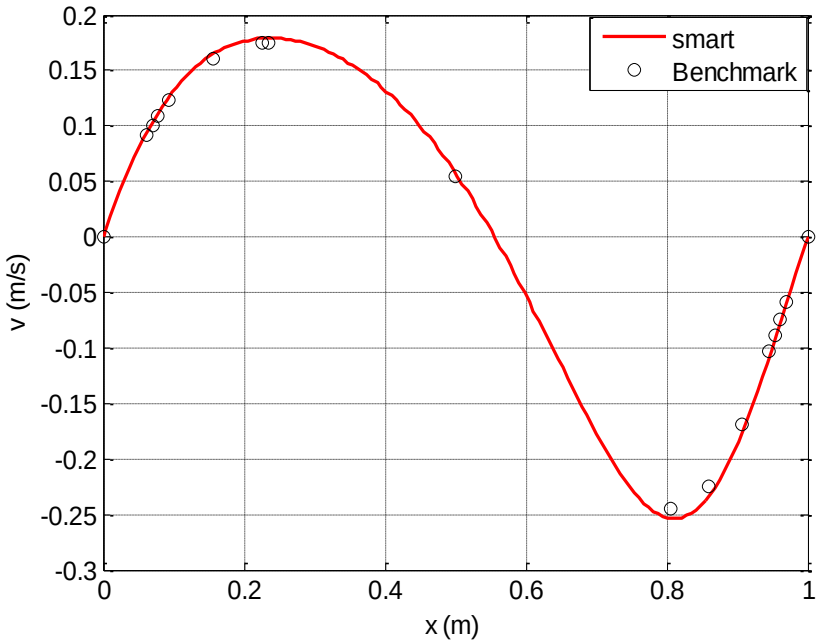

Figure 5.5: Results of v-velocity along the horizontal axis passing through geometric centre of cavity Re=100 (150*150 CV)

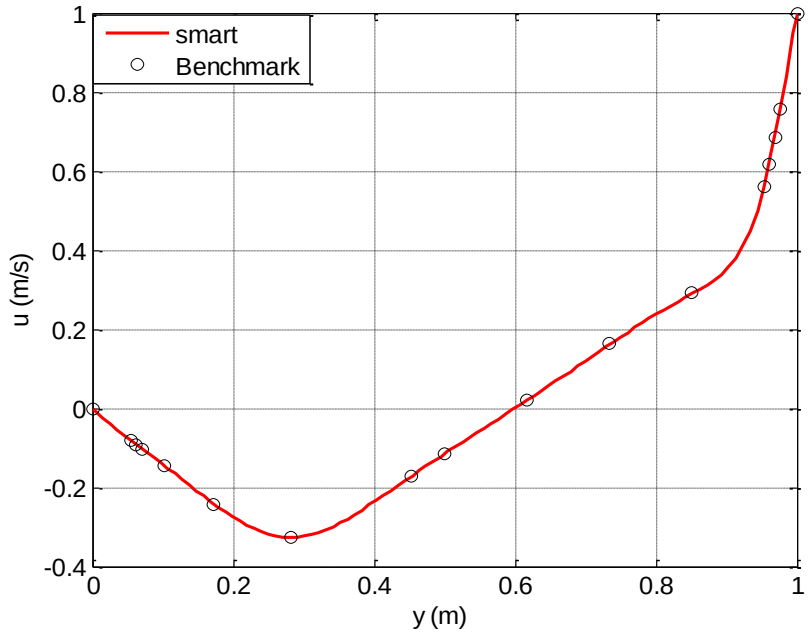

Figure 5.6: Results of u-velocity along the horizontal axis passing through geometric centre of cavity Re=400 (150*150 CV)

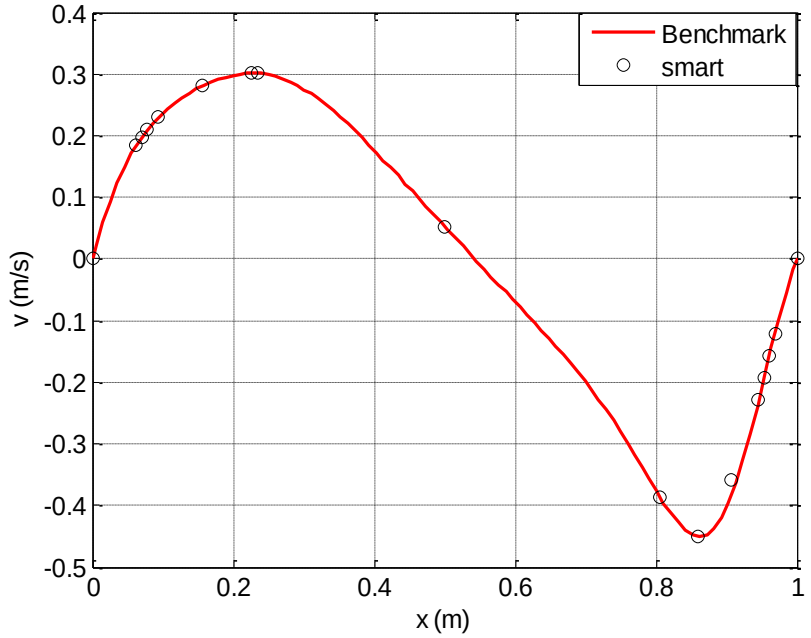

Figure 5.7: Results of v-velocity along the horizontal axis passing through geometric centre of cavity Re=400 (150*150 CV)

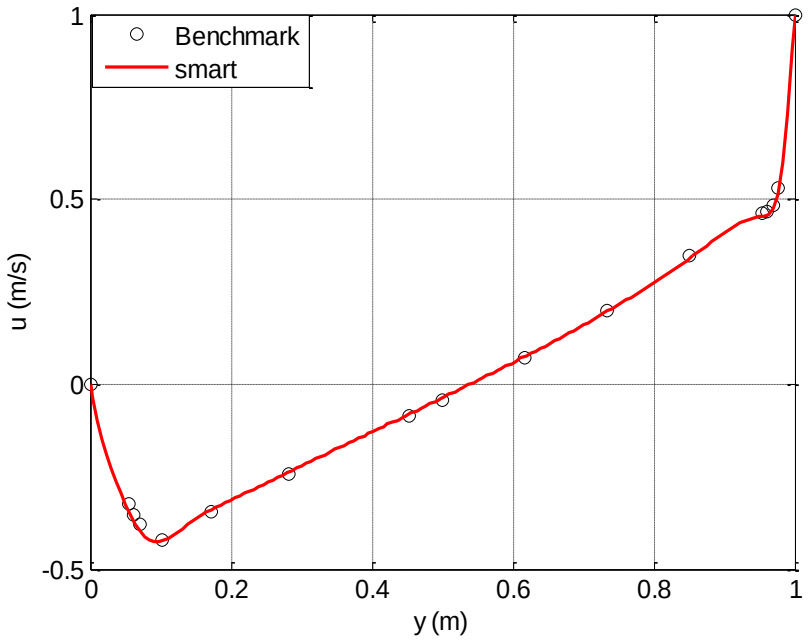

Figure 5.8: Results of u-velocity along the horizontal axis passing through geometric centre of cavity Re=3200 (150*150 CV)

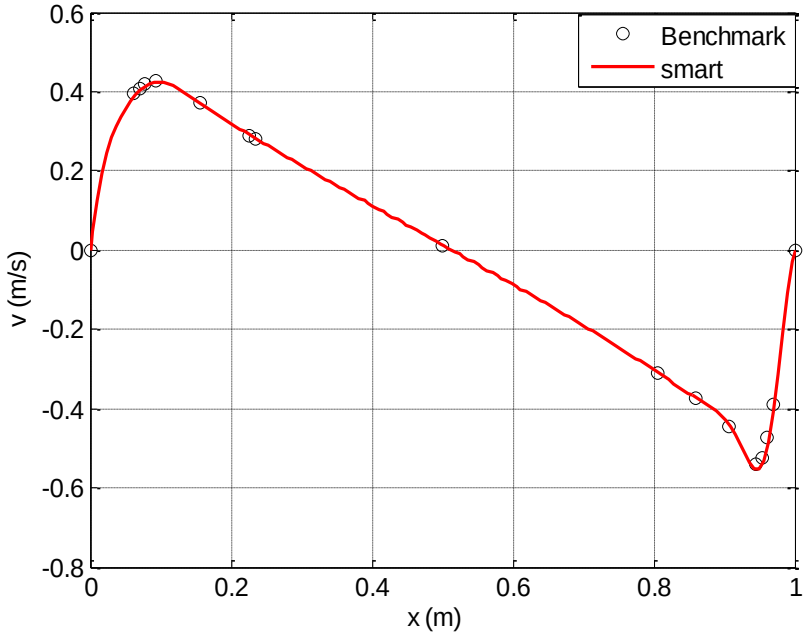

Figure 5.9: Results of v-velocity along the horizontal axis passing through geometric centre of cavity Re=3200 (150*150 CV)

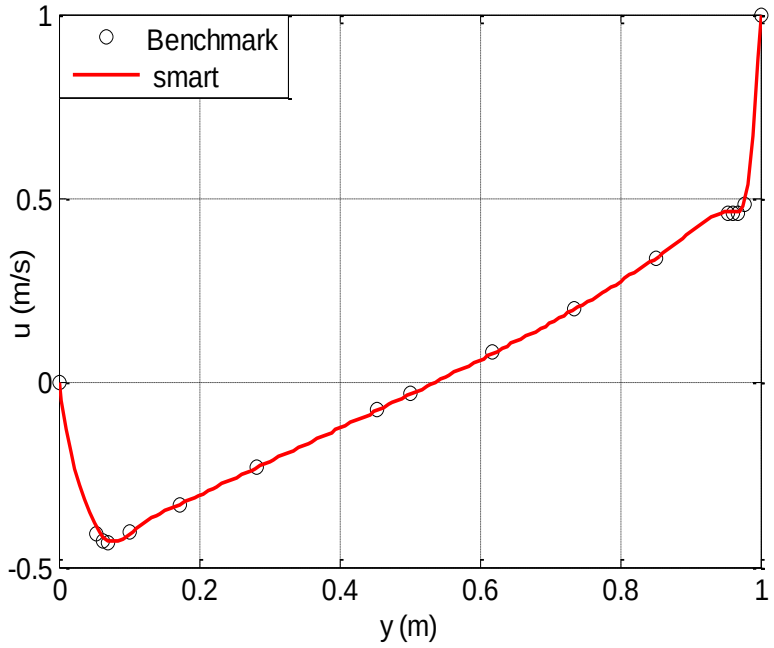

Figure 5.10: Results of u-velocity along the horizontal axis passing through geometric centre of cavity Re=5000 (150*150 CV)

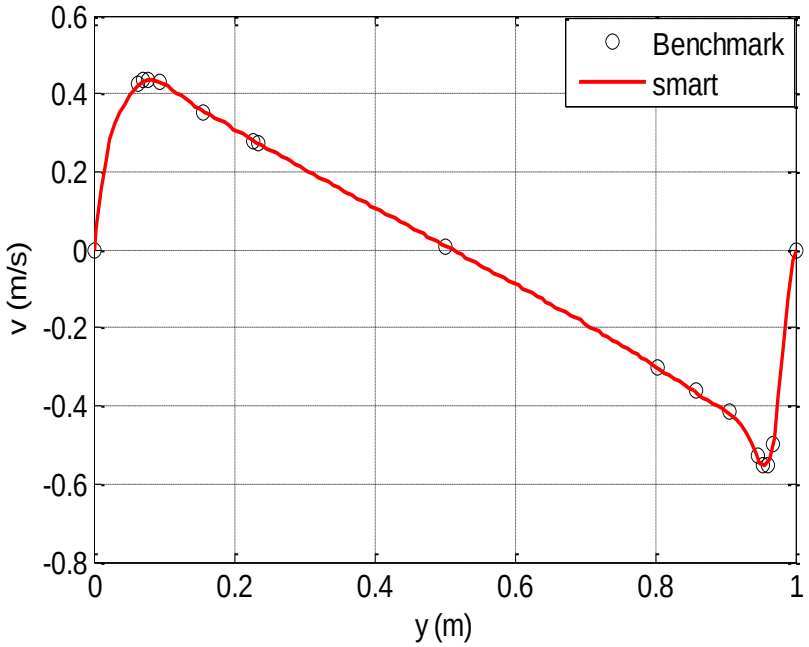

Figure 5.11: Results of v-velocity along the horizontal axis passing through geometric centre of cavity Re=5000 (150*150 CV)

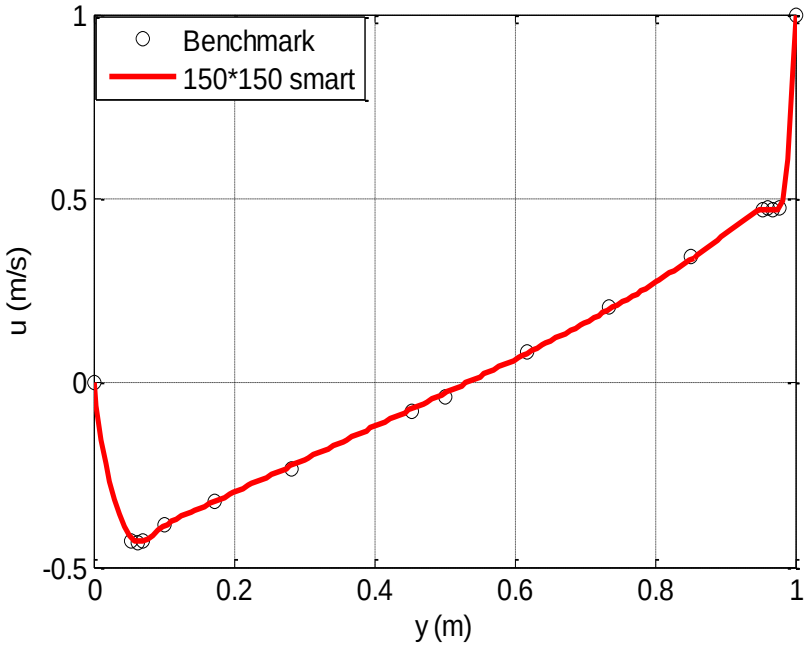

Figure 5.12: Results of u-velocity along the horizontal axis passing through geometric centre of cavity Re=7200 (150*150 CV)

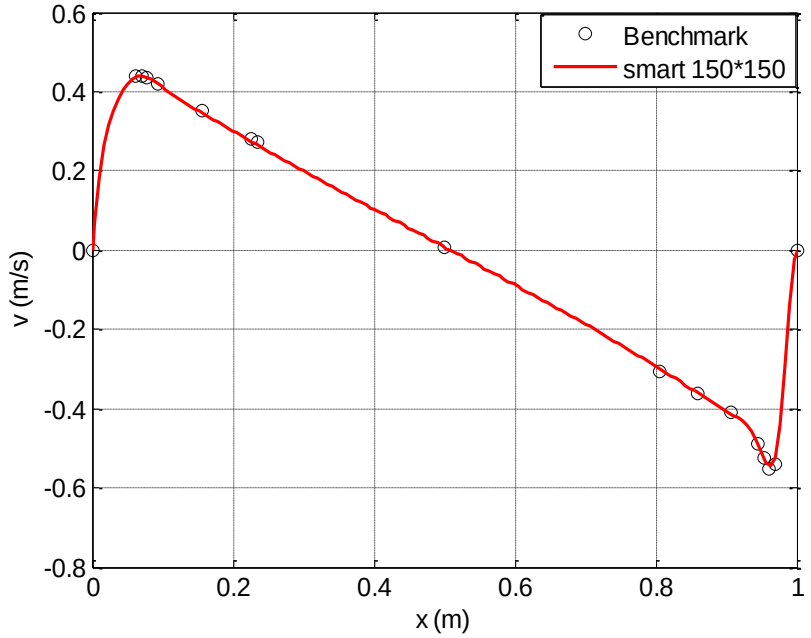

Figure 5.13 : Results of v-velocity along the horizontal axis passing through geometric centre of cavity Re=7200 (150*150 CV)

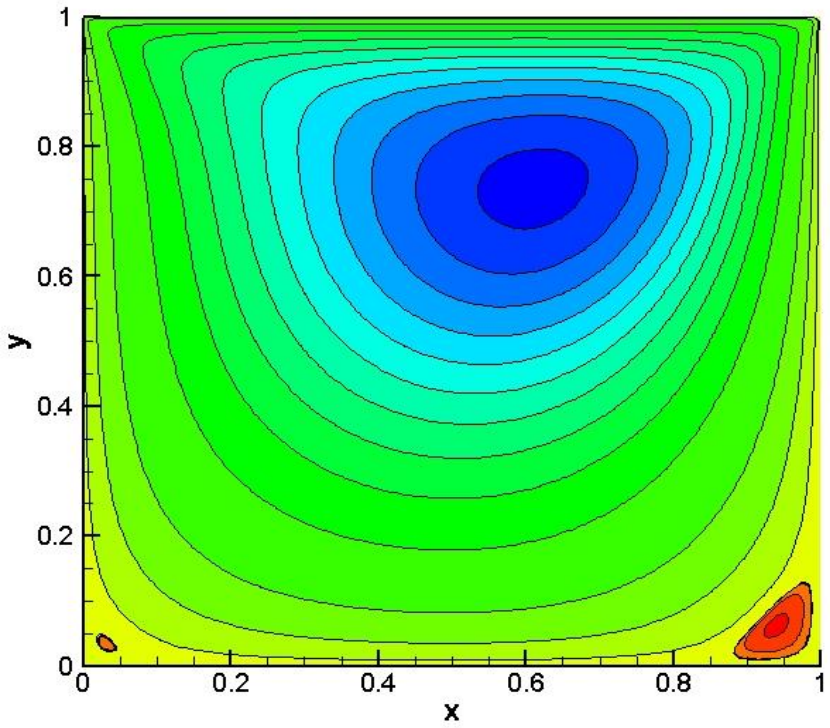

Figure 5.14: streamlines at Re=100

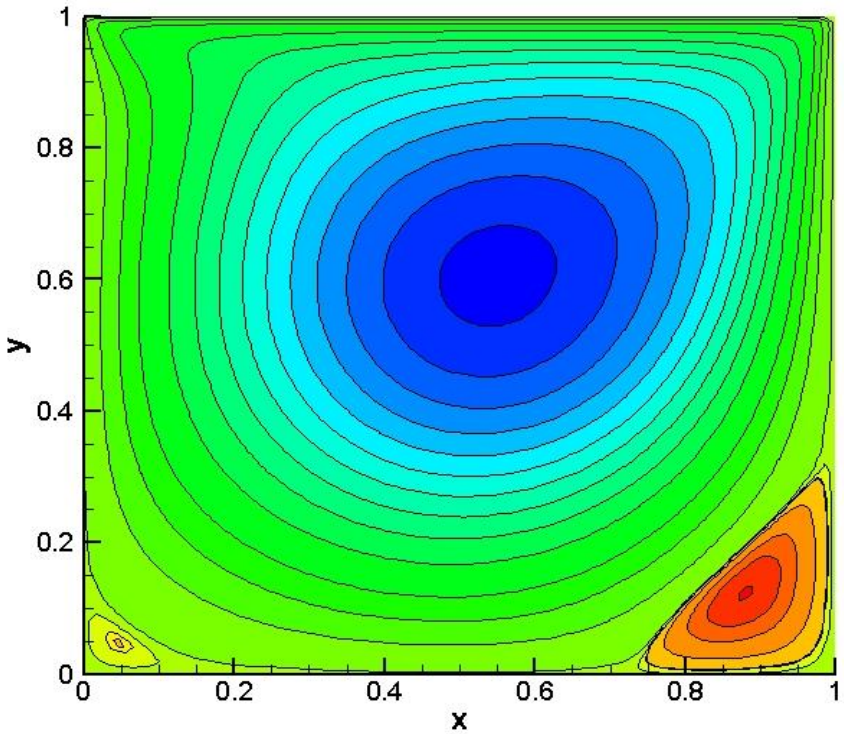

Figure 5.15: streamlines at Re=400

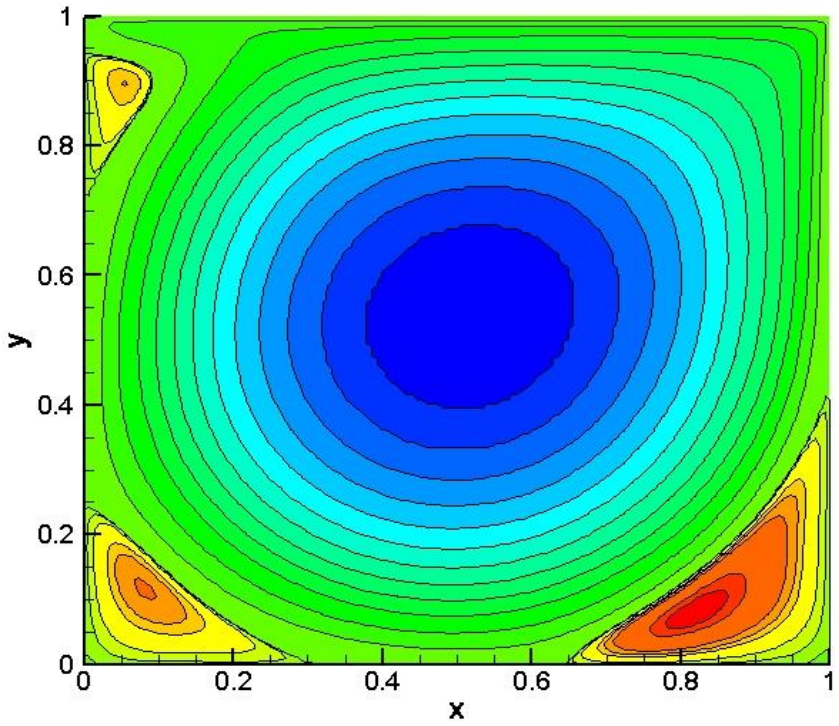

Figure 5.16: streamlines at Re=3200

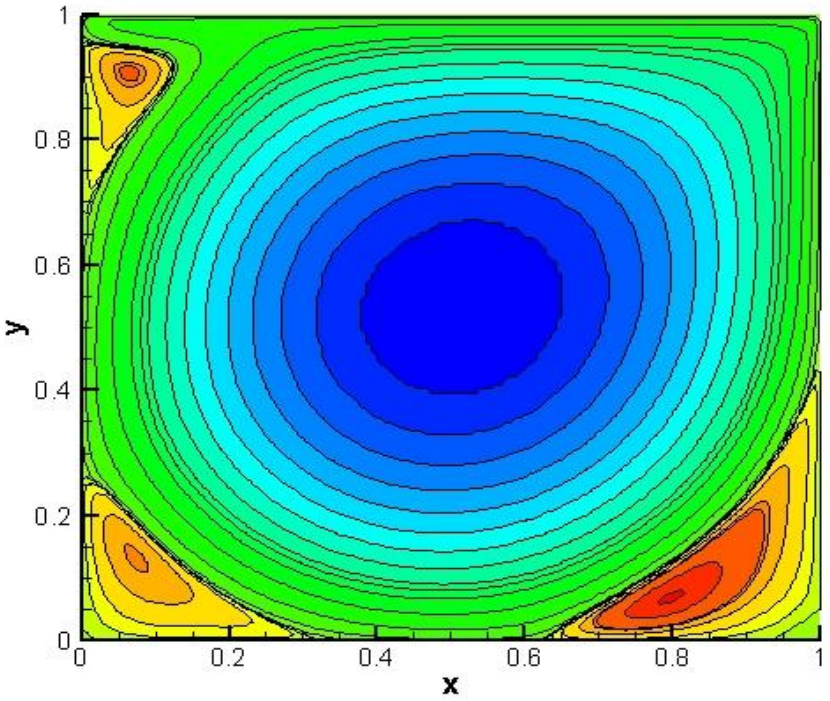

Figure 5.17: streamlines at Re=5000

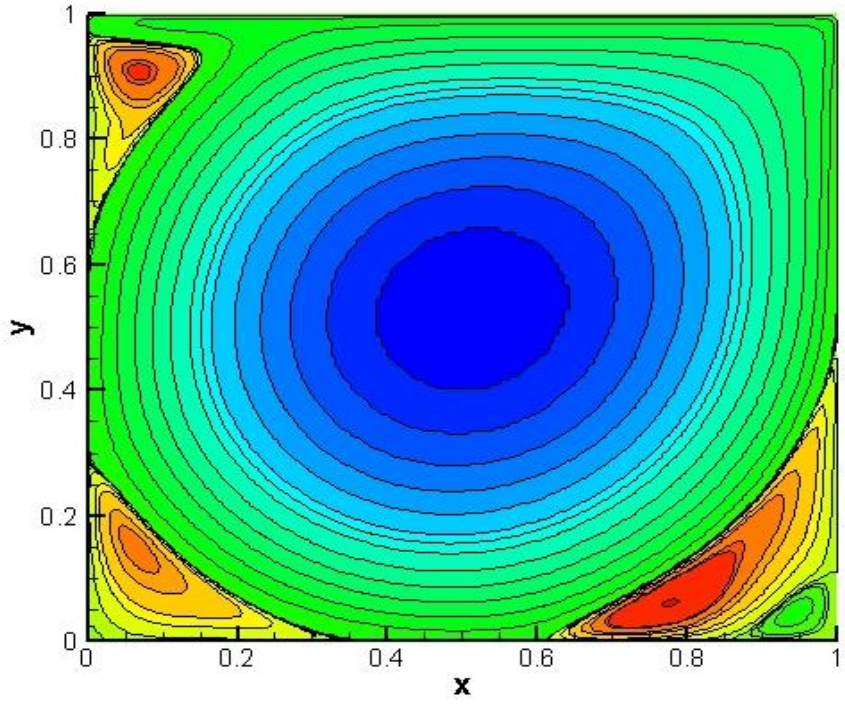

Figure 5.18: streamlines at Re=72000

The steady-state u and v profiles along the vertical and horizontal center lines showed a good agreement with benchmark solutions at different Reynold numbers. As Reynold number increases, a new secondary vortex appear in the top left side of the corner as shown in the streamlines drawing at Re=3200, 5000 and 7200 Figure 5.16 , Figure 5.17 & Figure 5.18.

5.1.3 Differentially heated cavity

The objective of comparing our results with the benchmark solution of the differentially heated cavity case is to ensure that continuity, Navier-Stokes equations and energy equations for incompressible flow have been modelled correctly in our code.

5.1.3.1 Problem description

The flow being considered is two dimensional incompressible flow of Prandtl number 0.71 in an upright square cavity of length L. Boussinesq approximation is describing continuity and momentum equations which assume that density variation is negligible in continuity equation and inertia terms in momentum equation, while density variation in buoyancy terms in momentum equation in the vertical direction cannot be neglected. Both velocity components are zero on the boundaries. The horizontal walls are insulated, and the vertical sides are at temperatures T_h and T_c. The solutions of this problem-velocities, temperature and rates of heat transfer-have been obtained at Rayleigh number of 10^3, 10^4, 10^5 and 10^6.

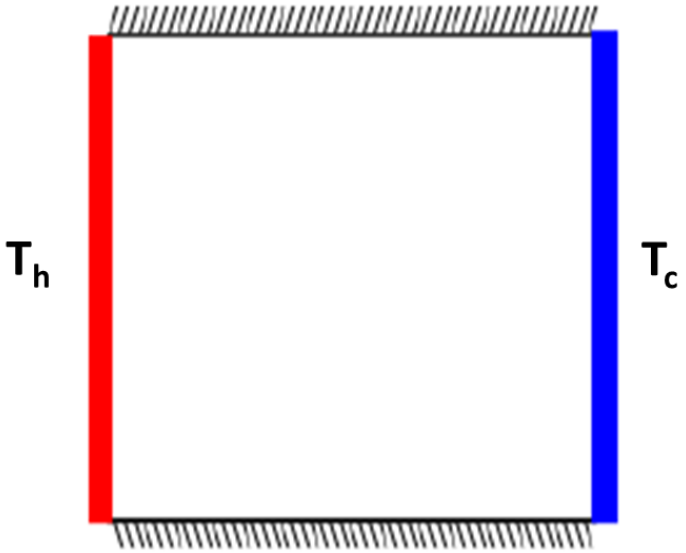

Figure 5.19: Differentially heated cavity problem description

5.1.3.2 Boundary conditions

The velocity components in tangential and normal direction are equal to zero for all the walls (u=v=0 m/s).

For pressure boundary conditions, zero pressure gradients in the normal direction are assumed for all the walls $\left(\frac{\partial p}{\partial n} = 0\right)$. As the Poisson equation is solved by TDMA solver, so it will have infinite number of solutions with the zero gradients boundary condition for all the walls. In order to avoid this problem, the pressure is set to fixed value at one control volume in the problem domain.

For temperature boundary conditions, top and bottom walls are insulated, so the temperature gradient in direction normal to wall is equal to zero $\left(\frac{\partial T}{\partial n} = 0\right)$.while the vertical walls temperatures are fixed to T_h and T_c.

5.1.3.3 Results

The results at different Rayleigh number 10^3, 10^4, 10^5 and 10^6 are calculated using different mesh sizes. For Rayleigh number 10^3 and10^4 uniform mesh of 50*50 is used as this mesh size was sufficient to get quite similar solution to benchmark solution [18, 19], while for higher Rayleigh 10^5 and 10^6 a finer concentrated mesh of 100*100 is utilized.

To compare our results with the benchmark solution, the following quantities are showed in Table 5.6 to Table 5.9

$\|\psi_{mid}\|$	The stream function at the mid-point of the cavity
$\|\psi\|_{max}$	The maximum absolute value of the stream function (together with its location): for Ra= 10^5 and 10^6**,** the maximum does not occur at the cavity mid-point
U_{max}	The maximum horizontal velocity on the vertical mid-plane of the cavity (together with its location)
w_{max}	The maximum vertical velocity on the horizontal mid-plane of the cavity (together with its location)
$NU_{1/2}$	The average Nusselt number on the vertical mid-plane of the cavity
NU_0	The average Nusselt number on the vertical boundary of the cavity at x = 0
NU_1	The average Nusselt number on the vertical boundary of the cavity at x = 1
NU_{max}	The maximum value of the local Nusselt number on the boundary at x = 0 (together with its location)
NU_{min}	The minimum value of the local Nusselt number on the boundary at x = 0 (together with its location).

$Ra=10^3$							
Mesh type		Uniform mesh		Concentrated mesh (k=2)			
No of control volumes		50*50		50*50		50*50	
Numerical scheme for convective terms		Central scheme		Central scheme		Smart scheme	
	Reference value	**Obtained value**	**Error (%)**	**Obtained value**	**Error (%)**	**Obtained value**	**Error (%)**
$\|\psi_{mid}\|$	1.174	1.1815	0.621	1.177	0.256	1.1765	**0.212**
$\|\psi\|_{max}$	----	----	----	----	----	----	----
X	-----	-----	-----	-----	-----	-----	-----
Z	-----	-----	-----	-----	-----	-----	-----
u_{max}	3.649	3.663	**0.685**	3.677	0.767	3.676	0.739
Z	0.813	0.8229	0.516	0.815	**0.344**	0.8158	**0.344**
w_{max}	3.697	3.721	**0.676**	3.727	0.811	3.726	**0.784**
X	0.178	0.1771	**2.696**	0.184	3.483	0.1842	3.483
$NU_{1/2}$	1.117	1.119	0.242	1.118	0.132	1.11809	**0.008**
NU_0	1.118	1.119	**0.172**	1.122	0.424	1.12286	0.524
NU_1	-----	1.119	-----	1.115	-----	1.11534	-----
NU_{max}	1.505	1.512	**0.525**	1.513	0.593	1.51391	0.592
Z	0.092	0.093	9.597	0.0964	**4.866**	0.0964	4.867
NU_{min}	0.692	0.689	0.394	6.931	**0.171**	0.693	0.194
Z	1	1	0	1	0	1	0

Table 5.6: Comparing results at $Ra=10^3$

$Ra=10^4$			
Mesh type		Uniform mesh	
No of control volumes		50*50	
Numerical scheme for convective terms		Central scheme	
	Reference value	**Obtained results**	**Error (%)**
$\|\psi_{mid}\|$	5.071	5.064	0.138
$\|\psi\|_{max}$	-----	-----	-----
X, Z	------	-----	-----
U_{max}	16.178	16.14	0.234
Z	0.823	0.8229	0.012
w_{max}	19.617	19.6	0.086
X	0.119	0.1146	3.697
$NU_{1/2}$	2.243	2.25	0.312
NU_0	2.238	2.25	0.536
NU_1	-----	2.25	-----

NU_{max}	3.528	3.5571	0.824
Z	0.143	0.135	5.594
NU_{min}	0.586	0.5819	0.699
Z	1	1	0

Table 5.7: Comparing results at $Ra=10^4$

$Ra=10^5$					
Mesh type		Uniform mesh		Uniform mesh	
Mesh size		50*50		100*100	
Numerical scheme for convective terms		Central scheme		Central scheme	
	Reference values	**Obtained values**	**Error (%)**	**Obtained values**	**Error (%)**
$\|\psi_{mid}\|$	9.111	9.111	0	9.1135	0.0274
$\|\psi\|_{max}$	9.612	9.617	0.052	9.617	0
X	0.285	0.2917	2.35	0.285	0
Z	0.601	0.5938	1.212	0.5969	0.6
U_{max}	34.73	34.44	0.835	34.68	0.14
z	0.855	0.8646	1.122	0.852	0.35
w_{max}	68.59	67.72	1.2684	68.57	0.0291
x	0.066	0.07292	10.484	0.066	0
$NU_{1/2}$	4.519	4.538	0.420	4.52545	0.14
NU_0	4.519	4.538	0.420	4.52515	0.136
NU_1	-----	4.539	-----	4.52507	-----
NU_{max}	7.717	7.9795	3.401	7.7837	0.864
Z	0.081	0.0729	10	0.0765	5.55
NU_{min}	0.729	0.7124	2.277	0.724123	0.669
Z	1	1	0	1	0

Table 5.8: Comparing results at $Ra=10^5$

$Ra=10^6$					
Mesh type		Concentrated mesh (k=2)			
Mesh size		50*50		100*100	
Numerical scheme for convective terms		Central scheme		Central scheme	
	Reference value	**Obtained values**	**Error (%)**	**Obtained values**	**Error (%)**
$\|\psi_{mid}\|$	16.32	16.345	0.153186	16.38	0.368
$\|\psi\|_{max}$	16.750	16.81	0.358209	16.82	0.418
X	0.151	0.1461	3.4437	0.1509	0.066
Z	0.547	0.5216	4.64351	0.5317	2.797
U_{max}	64.63	64.32	0.4796	64.78	0.232
z	0.850	0.8648	1.741176	0.8547	0.553
w_{max}	219.36	220.5	0.52	220.395	0.472
x	0.0379	0.03475	8.311346	0.0355	6.095
$NU_{1/2}$	8.799	8.82753	0.324	8.8255	0.302
NU_0	8.817	8.82956	0.142452	8.8345	0.199
NU_1	-----	8.82583	-----	8.8173	-----
NU_{max}	17.925	17.6515	1.525802	17.5791	1.930
Z	0.0378	0.0347515	8.064815	0.03993	5.656
NU_{min}	0.989	0.988328	0.067947	0.9833	0.572
Z	1	1	0	0	0

Table 5.9: Comparing results at $Ra=10^6$

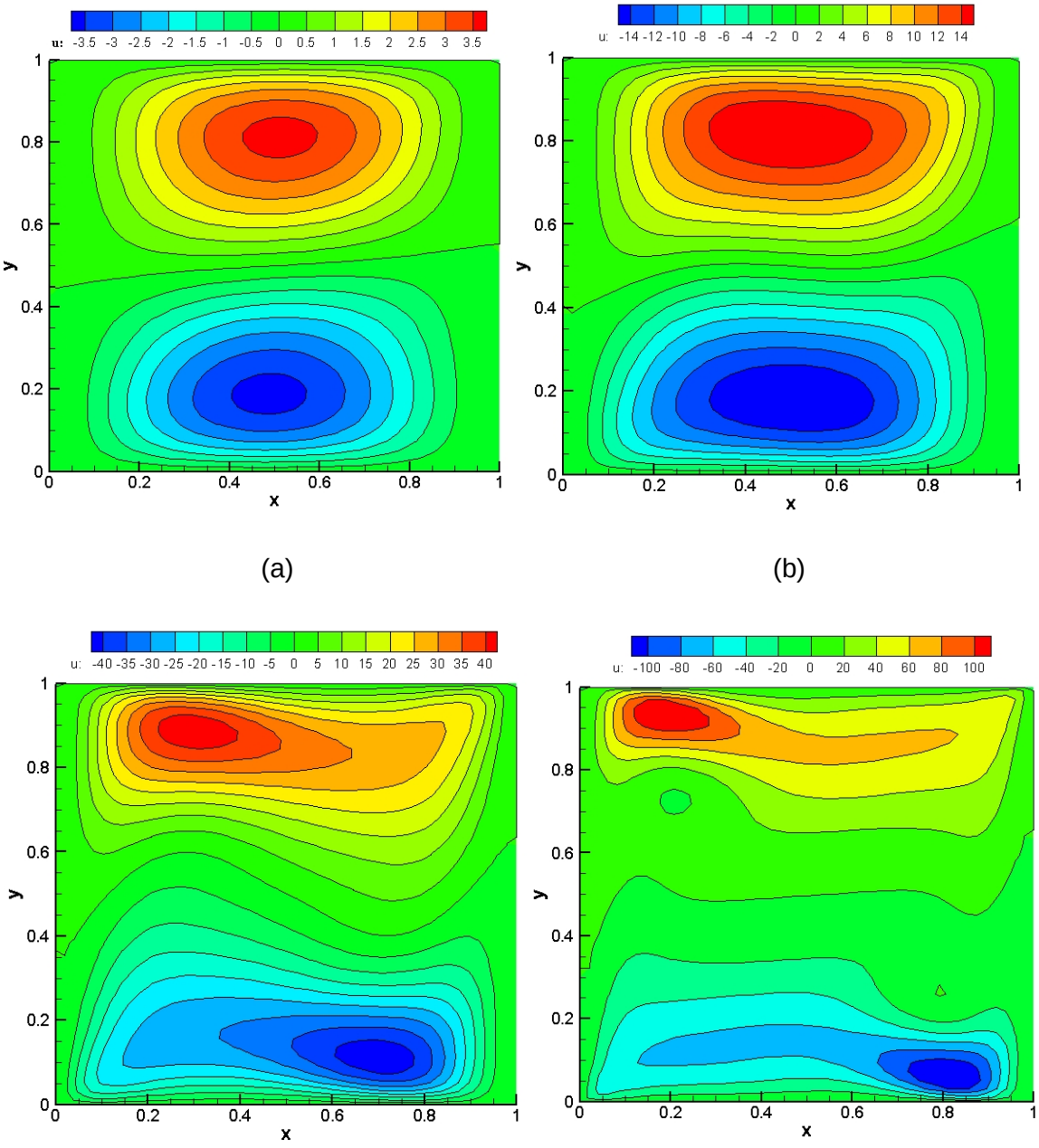

Figure 5.20: Contour maps of horizontal velocity u

(a)Re=10^3, (b) Re=10^4, (c) Re=10^5, (d) Re=10^6

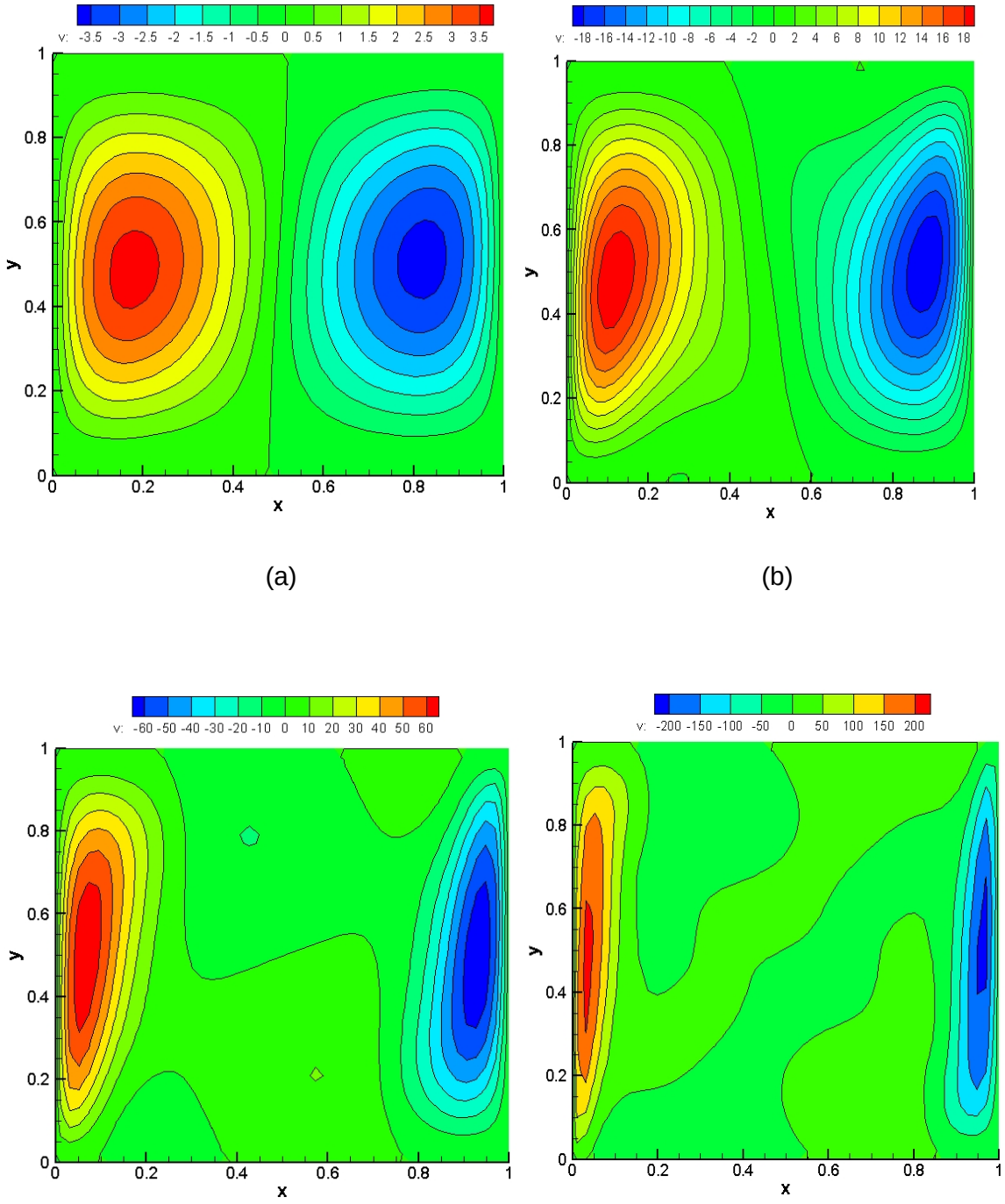

Figure 5.21: Contour maps of horizontal velocity v

(a)Re=10^3, (b) Re=10^4, (c) Re=10^5, (d) Re=10^6

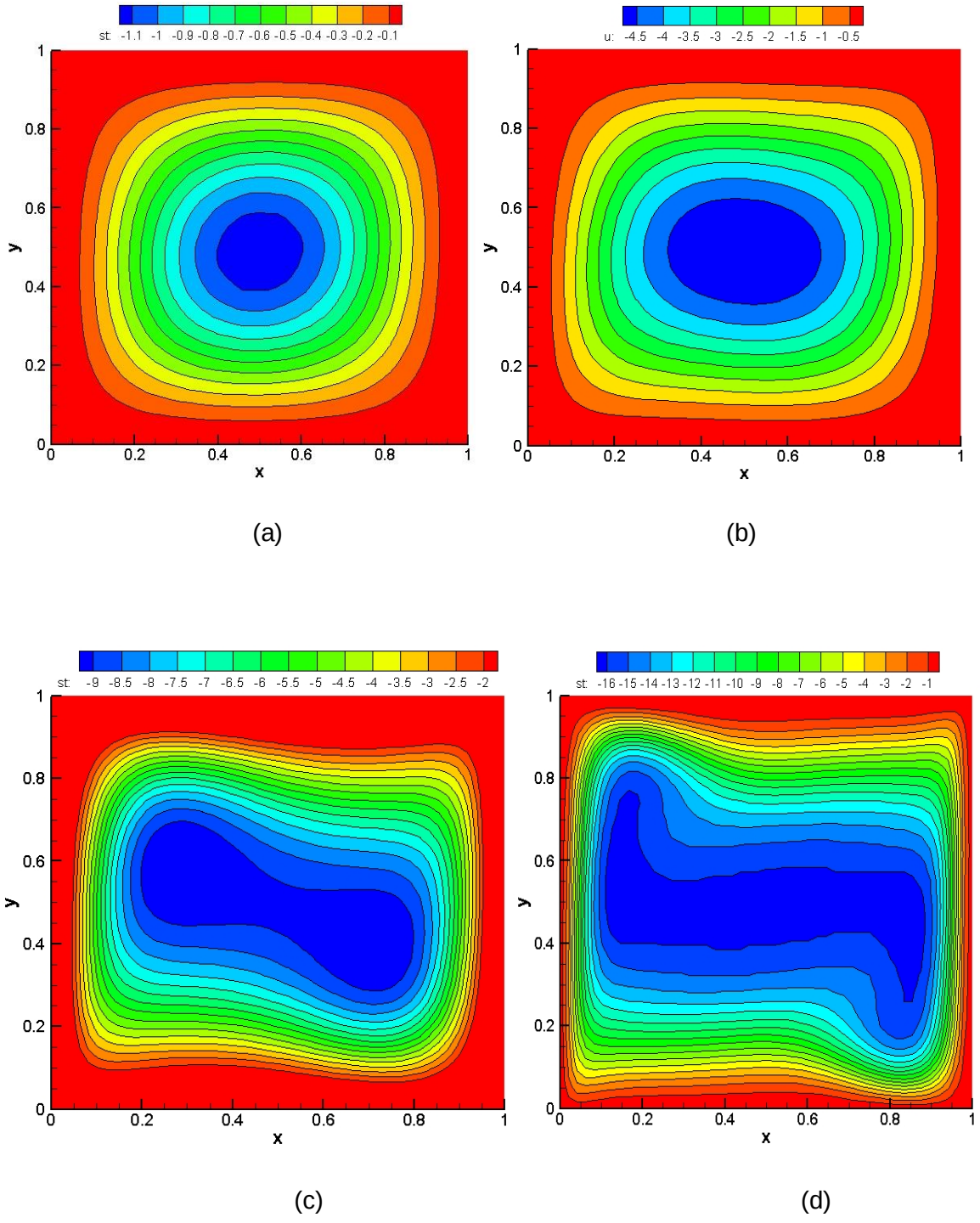

Figure 5.22: contour maps of streamline function ψ

(a)Re=10^3, (b) Re=10^4, (c) Re=10^5, (d) Re=10^6

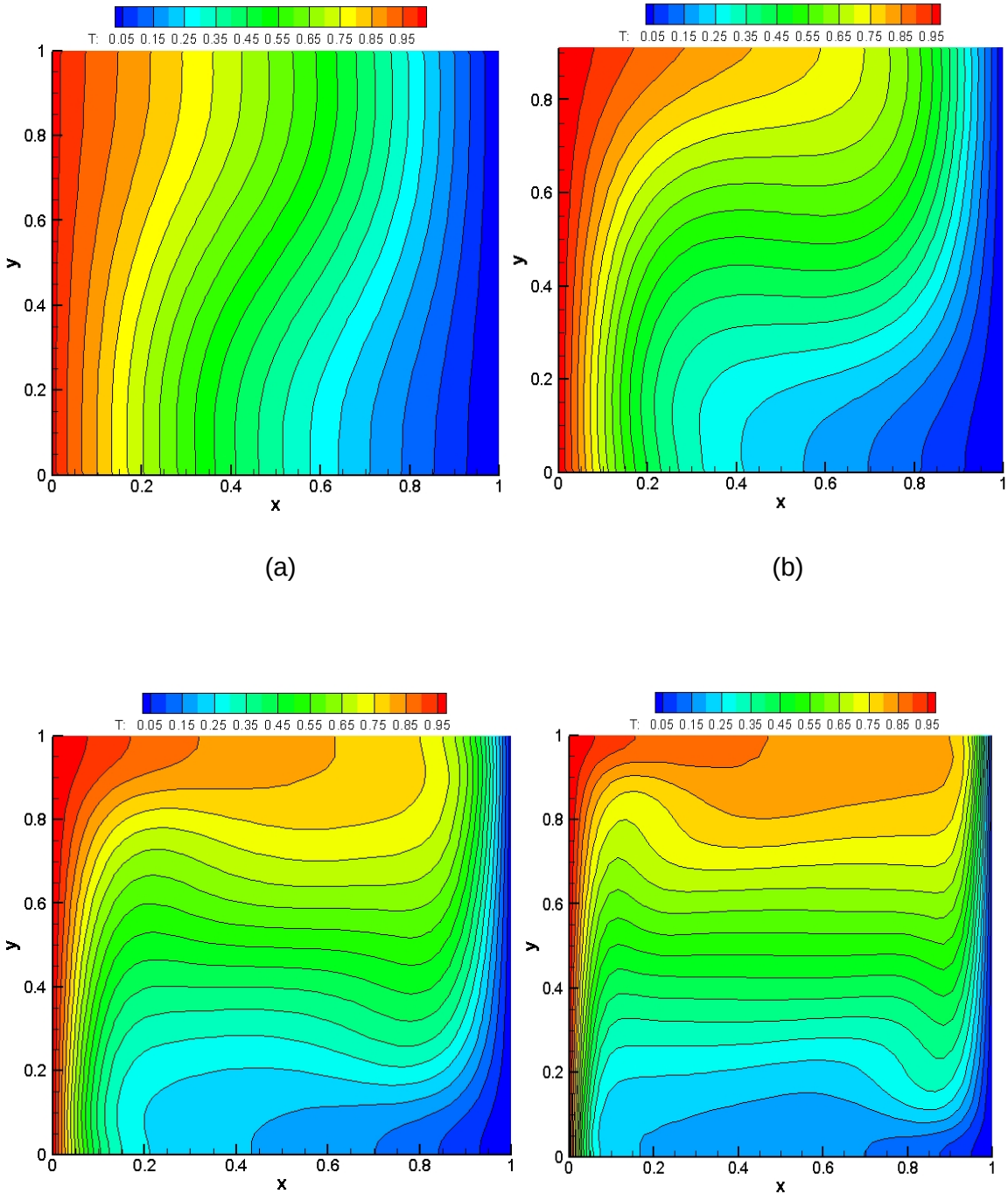

Figure 5.23: Contour maps of Temperature T

(a)Re=10^3, (b) Re=10^4, (c) Re=10^5, (d) Re=10^6

The result for Ra=10^3 and 10^4 showed that mesh of 50*50 gives a solutions with error percent less than 1% for all calculated quantities but error percent was higher for location of these quantities. Both uniform mesh and concentrated mesh are tested and results showed that both give good results for the calculated quantity while the concentrated mesh gives better results for the location of these quantities especially for that calculated at boundaries as more control volumes are concentrated in these regions. Comparing the results using smart scheme to central scheme for convective term, results do not show considerable improvement.

For Ra=10^5 and 10^6, a finer mesh of 100*100 is used to get error percent less than 1% for the calculated quantities. At high Rayleigh number the velocity and temperature gradients near the walls are high so concentrated mesh near the walls gives more precise results compared to uniform mesh.

5.2 Compressible flow with low Mach number

Compressible flow program code will be checked by comparing its results with benchmark solution for differentially heated cavity with large temperature difference.

5.2.1 Differentially heated cavity with high temperature difference

The objective of comparing our results with the benchmark solution of the differentially heated cavity case is to ensure that continuity, Navier-Stokes equations and energy equations for compressible flow with low Mach number have been modelled correctly in our code.

5.2.1.1 Problem description

Flow of compressible fluid is considered in a differentially heated square cavity of length L in which a large temperature difference is applied to the vertical walls (ΔT=720 ^{0}C) while horizontal walls are thermally insulated. The left wall is at high temperature (T_h) and the right is at low temperature (T_c).The temperatures difference can be represented by dimensionless parameter ϵ

$$\epsilon = \frac{T_h - T_c}{T_0} \qquad \textbf{(5.12)}$$

Where,

T_0: Reference temperature

The fluid filling the cavity is air of constant prandtl number of 0.71 and constant specific heat (C_p=1004.5 KJ/kg.k) neglecting temperature influence on C_p while the dynamic viscosity is calculated using Sutherland's law equation (5.13) and thermal conductivity is calculated from equation (5.14)

$$\frac{\mu(T)}{\mu^*} = \left(\frac{T}{T^*}\right)^{\frac{3}{2}} \frac{T^* + S}{T + S} \quad \textbf{(5.13)}$$

$$k(T) = \frac{\mu(T) C_p}{Pr} \quad \textbf{(5.14)}$$

Where,

T^*: Reference temperature $(T^* = 273\ k)$

μ^*: Reference viscosity $(\mu^* = 1.68 * 10^{-5} kg/m.s)$

S: Sutherland constant $(\mathrm{S} = 110.5\ \mathrm{K})$

The case is defined by Rayleigh number, value of ∈ , fluid properties ,cavity dimensions , initial mass content in the cavity and reference state: p_0=101.325 Kpa,T_0= 600K and $\rho_0 = \frac{p_0}{R\,T_0}$.

5.2.1.2 Boundary conditions

The same boundary conditions are the same conditions mentioned in section (7.1.3.2) for differentially heated cavity for incompressible flow.

5.2.1.3 Results

We compare our results for Ra=10^5 and 10^6 and Ɛ=0.6 with the benchmark solution[20]. The benchmark solution was computed on 1024*1024 stretched mesh. In our result, different uniform mesh sized is used and error convergence of different dimensionless quantities is computed for every mesh size. Mesh sizes tested are 64*64, 128*128 and 256*256. Table 5.10 and Table 5.11 show values for different dimensionless parameter at Ra=10^5 and 10^6 respectively and Ɛ=0.6.The parameters are:

NU_{max}	Maximum local Nussult number at wall plane and its location
NU_{min}	Minimum local Nussult number at wall plane and its location
NU_{mid}	Local Nussult number at mid-point of wall plane (y=0.5)

$\overline{NU}$	Average Nussult number over wall plane
p/p_0	Ratio between thermodynamic pressure (p) and its initial value (p_0)
V_{max} (y=0.5)	The maximum vertical velocity on the vertical mid-plane of the cavity (together with its location)
V_{min} (y=0.5)	The minimum vertical velocity on the vertical mid-plane of the cavity (together with its location)
U_{max} (x=0.5)	The maximum horizontal velocity on the horizontal mid-plane of the cavity (together with its location)
U_{min} (x=0.5)	The minimum horizontal velocity on the horizontal mid-plane of the cavity (together with its location)
ψ_{mid}	Streamline function at the centre of the cavity
ψ_{max}	The maximum value for streamline function and its location

Comparing the results for different mesh sizes with benchmark reference solution, we can conclude that error percentage decreases with increasing mesh size and results show a good agreement with reference solution. For the finest mesh with (256*256) nodes, error percentages for all variables are less than 1%, while error percentages of the locations for these variables have higher error but still less than 2.5%.

The contour maps for Ra=10^5 and 10^6 with Ɛ=0.6 for horizontal velocity component (u), vertical velocity component (v), streamline function (**ψ)** and temperature (T) are shown in Figure 5.24 , Figure 5.25, Figure 5.26 & Figure 5.27 respectively

variable	64*64	Error (%)	128*128	Error (%)	256*256	Error (%)	Reference values
Left							
NU_{max}	8.91611	3.183775	8.70537	0.74493	8.63057	-0.1207	8.641
location	0.07258	-3.73926	0.075397	-0.00424	0.076772	1.81923	0.0754
NU_{min}	0.85281	0.567689	0.849215	0.14327	0.846921	-0.1272	0.848
location	1	0	1	0	1	0	1
NU_{mid}	4.225	0.523436	4.20896	0.14180	4.19597	-0.1672	4.203
$\overline{NU}$	4.54612	1.475893	4.49597	0.35647	4.47346	-0.1459	4.48
Right							
NU_{max}	7.18226	3.595269	7.03298	1.44208	6.96903	0.51968	6.933
location	0.94354	1.304273	0.940476	0.97444	0.935039	0.39070	0.9314
NU_{min}	0.49090	-4.67864	0.509007	-1.16369	0.515903	0.17534	0.515
location	0	0	0	0	0	0	0
NU_{mid}	4.79075	1.070675	4.74754	0.15907	4.74921	0.19430	4.74
$\overline{NU}$	4.54743	1.505134	4.5	0.44642	4.49349	0.30111	4.48
p/p_0	0.919	-0.32106	0.9213	-0.07159	0.9229	0.10195	0.92196
V_{max} (y=0.5)	0.31804	0.454833	0.316932	0.10493	0.31624	-0.1136	0.3166
location	0.08871	-6.42437	0.09127	-3.72384	0.096457	1.74757	0.0948
V_{min} (y=0.5)	-0.29285	-0.35726	-0.29317	-0.24995	-0.29393	0.01041	-0.2939
location	0.95967	0.19597	0.956349	-0.15149	0.958661	0.08989	0.9578
U_{max} (x=0.5)	0.1953	0.359712	0.194884	0.146	0.194535	-0.0333	0.1946
location	0.83064	-0.68807	0.837302	0.10784	0.836614	0.02558	0.8364
U_{min} (x=0.5)	-0.1108	-0.22502	-0.11111	0.01214	-0.11152	0.38118	-0.1111
location	0.13709	-1.65208	0.138889	-0.36657	0.139764	0.26111	0.1394
ψ_{mid}	0.04104	0.30303	0.04094	0.04887	0.040931	0.02631	0.04092
ψ_{max}	0.04251	0.44896	0.042379	0.13837	0.042337	0.03948	0.04232
X	0.34677	-0.38093	0.345238	-0.82218	0.348425	0.09336	0.3481
Y	0.51612	0.199767	0.515873	0.15006	0.515748	0.12580	0.5151

Table 5.10: comparing results at $Ra=10^5$ and $\varepsilon=0.6$

variable	64*64	Error (%)	128*128	Error (%)	256*256	Error (%)	Reference values
Left							
NU_{max}	22.7675	12.3211	20.9027	3.12136	20.4054	0.66798	20.27
location	0.02419	-33.7164	0.035714	-2.1526	0.037402	2.47013	0.0365
NU_{min}	1.06608	-0.08622	1.07217	0.48453	1.06801	0.09465	1.067
location	1	0	1	0	1	0	1
NU_{mid}	7.454	-0.06703	7.48895	0.40152	7.46485	0.07842	7.459
$\overline{NU}$	8.9472	2.99516	8.78024	1.07332	8.70621	0.22113	8.687
Right							
NU max	15.3635	-1.002	16.0834	3.63683	15.7753	1.65152	15.519
location	0.95967	-0.81883	0.972222	0.47767	0.970472	0.29681	0.9676
NU min	0.67213	-11.3281	0.723573	-4.5418	0.749291	-1.1489	0.758
location	0	0	0	0	0	0	0
NU_{mid}	9.02605	4.310302	8.6916	0.63216	8.645595	0.09951	8.637
$\overline{NU}$	8.9481	3.00575	8.78283	1.10314	8.71814	0.35846	8.687
p/p_0	0.91927	-0.56464	0.92138	-0.3364	0.9239	-0.0638	0.92449
V_{max} (y=0.5)	0.32264	0.73185	0.3222	0.59319	0.320744	0.13863	0.3203
location	0.0565	5.12402	0.05159	-3.9292	0.05315	-1.0249	0.0537
V_{min} (y=0.5)	-0.2959	-1.38703	-0.29614	-1.3181	-0.29938	-0.2403	-0.3001
location	0.97580	0.02115	0.9802	0.47150	0.974409	-0.1220	0.9756
U_{max} (x=0.5)	0.11947	0.14501	0.12003	0.61190	0.119742	0.37034	0.1193
location	0.8468	-0.8547	0.8532	-0.1053	0.852362	-0.2034	0.8541
U_{min} (x=0.5)	-0.0779	-2.17097	-0.07948	-0.2985	-0.07998	0.3247	-0.07972
location	0.08871	-1.9779	0.09127	0.85082	0.088583	-2.1185	0.0905
ψ_{mid}	0.02223	0.63377	0.022189	0.44816	0.022139	0.22004	0.02209
ψ_{max}	0.02355	0.18502	0.02359	0.34028	0.023547	0.15614	0.02351
X	0.8629	-0.6791	0.869	0.02302	0.86811	-0.0794	0.8688
Y	0.4032	2.69994	0.3889	-0.9424	0.389764	-0.7223	0.3926

Table 5.11: comparing results at $Ra=10^6$ and $\varepsilon=0.6$

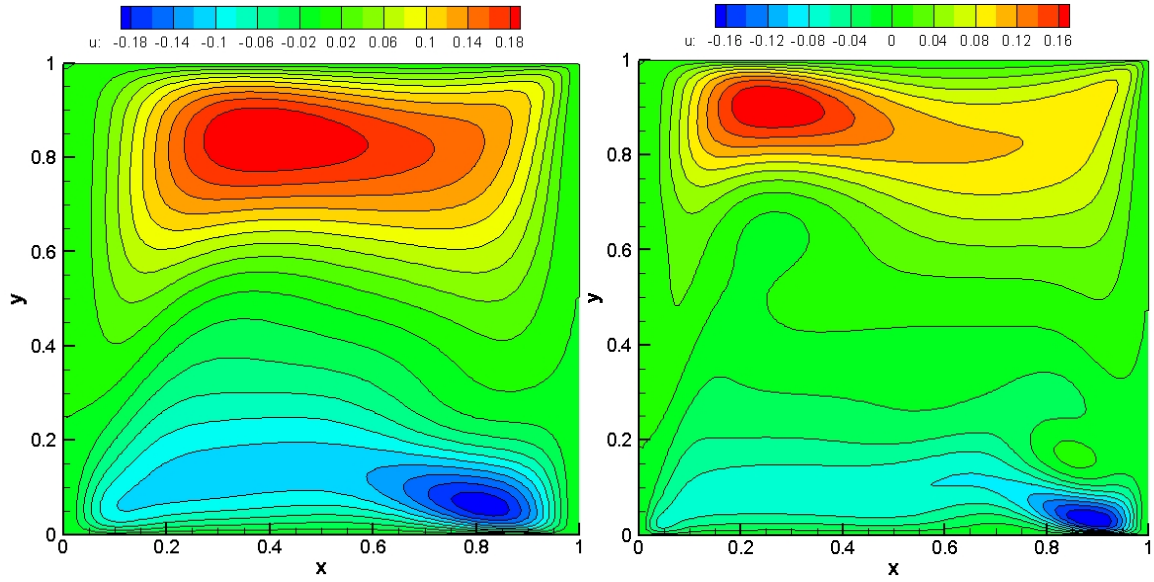

Figure 5.24: Contour maps of horizontal velocity u

(a) $Re=10^5$, (b) $Re=10^6$

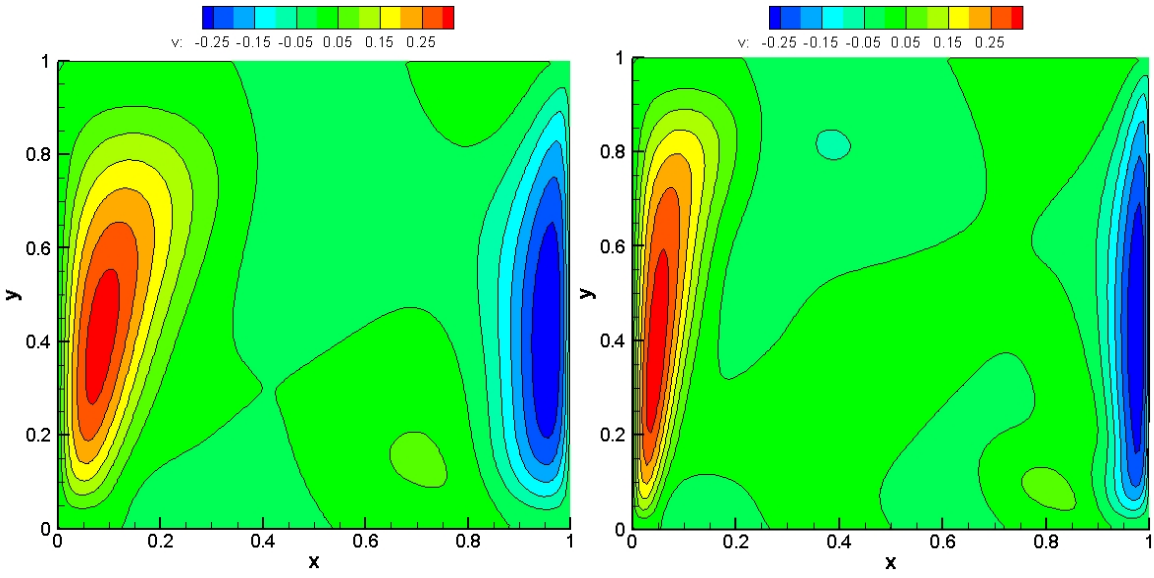

Figure 5.25 Contour maps of horizontal velocity v

(a) $Re=10^5$, (b) $Re=10^6$

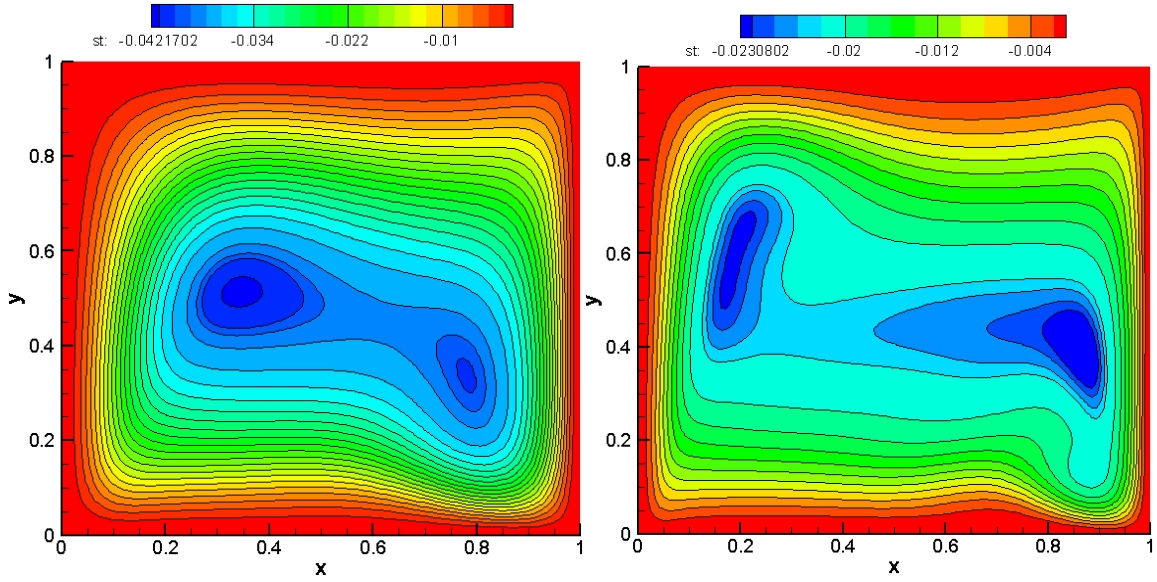

Figure 5.26: contour maps of streamline function ψ

(a)Re=10^5, (b) Re=10^6

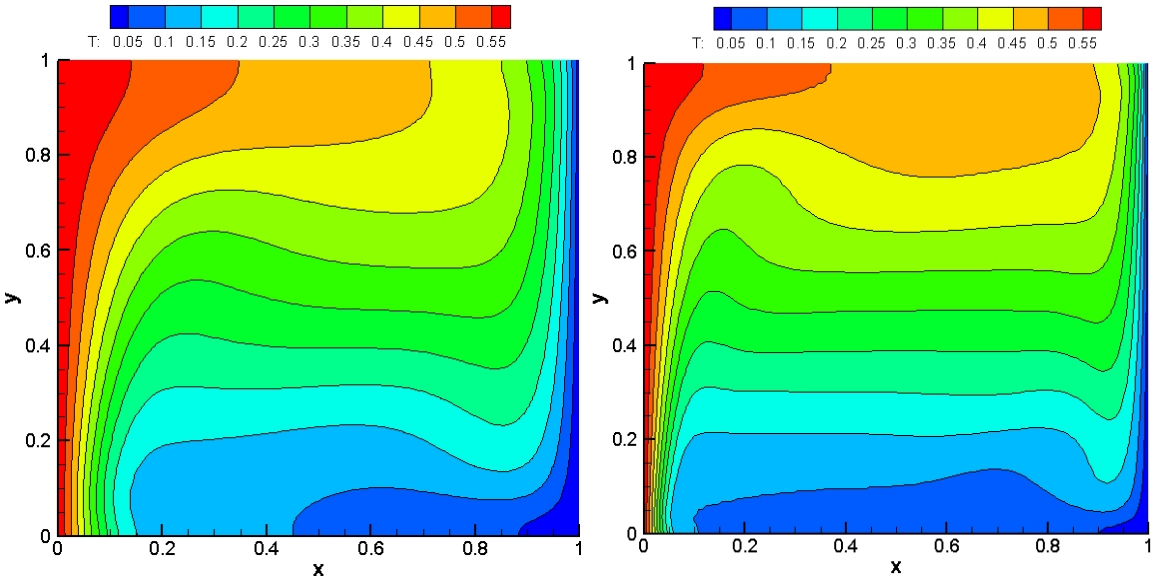

Figure 5.27: Contour maps of Temperature T

(a) Re=10^5, (b) Re=10^6

The verification process for our code using analytical solution and comparing results to highly accurate solution showed that our code is reliable and gives accurate results as the verification process using Method of manufactured solutions (MMS) showed the the logarithms of the quotients of consecutive error is nearly equal to the order of the scheme used for discretizing convective terms that are dominant over other terms and for comparison of our results with benchmark solutions, a good agreement between our results and benchmark solution are shown.

6 Case study: Modeling laminar diffusion flame using SCRS

Computational fluid dynamics (CFD) can be used for modelling combustion process. Combustion is defined as a chemical reaction of hydrocarbon fuels and oxidizer to form combustion products with the release of heat energy. It is one of the most important process in engineering include in various engineering applications: internal combustion engines, power station combustors, aero engines, gas turbine combustors, boilers, furnaces, and much other combustion equipment. Modelling of combustion process is governed by basic transport equation for fluid flow and heat transfer with additional models for combustion chemistry.

There are many types of combustion process that can be classified into: Gaseous fuel combustion, liquid fuel combustion, spray combustion, solid fuel combustion, and pulverized fuel combustion[4].The gaseous combustion is defined as a chemical reaction between fuel and oxidizer in the gas phase. The gaseous combustion is classified into: premixed combustion and non-premixed combustion. In premixed flame, the fuel is mixed with oxidizer before combustion process. The stoichiometry of the fuel and oxidizer mixture can be controlled by adjusting fuel to oxidizer ratio and flame temperature can be controlled by diluting the reactants by increasing inert gas (nitrogen) percent. Examples of premixed flames are spark ignition engines and Bunsen burner. While, in non-premixed flame gaseous fuel mixes with the oxidizer stream and at the same time combustion takes place at region with suitable conditions for combustion. It is also known as diffusion flame as fuel and oxidizer are introduced from separate streams, so they are mixed together by diffusion prior to combustion.

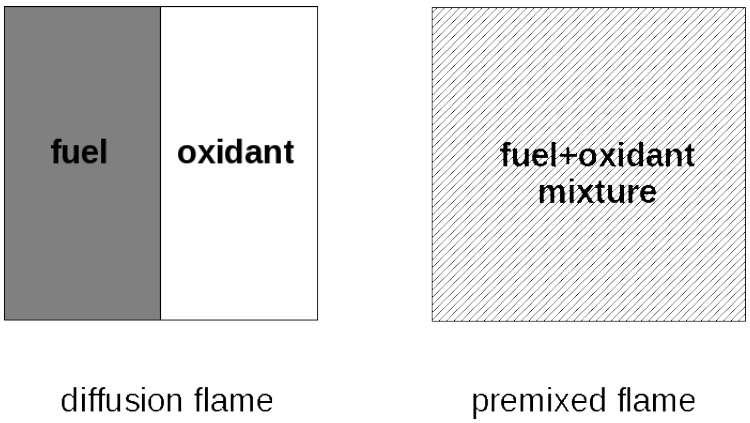

Figure 6.1: Difference between premixed and diffusion flames[21]

Different combustion models are used for simulating the gaseous combustion like Simple chemical reacting system model, Eddy break–up model, laminar flamelet model and

presumed probability distribution function model. For our case study, we will use simple chemical reacting model that will be explained in the following section.

6.1 Simple chemical reacting system (SCRS)

This model is concerned only with the global nature of the combustion process and the final major species concentrations as it assumes that the reaction infinitely fast and takes place in a single step process neglecting the detailed kinetics involved in the combustion process[4]. Combustion occurs where the fuel and oxidizer are mixed in stoichiometric proportions to form combustion products. This model is suitable to be applied to combustion process where diffusion effects are dominant and combustion takes place by non-premixed streams of fuel and oxidizer which are diffusing into each forming the flame structure.

In SCRS, fuel and oxidizer combine together in fixed mass portions to form products, where s is stoichiometric oxygen/fuel ratio by mass.

$$1\ kg\ of\ fuel\ + s\ kg\ of\ oxidizer \rightarrow (1+s) kg\ of\ products \qquad \textbf{(6.1)}$$

For methane combustion, when it burns with air, it is believed to proceed according to the following reactions shown in Figure 6.2.

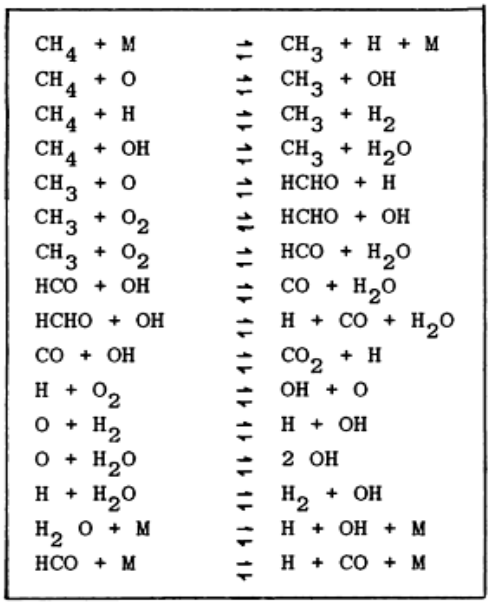

Figure 6.2: Detailed mechanism for methane oxidation

While in SCRS model methane combustion is simplified to the following one step fast reaction

$$CH_4 + 2O_2 \rightarrow CO_2 + 2H_2O \quad \textbf{(6.2)}$$

This simplification means that intermediate species (CH_3, OH, HCHO, H, H_2, O, HCO, CO) do not have concentrations of the same order of those of main reactants (CH_4, O_2) and the main products (CO_2, H_2O).

Ordinary nitrogen gas that can be present with fuel or oxygen streams can in practice lead to additional chemical reactions as shown in Figure 6.3 reactions between nitrogen and oxygen. While in SCRS nitrogen is considered as a simple dilute that does not enter any chemical reactions.

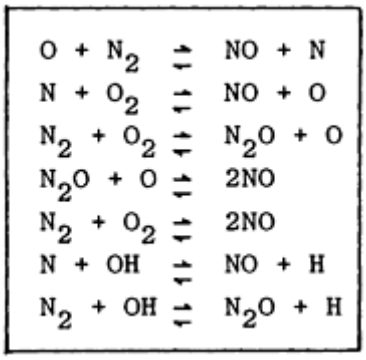

Figure 6.3: chemical reaction between nitrogen and oxygen

The stoichiometric oxygen/fuel ratio by mass s is equal to 4 for pure methane combustion. From equation (6.1), it can be deduced that rate of fuel consumption is 1/s time consumption rate of oxygen.

$$\dot{\omega}_{fu} = \frac{1}{s}\,\dot{\omega}_{ox} \quad \textbf{(6.3)}$$

As in SCRS intermediate reactions are ignored as the chemical reaction is infinitely fast, so the transport equations of fuel and oxygen mass fraction can be written as shown

$$\frac{\partial(\rho Y_{fu})}{\partial t} + div(\rho Y_{fu} U) = div(\Gamma_{fu}\, grad\, Y_{fu}) + \dot{\omega}_{fu} \quad \textbf{(6.4)}$$

$$\frac{\partial(\rho Y_{ox})}{\partial t} + div(\rho Y_{ox} U) = div(\Gamma_{ox}\, grad\, Y_{ox}) + \dot{\omega}_{ox} \quad \textbf{(6.5)}$$

Where,

Y_{fu}: Fuel mass fraction

Y_{ox}: Oxygen mass fraction

Γ_{fu}: Fuel diffusion coefficient $\left(\Gamma_{fu} = \rho D_{fu}\right)$

Γ_{ox}: Oxygen diffusion coefficient $(\Gamma_{ox} = \rho D_{ox})$

Nitrogen gas that can be present in fuel or oxidant streams does not participate in the chemical reaction so the mass fraction of inert gas (Y_{in}) will remain constant before and after combustion and there is no need for writing transport equation for inert gas. Also the mass fraction of the product can be determined from mass fractions of fuel, oxygen and inert gas equation (6.6) , so that it is not necessary to solve separate equation for Y_{pr} .

$$Y_{pr} = 1 - \left(Y_{fu} + Y_{ox} + Y_{in}\right) \quad \textbf{(6.6)}$$

It is possible to decrease the number of transport equations by introducing variable ∅ that is defined as follows:

$$\emptyset = sY_{fu} - Y_{ox} \quad \textbf{(6.7)}$$

Single transport equation can be deduced by subtracting equation (6.5) from s times equation (6.4) after assuming single diffusion coefficient for fuel and oxygen $\left(\Gamma_{fu} = \Gamma_{ox} = \rho D = \Gamma_{\emptyset}\right)$ .The new transport equation can be written as follows:

$$\frac{\partial(\rho\emptyset)}{\partial t} + div(\rho\emptyset U) = div(\Gamma_{\emptyset}\, grad\, \emptyset) + \left(s\dot{\omega}_{fu} - \dot{\omega}_{ox}\right) \quad \textbf{(6.8)}$$

From equation (6.3), we can conclude that$\left(s\dot{\omega}_{fu} - \dot{\omega}_{ox}\right) = 0$, so the transport equation (6.8) can be reduced to the following form:

$$\frac{\partial(\rho\emptyset)}{\partial t} + div(\rho\emptyset U) = div(\Gamma_{\emptyset}\, grad\, \emptyset) \quad \textbf{(6.9)}$$

Since ∅ is a passive quantity, it obeys the scalar transport equation without source terms. A non-dimensional variable ξ called mixture fraction can be defined as function of ∅.

$$\xi = \frac{\emptyset - \emptyset_0}{\emptyset_1 - \emptyset_0} \quad \textbf{(6.10)}$$

Where, suffix 0 denotes stands for oxidant stream and 1 stands for fuel stream. The local value of ξ range is from 0 to 1.It is equal 0 when mixture at point contains only oxidant and equal 1 when mixture contains only fuel.

Equation (6.10) for mixture fraction can be expanded as follows:

$$\xi = \frac{\left[sY_{fu} - Y_{ox}\right] - \left[sY_{fu} - Y_{ox}\right]_0}{\left[sY_{fu} - Y_{ox}\right]_1 - \left[sY_{fu} - Y_{ox}\right]_0} \quad \textbf{(6.11)}$$

If the oxidant stream has no fuel we have

$$[\mathrm{Y_{fu}}]_0 = 0 \quad \textbf{(6.12)}$$

If the fuel stream has no oxidant we have

$$[\mathrm{Y_{ox}}]_1 = 0 \quad \textbf{(6.13)}$$

Using the two previous conditions, equation (6.11) can be simplified as follows

$$\xi = \frac{\left[sY_{fu} - Y_{ox}\right] - [-Y_{ox}]_0}{\left[sY_{fu}\right]_1 - [-Y_{ox}]_0} = \frac{sY_{fu} - Y_{ox} + Y_{ox,0}}{s\,Y_{fu,1} + Y_{ox,0}} \quad \textbf{(6.14)}$$

In stoichiometric mixture where neither fuel nor oxygen is present in the product, the stoichiometric mixture fraction ξ_{st} can be written as follows

$$\xi_{st} = \frac{Y_{ox,0}}{s\,Y_{fu,1} + Y_{ox,0}} \quad \textbf{(6.15)}$$

Fast chemistry reaction implies that at certain region the mixture is lean. In this region, there is excess of oxidant and no fuel is present in the product. The mixture fraction is calculated using equation

$$Y_{fu} = 0 \quad Y_{ox} > 0 \quad \textbf{(6.16)}$$

$$if \quad \xi < \xi_{st} \quad then \quad \xi = \frac{-Y_{ox} + Y_{ox,0}}{s\,Y_{fu,1} + Y_{ox,0}} \quad \textbf{(6.17)}$$

While in region with rich mixture, there is excess of fuel and there is no oxidant in the product. The mixture fraction is calculated as follows

$$Y_{ox} = 0 \quad Y_{fu} > 0 \quad \textbf{(6.18)}$$

$$if \quad \xi > \xi_{st} \quad then \quad \xi = \frac{sY_{fu} + Y_{ox,0}}{s\,Y_{fu,1} + Y_{ox,0}} \quad \textbf{(6.19)}$$

From equation (6.10), ξ is linearly related to ∅ , so the mixture fraction is also a passive scalar and obeys the transport equation.

$$\frac{\partial(\rho\xi)}{\partial t} + div(\rho\xi U) = div\left(\Gamma_\xi \, grad\, \xi\right) \quad \textbf{(6.20)}$$

The previous can be also written using index notation as shown in the following equation

$$\frac{\partial(\rho\xi)}{\partial t} + \frac{\partial(\rho u_i \xi)}{\partial x_i} = \frac{\partial}{\partial x_i}\left(\Gamma_\xi \, \frac{\partial \xi}{\partial x_i}\right) \quad \textbf{(6.21)}$$

To obtain the distribution of ξ , the transport equation of mixture fraction has to be solved. A suitable boundary conditions should be used, e.g. mixture fraction for fuel and oxidant inlet streams are known, zero normal flux of ξ across solid walls and zero gradient of ξ for outflow boundaries.

From the previous equations (6.14) - (6.19) for the mixture fraction, we can calculate the mass fraction of oxygen (Y_{ox}), fuel (Y_{fu}), inert gas (Y_{in}) and product (Y_{pr}) after combustion as shown below

$$Y_{ox} = \begin{cases} \dfrac{\xi_{st} - \xi}{\xi_{st}} \; Y_{ox,0} & , \quad 0 \le \xi < \xi_{st} \\ 0 & , \quad \xi_{st} \le \xi < 1 \end{cases} \quad \textbf{(6.22)}$$

$$Y_{fu} = \begin{cases} 0 & , \quad 0 \le \xi < \xi_{st} \\ \dfrac{\xi - \xi_{st}}{1 - \xi_{st}} \; Y_{fu,1} & , \quad \xi_{st} \le \xi < 1 \end{cases} \quad \textbf{(6.23)}$$

$$Y_{in} = Y_{in\,,0}\,(1 - \xi) + Y_{in\,,1}\,\xi \quad \textbf{(6.24)}$$

$$Y_{pr} = 1 - \left(Y_{fu} + Y_{ox} + Y_{in}\right) \quad \textbf{(6.25)}$$

The above formulae show that mixture fraction of oxygen and fuel are linearly related to the mixture faction and these formulae can be illustrated graphically as shown in figure Figure 6.4

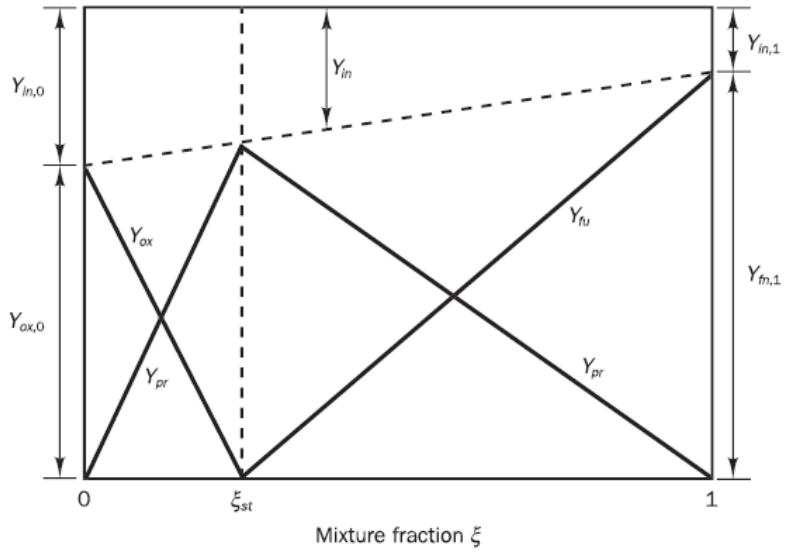

Figure 6.4: Mixing and fast reaction between fuel and oxidant streams (SCRC relationships)[4]

When the reaction products contain many species, the ratio of the mass fraction of each component to the total product mass fraction is known from the chemical reaction equation and this ratio is used for deducing the mass fraction of different product components. For example, consider combustion of methane with oxygen:

$$CH_4 + 2O_2 \rightarrow CO_2 + 2H_2O \qquad \textbf{(6.26)}$$

The ratios of H_2O $(r_{H_2O})$and CO_2 (r_{CO_2}) to the total product by mass are equal to 44/80 and 36/80 respectively. Using the product mass fraction calculated in equation (6.25) the CO_2 mass fraction (Y_{CO_2}) in product is $r_{CO_2}Y_{pr}$ and H_2O mass fraction in product is $r_{H_2O}Y_{pr}$.

6.2 Modelling of a laminar diffusion flame

The SCRS combustion model can be applied in planer laminar diffusion flame to calculate temperature and chemical species distribution in the laminar diffusion flame. First we will discuss the governing equation for laminar compressible low Mach number flow in Cartesian coordinates.

6.2.1 Governing equations

- Continuity equation

$$\frac{\partial \rho}{\partial t} + \frac{\partial \rho u_i}{\partial x_i} = 0 \qquad \textbf{(6.27)}$$

- Momentum equation

$$\frac{\partial \rho u_i}{\partial t} = -\frac{\partial \rho u_i u_j}{\partial x_j} - \frac{\partial p}{\partial x_i} + \frac{\partial \tau_{ij}}{\partial x_j} + \rho g_i \quad \textbf{(6.28)}$$

Where,

$$\tau_{ij} = \mu\left(\frac{\partial u_i}{\partial x_j} + \frac{\partial u_j}{\partial x_i} - \frac{2}{3}\delta_{ij}\frac{\partial u_k}{\partial x_k}\right) \quad \textbf{(6.29)}$$

- Mixture fraction

$$\frac{\partial(\rho\xi)}{\partial t} + \frac{\partial(\rho u_i \xi)}{\partial x_i} = \frac{\partial}{\partial x_i}\left(\Gamma_\xi \frac{\partial \xi}{\partial x_i}\right) \quad \textbf{(6.30)}$$

- Energy equation

The energy equation for open system with compressible flow at low Mach number with the following assumption:

1. Neglecting radiation energy loss or gain
2. Negligible pressure work
3. Assuming constant specific heat ,can be written as follows:

$$\frac{\partial(\rho h)}{\partial t} + \frac{\partial(\rho u_i h)}{\partial x_i} = \frac{\partial}{\partial x_i}(k\frac{\partial T}{\partial x_i}) \quad \textbf{(6.31)}$$

After simplifying the energy equation, it becomes another conserved scalar equation like mixture fraction equation. We can conclude that both enthalpy and mixture fraction are scalar quantities and linearly related.

Since enthalpy (h) is a passive quantity, it obeys the scalar transport equation without source terms. A non-dimensional variable (h^*) called non-dimensional enthalpy can be defined.

$$h^* = \frac{h - h_{air,in}}{h_{fu,in} - h_{air,in}} \quad \textbf{(6.32)}$$

Where,

$h_{air,in}$: Enthalpy of air stream

$h_{fu,in}$: Enthalpy of fuel stream

Taking the reference temperature as ambient temperature (298^0K), the enthalpy is defined as shown below for combustion of methane as example

$$h = Y_{fu}h_{f_{fu}} + Y_{H_20}h_{f_{H_20}} + Y_{CO_2}h_{f_{CO_2}} + \overline{C_p}(T - 298) \quad \textbf{(6.33)}$$

Where,

h_f: Enthalpy of formation at 298^0K

Enthalpy of the fuel stream where $\xi = 1$ is

$$h_{fu,in} = Y_{fu}\left(h_{f_{fu}} + C_{p_{fu}}(T_{fu,in} - 298)\right) + Y_{in,1}C_{p_{in,1}}(T_{fu,in} - 298) \quad \textbf{(6.34)}$$

Enthalpy of the air stream where $\xi = 0$ is

$$h_{air,in} = C_{p_{air}}(T_{air,in} - 298) \quad \textbf{(6.35)}$$

We can see that when $\xi = 0$, $Y_{fu} = 0$, $h^* = 0$ and when $\xi = 1$, $Y_{fu} = 1$, $h^* = 1$.By adding simplifying assumptions for mixture fraction and enthalpy transport equations which are single diffusion coefficient $(\Gamma_{fu} = \Gamma_{ox} = \rho D = \Gamma_{\phi})$,unity Lewis number and negligible pressure work and radiation source. The distribution of non-dimensional enthalpy (h^*) and mixture fraction (ξ) will be the same, so that there is no need to solve both equations only solving mixture fraction will be sufficient and enthalpy can be calculated using mixture fraction using the following equation

$$\xi = h^* = \frac{h - h_{air,in}}{h_{fu,in} - h_{air,in}}$$
$$h = h_{air,in} + \xi(h_{fu,in} - h_{air,in}) \quad \textbf{(6.36)}$$

After calculating enthalpy and mass fractions for different components from SCRS model relationships, the temperature can be obtained from equation

$$T = 298 + \frac{1}{\overline{C_p}}\left[h - \left(Y_{fu}h_{f_{fu}} + Y_{H_20}h_{f_{H_20}} + Y_{CO_2}h_{f_{CO_2}}\right)\right] \quad \textbf{(6.37)}$$

6.2.2 Configuration of simulation

The geometry considered is shown in Figure 6.5 in which a planar fuel jet is surrounded by two planar air jets. The width of fuel jet (d_{fuel}) is 0.4 cm and the width of air jet (d_{air}) is 2.25 cm. The thickness of the wall between fuel and air streams is 0.05 cm. We will consider burning diluted methane (5% CH_4, 95% N_2) jet with co-flowing air (23.3% O_2, 76.7% N_2). Both fuel and air velocity are equal to 0.2 m/s and enter at ambient temperature 25 ^{0}C .The computational domain is rectangle of length L and width W. A staggered grid of 164*82 nodes is used.

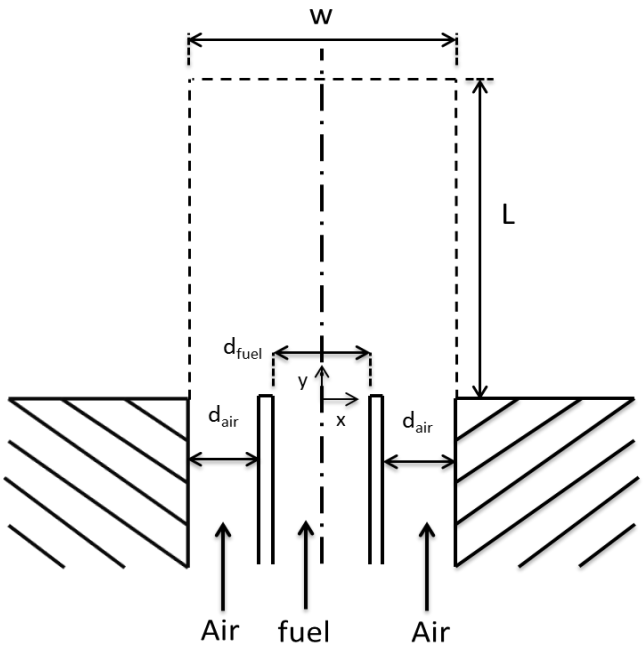

Figure 6.5: schematic diagram of the problem considered

6.2.2.1 Boundary conditions

For velocity boundary conditions, at inlet the normal velocity component is constant and equal to 0.2 m/s (v=0.2 m/s) for fuel and oxygen streams and the tangential component is equal to zero (u=0 m/s).At the axis of symmetry are applied, the horizontal velocity component is zero (u=0 m/s) and gradient of vertical component in normal direction is zero $\left(\frac{\partial \mathrm{v}}{\partial \mathrm{x}} = 0\right)$.For top and right boundary conditions the velocity gradient for both velocity components in the normal direction are zero, so for the top boundary the conditions are $\left(\frac{\partial \mathrm{u}}{\partial \mathrm{y}} = \frac{\partial \mathrm{v}}{\partial \mathrm{y}} = 0\right)$ and for right boundary the conditions are $\left(\frac{\partial \mathrm{u}}{\partial \mathrm{x}} = \frac{\partial \mathrm{v}}{\partial \mathrm{x}} = 0\right)$.

For pressure boundary conditions, the pressure is set to zero at the top boundary (p=0), while the other boundaries, the pressure gradient in the normal direction is set to zero$\left(\frac{\partial \mathrm{p}}{\partial \eta}=0\right)$.

For mixture fraction boundary conditions, at the inlet of fuel stream, the mixture fraction is equal to 1 $(\xi=1)$ for fuel stream and for air stream mixture fraction is zero $(\xi=0)$.For other boundaries, the gradient of mixture fraction in normal direction is zero, for the top boundary the condition is $\left(\frac{\partial \xi}{\partial \mathrm{y}}=0\right)$ and for the left and right boundary $\left(\frac{\partial \xi}{\partial \mathrm{x}}=0\right)$.

6.2.3 Results

After solving fluid flow equations and mixture fraction equation, the pressure, velocity and mixture fraction distributions are obtained. Mixture fraction defines flame structure and different species distribution. Species mass fractions are obtained using equation (6.22)-(6.25) and enthalpy and temperature fields are calculated from (6.36) and (6.37) respectively. The pressure contour map is shown in Figure 6.6 in which pressure reaches its maximum values at the walls separating fuel and air stream as the velocity at the walls boundaries is zero.The horizontal and vertical velocity components contour maps and streamline function are shown in Figure 6.7 , Figure 6.8 and Figure 6.9 respectively. Mixture fraction and temperature distribution shown in Figure 6.11 and Figure 6.10 respectively has the same pattern as temperature is linearly related to mixture fraction equation (6.36), so the stoichiometric contour $(\xi = \xi_{st})$ is corresponding to contour of maximum flame temperature. In this case flame length is equal to 1.594 cm and maximum flame temperature is 1275 k .The flame length is defined as the height at flame axis of symmetry where temperature reaches its maximum value.

To highlight the consequences of fast chemistry assumption in SCRS model, the temperature, mixture fraction and species mass fraction will be shown at three different horizontal levels shown in Figure 6.12. The first level is at y=0.781 cm. At this level from centreline to stoichiometric contour fuel is found without oxygen. Fuel concentration decreases gradually till it is consumed completely at stoichiometric contour where temperature peaks. The second level is at y=1.594 cm that is equal to flame length, at centreline where $\xi = \xi_{st}$ neither oxygen nor fuel exist and temperature is at a maximum. In third level at y=3.281 cm that lies outside stoichiometric contour($\xi < \xi_{st}$), where no fuel exist and the temperature is lower.

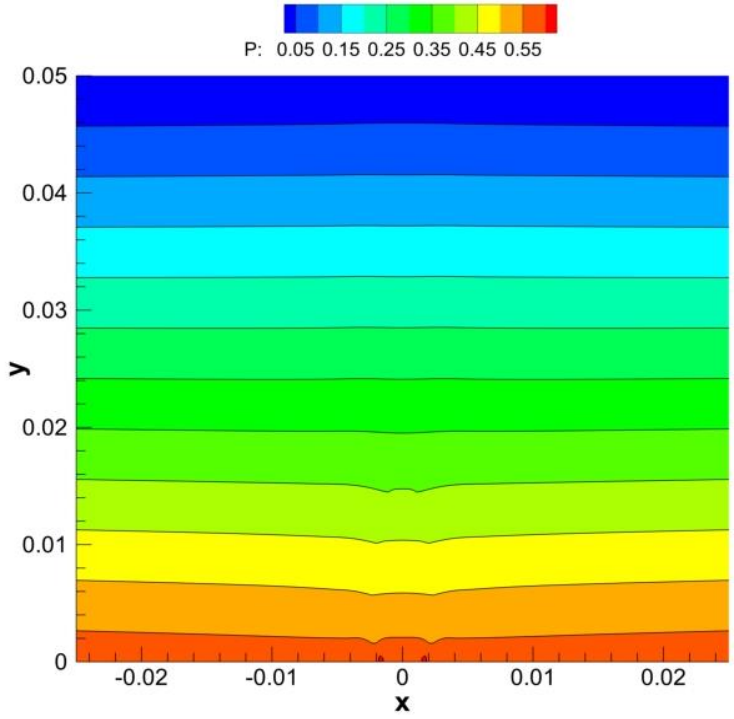

Figure 6.6: contour map of dynamic pressure

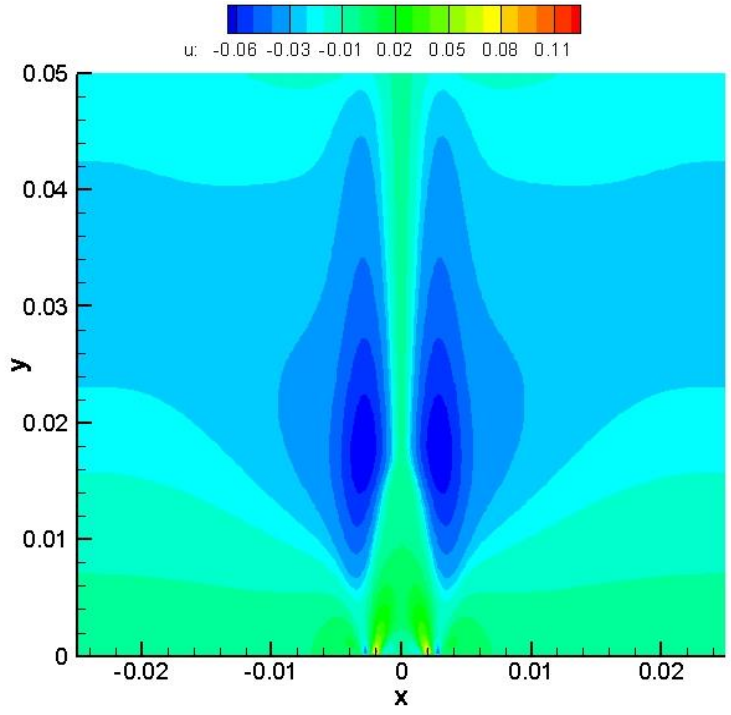

Figure 6.7: contour map of horizontal velocity components u

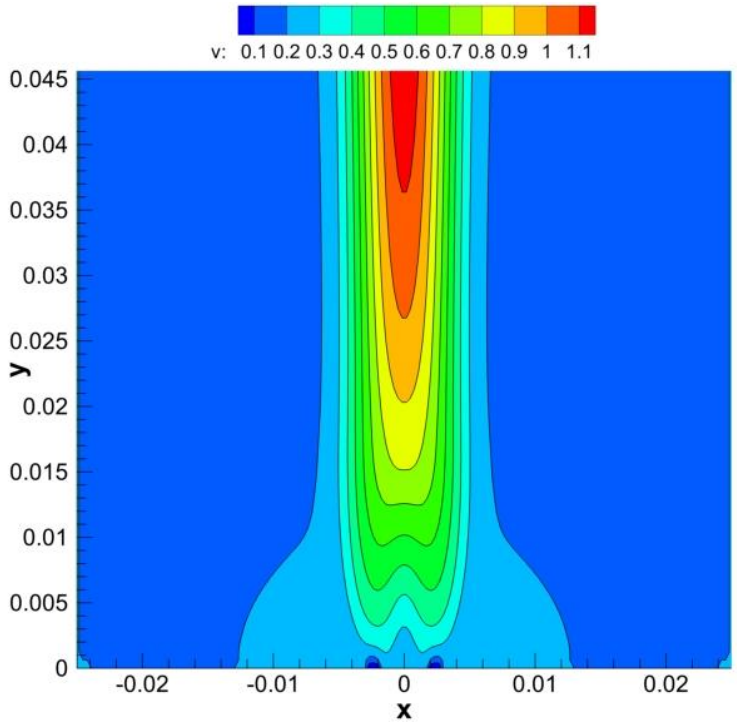

Figure 6.8: contour map of vertical velocity component v

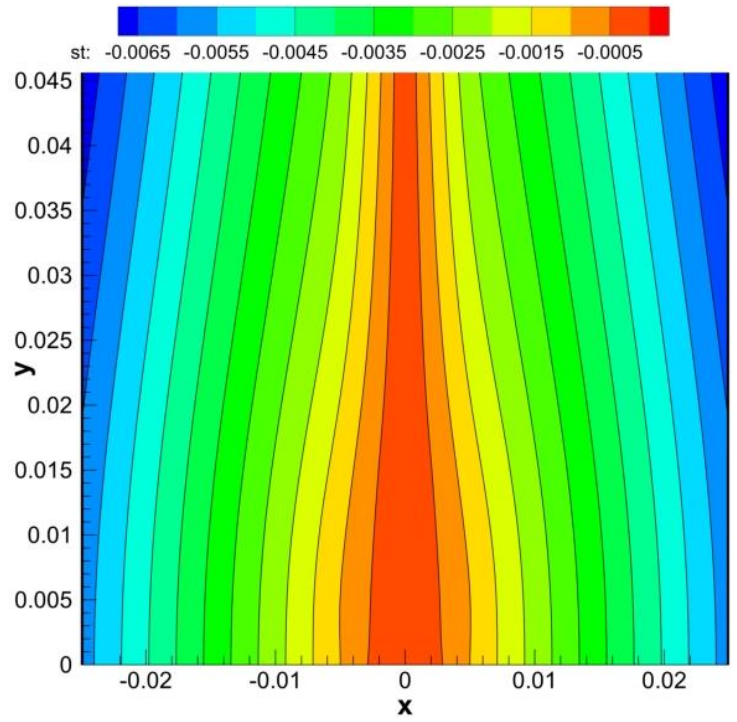

Figure 6.9: contour map of streamline function (ψ)

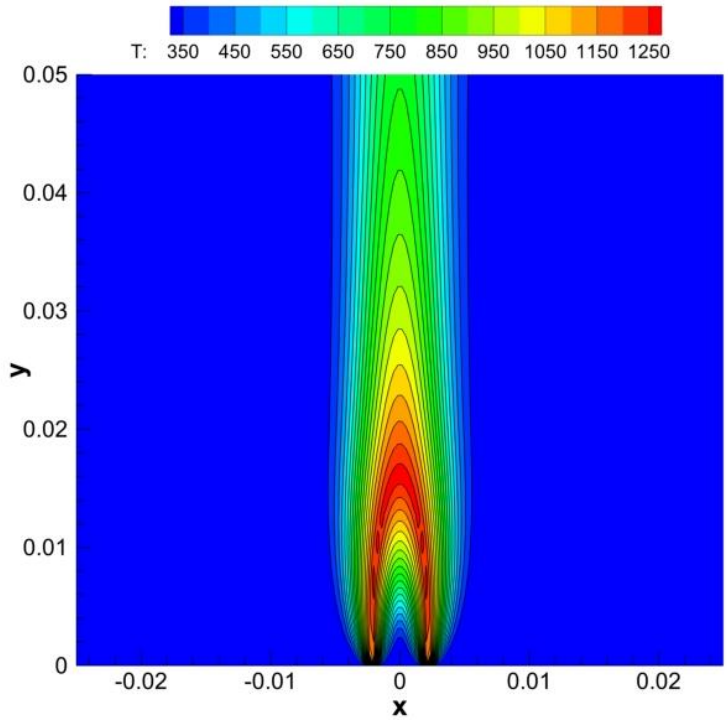

Figure 6.10: contour map of temperature

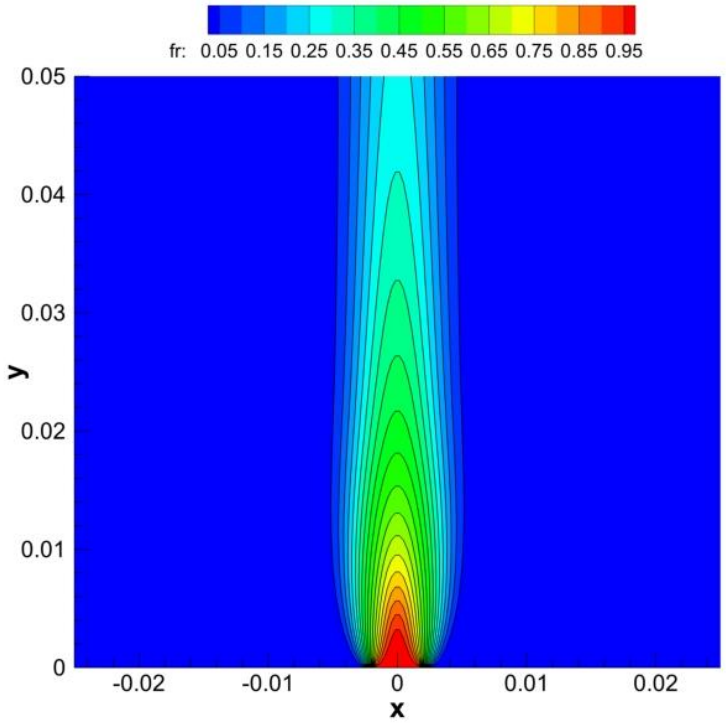

Figure 6.11: contour map of mixture fraction

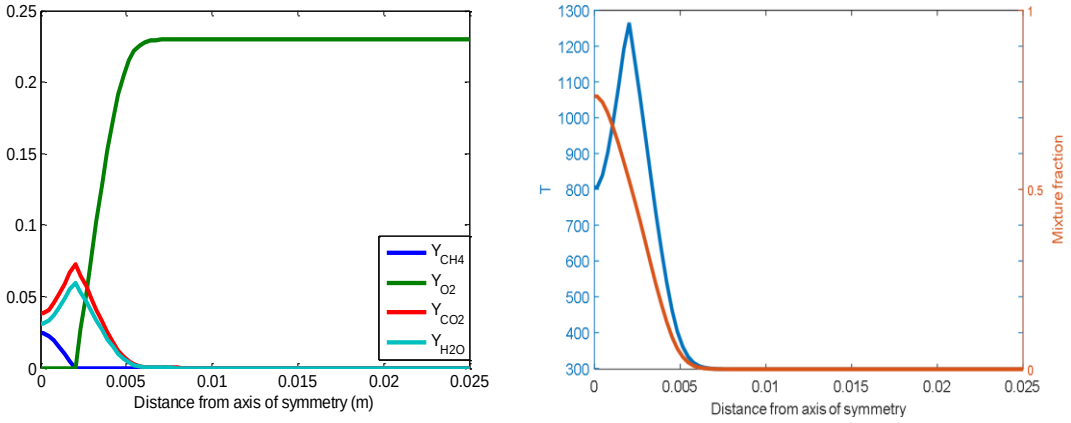

(a)

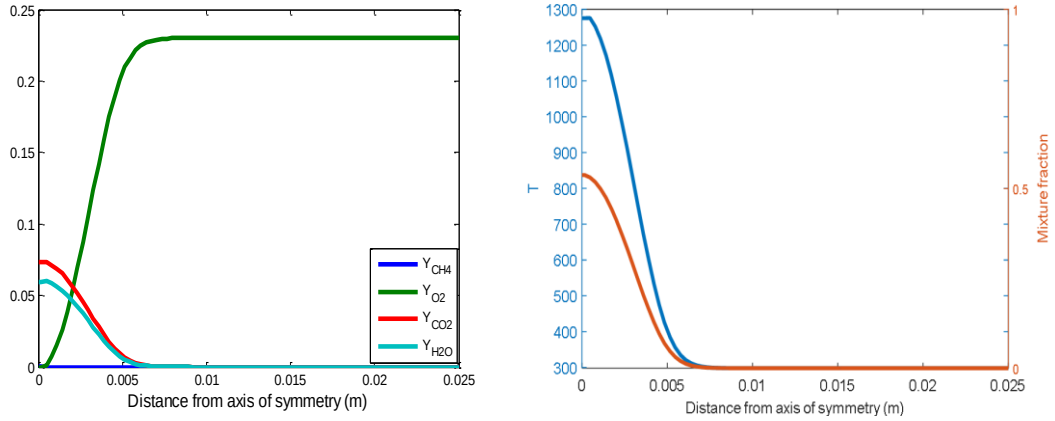

(b)

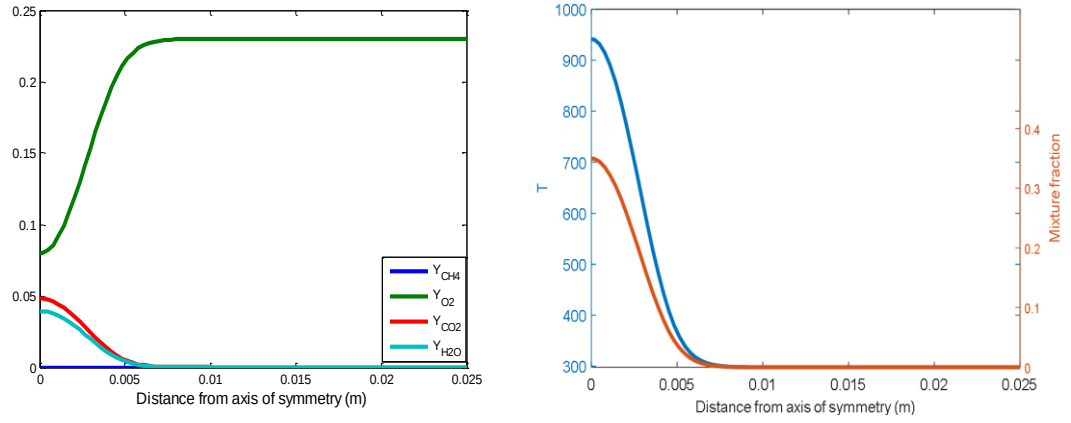

(c)

Figure 6.12: species mass fraction, mixture fraction and temperature distribution at different horizontal planes (a) y=0.781 cm (b) y=1.594 cm (c) y=3.281 cm

6.2.3.1 Effect of changing fuel stream velocity

The effect of changing fuel jet velocity is studied in this section, in which air jet velocity is kept constant (0.2 m/s) while fuel jet speed is changed. Different fuel jet velocities are tested and the results are at fuel jet velocity 0.1, 0.15, 0.2 and 0.25 m/s are shown in Figure 6.13. The results show that as fuel jet velocity increases, the flame height increases.

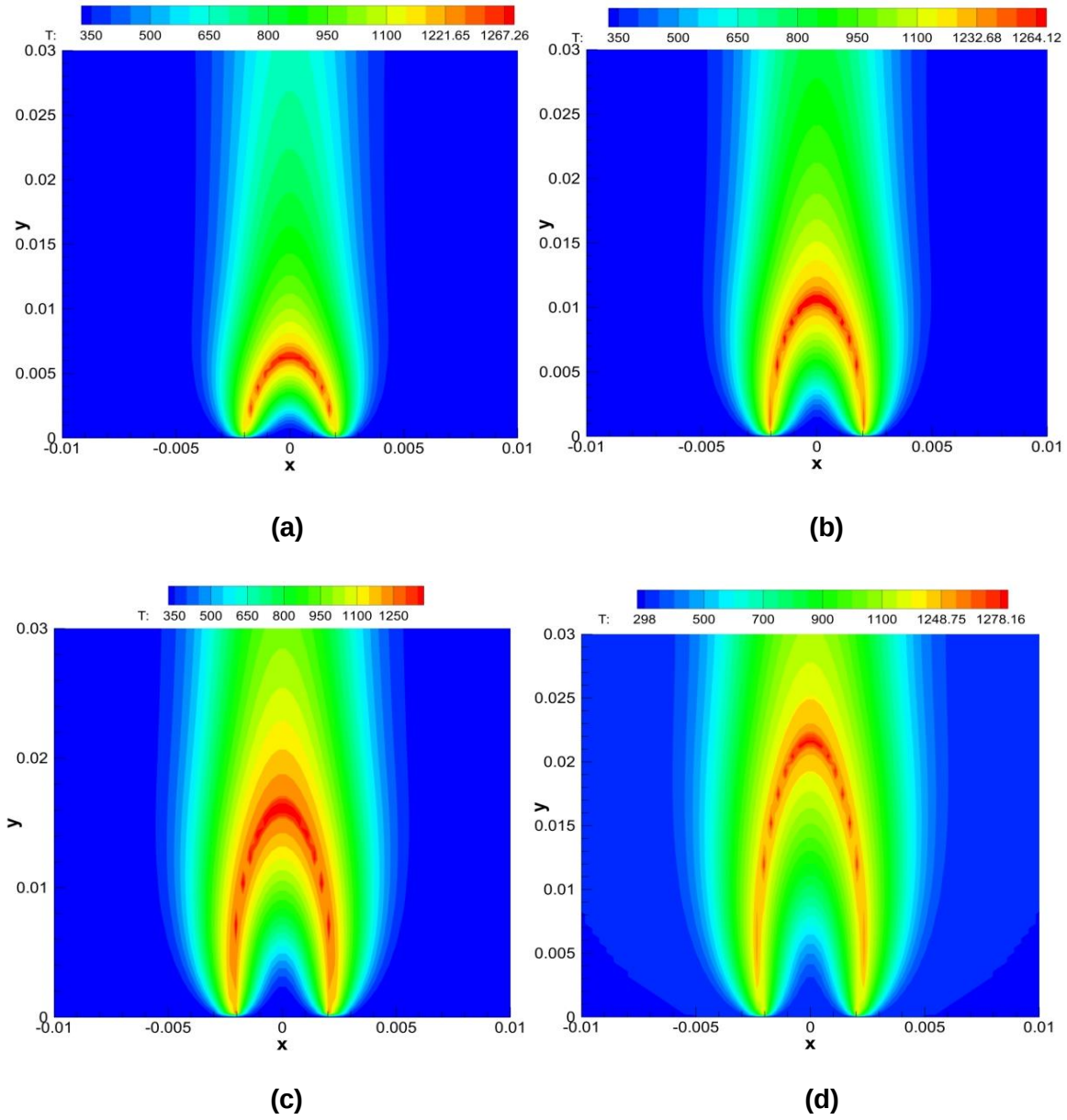

Figure 6.13: Effect of changing fuel jet velocity with constant air jet velocity (0.2 m/s)

(a) V_{fuel}=0.1 m/s, (b) V_{fuel}=0.15 m/s, (c) V_{fuel}=0.2 m/s, (d) V_{fuel}=0.25 m/s

Flame lengths are plotted versus fuel jet velocity in Figure 6.14 and from the figure it can be concluded that fuel flame length is linearly related to fuel jet velocity.

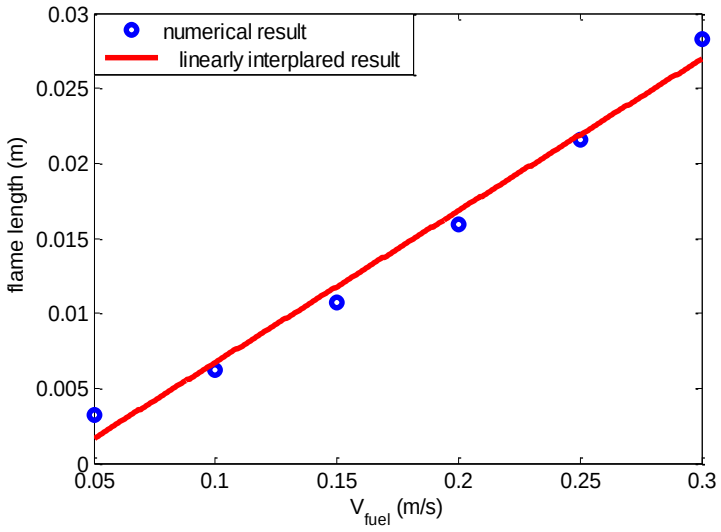

Figure 6.14: flame length variation with increasing fuel stream velocity

6.2.3.2 Effect of changing air stream velocity

The effect of changing air jet velocity is studied in this section, in which fuel jet velocity is kept constant (0.2 m/s) while air jet speed is changed. Different air jet velocities are tested and the results are at air jet velocity 0.1, 0.3, 0.5 and 0.7 m/s are shown in Figure 6.16. The results show that as air jet velocity increases, the flame height decreases. As shown in following figure that flame length is linearly related to air stream velocity.

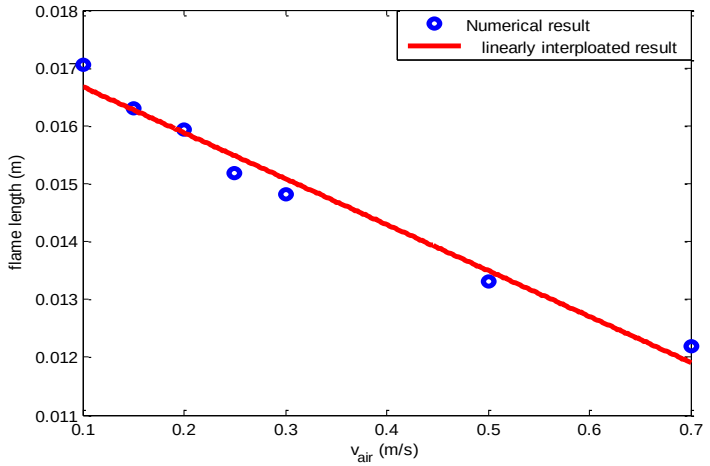

Figure 6.15: flame length variation with increasing air stream velocity

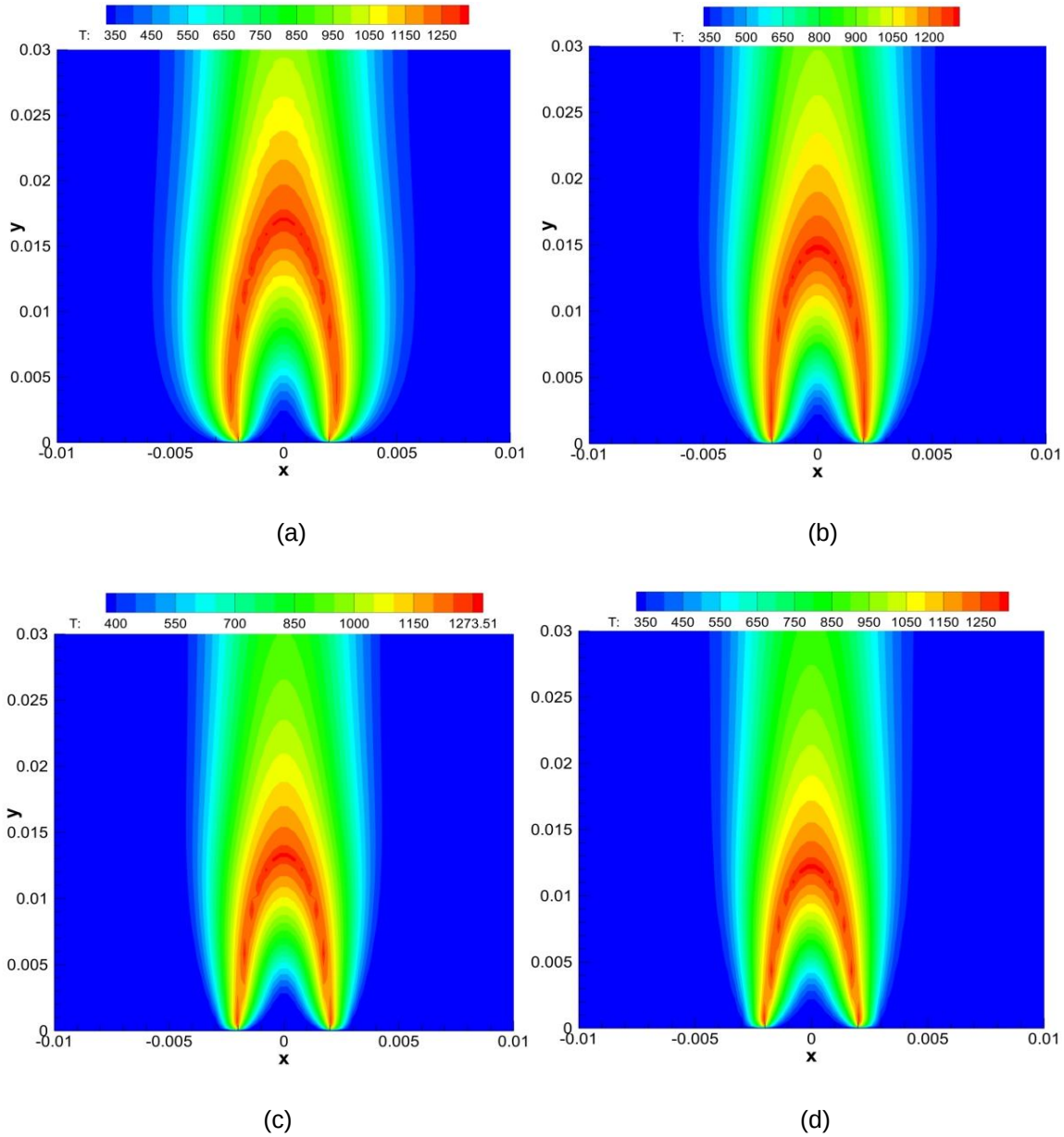

Figure 6.16: Effect of changing air stream velocity with constant fuel jet velocity (0.2 m/s)

(a) V_{fuel}=0.1 m/s, (b) V_{fuel}=0.2 m/s, (c) V_{fuel}=0.3 m/s, (d) V_{fuel}=0.4 m/s

6.2.3.3 Effect of increasing oxygen concentration in oxidant stream

In this section, the effect of increasing oxygen concentration in oxidant stream is studied. The oxidant stream contains oxygen and nitrogen gas. From Figure 6.17, it can be observed that as oxygen mass fraction increases, flame length decreases. This is due to increasing available oxygen for fuel combustion, so there is no need for fuel to transverse farther distance from fuel nozzle. Also, maximum flame temperature increases by

increasing oxygen concentration in oxidant stream as shown in Figure 6.18 (a).This happen because nitrogen gas that does not enter any chemical reaction in SCRS model consumes a part of energy of released from combustion to raise its temperature from inlet temperature to combustion product final temperature, so as nitrogen gas mass fraction decrease, energy consume by nitrogen gas decreases leading to higher maximum flame temperature. As shown in Table 6.1 stoichiometric mixture fraction increases as oxygen gas concentration increases.

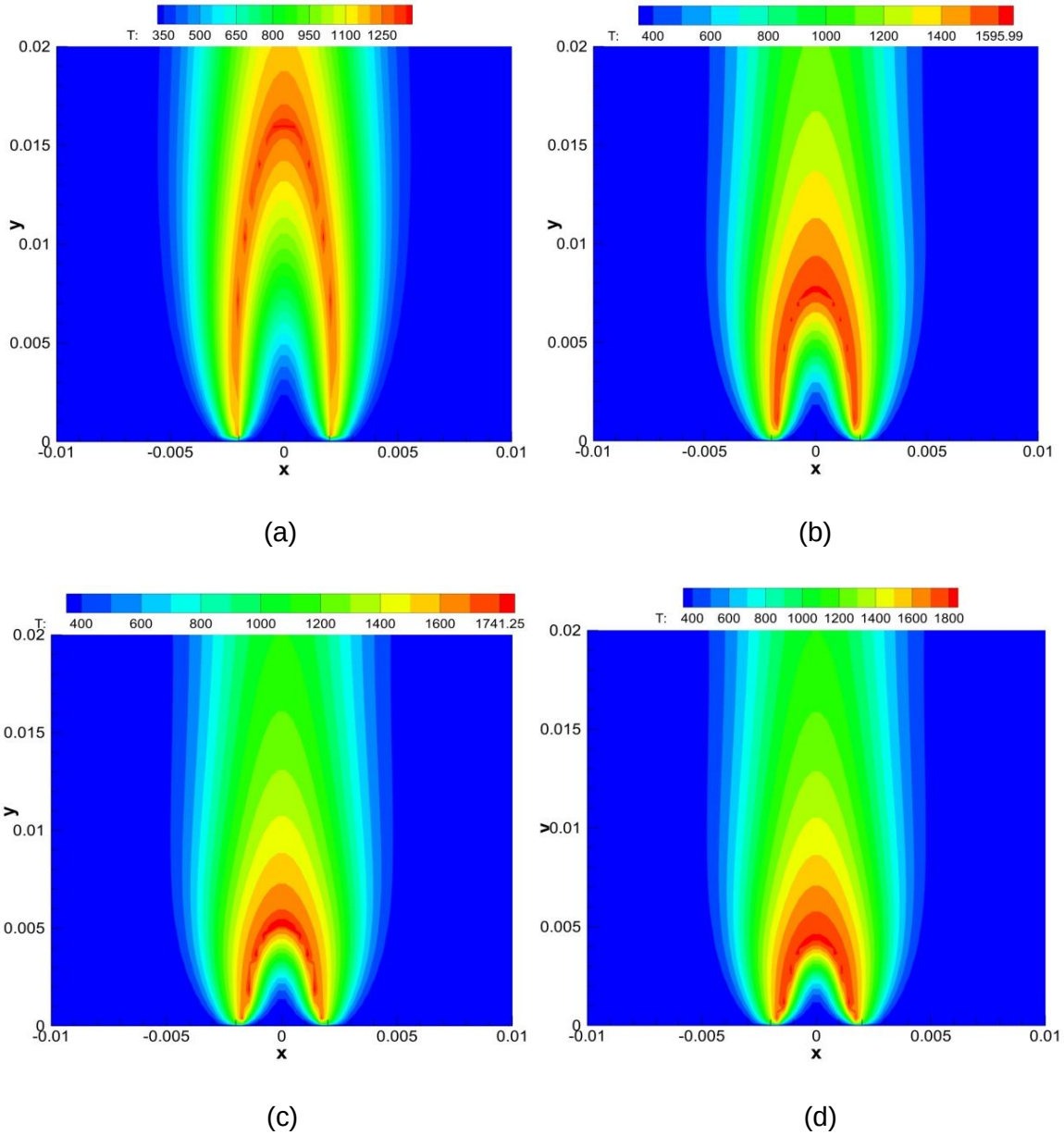

Figure 6.17: Effect of increasing oxygen concentration in oxidant stream

(a)Y_{ox} =23%, (b) Y_{ox} =50%,(c) Y_{ox} =80%,(d) Y_{ox} =100%

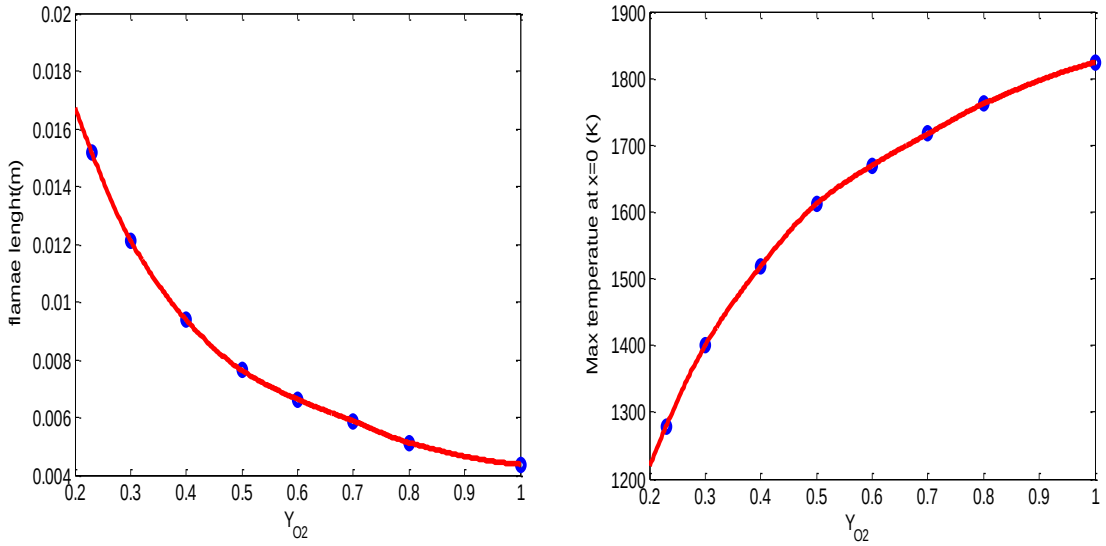

(a) (b)

Figure 6.18: Effect of increasing oxygen concentration on: (a) flame length and (b) max temperature at axis of symmetry

Oxidant stream composition by mass fraction	ξ_{st}	Flame length (cm)	Max flame temperature (K)
23% O_2 ,77 %N_2	0.5348	1.519	1279
30% O_2 ,70 %N_2	0.6	1.213	1400
40% O_2 ,60 %N_2	0.667	0.937	1519
50% O_2 ,50 %N_2	0.7142	0.762	1612
60% O_2 ,40 %N_2	0.75	0.6625	1670
70% O_2 ,30 %N_2	0.778	0.5875	1717
80% O_2 ,20 %N_2	0.8	0.5125	1762
100% O_2 ,0 %N_2	0.833	0.4375	1824

Table 6.1: Effect of increasing oxygen concentration in oxygen stream

6.2.3.4 Effect of diluting fuel stream with nitrogen

In this section, the effect of diluting fuel stream with nitrogen is investigated. The fuel stream consists of methane and nitrogen gas. Temperature contour maps for flames with different fuel concentration are shown in Figure 6.19.It can be seen that as nitrogen gas concentration increases, the flame length and maximum flame temperature decreases. The decreasing in flame length is due to the formation of stoichiometric mixture between fuel and oxidant streams at lower height from fuel nozzle as fuel concentration in fuel stream deceases. The maximum flame temperature decreases due to decreasing fuel concentration and increasing nitrogen gas concentration in fuel stream. As shown in Table 6.2 stoichiometric mixture fraction increases as nitrogen. gas concentration increases.

Fuel stream composition by mass fraction	ξ_{st}	Flame length (cm)	Max flame temperature (K)
10% CH_4 ,90 %N_2	0.365	2.906	1640
9% CH_4 ,91 %N_2	0.3898	2.656	1583
8% CH_4 ,92 %N_2	0.418	2.344	1523
7% CH_4 ,93 %N_2	0.4509	2.094	1455
6% CH_4 ,94 %N_2	0.489	1.844	1374
5% CH_4 ,95 %N_2	0.5348	1.519	1279

Table 6.2: Effect of diluting fuel stream with nitrogen gas

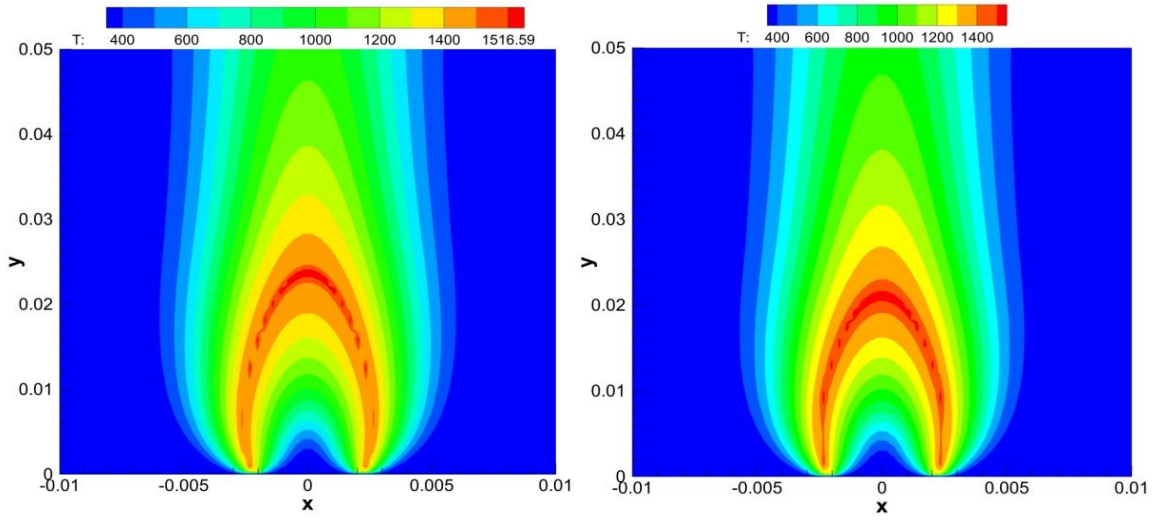

(a) (b)

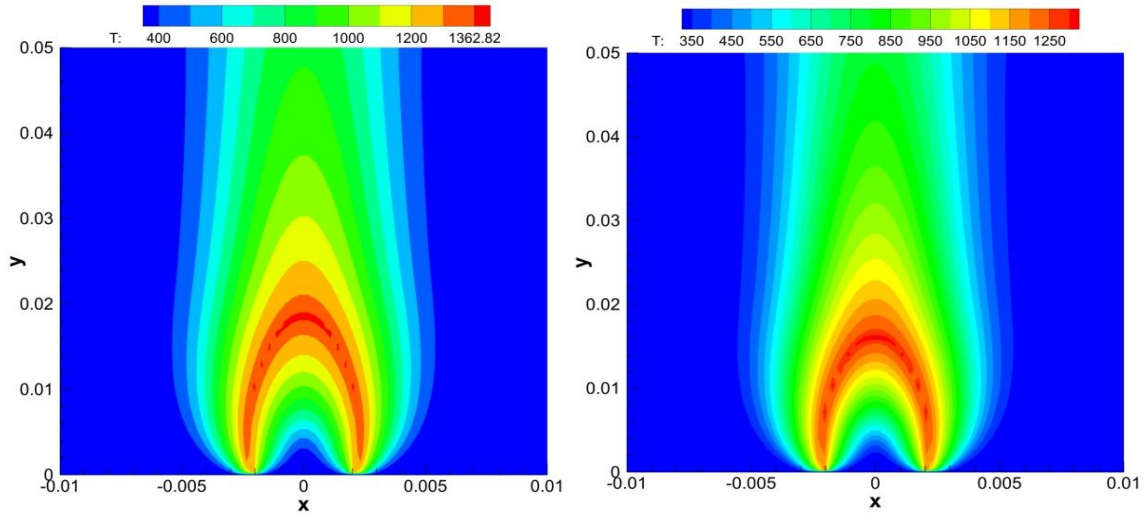

(c) (d)

Figure 6.19: Effect of diluting fuel stream with nitrogen gas

(a)Y_{CH4} =8%, (b) Y_{CH4} =7%,(c) Y_{CH4} =6%,(d) Y_{CH4} =5%

7 Conclusion

The goal our work is modelling laminar diffusion flame using simple chemical reacting system (SCRS) model which is simplified combustion model for modelling diffusion flames as it assumes that chemical reactions are infinitely fast and takes place in one step neglecting intermediate reactions as it is only concerted with final major species and it consider that combustion process occur when fuel and oxygen are mixed in stoichiometric proportions. For modelling diffusion flame, fractional step algorithm for compressible flow with low Mach number is used in which low Mach number approximation are utilized in simplifying momentum and energy transport equation. The code is verified by comparing its results with analytical and highly accurate benchmark solutions.

The verification process showed that the code is well implemented as the code results have good agreement with benchmark solution of driven cavity and differentially heated cavity for incompressible and compressible flow.

The results show that mixture fraction and temperature contour maps have the same pattern as the stoichiometric mixture fraction contour line is corresponding to maximum temperature contour line as the mixture fraction and energy transport equations are linearly related. The region inside stoichiometric contour line ($\xi > \xi_{st}$) only fuel is present and oxygen is completely consumed and on stoichiometric contour line ($\xi = \xi_{st}$) neither oxygen nor fuel is present, while at region outside stoichiometric contour line ($\xi < \xi_{st}$) only oxygen is present. Increasing fuel stream velocity leads to increasing flame length, while increasing air stream velocity decreases flame height and the flame maximum temperature is almost constant in both cases. Increasing oxygen concentration in oxidant stream leads to decreasing flame length and increasing flame maximum temperature, while diluting fuel stream with nitrogen also decreases both flame length and flame maximum temperature.

Future work

One of possible modification that can be done in the future is implementing the simulation code in cylindrical coordinates which is more convenient for modelling diffusion. Also included the detailed kinetics involved in combustion process, so we can compute species with minor concentration like OH and CO that are neglected in SCRS model.

References

1. *Mitchell Elliptic Test Problems for FREEFEM++*. 2015 15/2/2015 [cited 2015 22/7/2015]; Available from: http://people.sc.fsu.edu/~jburkardt/examples/mitchell_freefem++/mitchell_freefem++.html.

2. Tu, J., K. Inthavong, and K.K.L. Wong, *Generation of Computational Mesh for Haemodynamics Analysis*, in *Computational Hemodynamics–Theory, Modelling and Applications*. 2015, Springer. p. 155-181.

3. Craft, T.J., *Structured Finite Volume Schemes*.

4. Versteeg, H.K. and W. Malalasekera, *An introduction to computational fluid dynamics: the finite volume method*. 2007: Pearson Education.

5. Guerrero, J., *Introduction to Computational Fluid Dynamics: Governing Equations, Turbulence Modeling Introduction and Finite Volume Discretization Basics.* 2013.

6. Darwish, M. and F. Moukalled, *Normalized variable and space formulation methodology for high-resolution schemes.* Numerical Heat Transfer, 1994. **26**(1): p. 79-96.

7. Liu, F., H. Becker, and A. Pollard, *Spatial differencing schemes of the discrete-ordinates method.* Numerical Heat Transfer, 1996. **30**(1): p. 23-43.

8. Kim, J. and P. Moin, *Application of a fractional-step method to incompressible Navier-Stokes equations.* Journal of computational physics, 1985. **59**(2): p. 308-323.

9. MIT, *Systems of Linear Equations*. 2011.

10. Trivellato, F. and M.R. Castelli, *On the Courant–Friedrichs–Lewy criterion of rotating grids in 2D vertical-axis wind turbine analysis.* Renewable Energy, 2014. **62**: p. 53-62.

11. Simons, E., *An efficient multi-domain approach to large-eddy simulation of incompressible turbulent flows in complex geometries.* 2000.

12. Najm, H.N., P.S. Wyckoff, and O.M. Knio, *A semi-implicit numerical scheme for reacting flow: I. stiff chemistry.* Journal of Computational Physics, 1998. **143**(2): p. 381-402.

13. Jordi VENTOSA, j.C., Oriol LEHMKUHL,Carlos-David PEREZ-SEGARRA,Assensi OLIVA, *Low Mach Navier-Stokes Equations on Ustructured Meshes*, in *International conference on fluid flow Technologies*. 2012: Budapest,Hungary.

14. Oberkampf, W.L. and T.G. Trucano, *Verification and validation in computational fluid dynamics.* Progress in Aerospace Sciences, 2002. **38**(3): p. 209-272.

15. Roache, P.J., *Code verification by the method of manufactured solutions.* Journal of Fluids Engineering, 2002. **124**(1): p. 4-10.

16. Elias, R.N., A.L. Coutinho, and M.A. Martins, *Inexact Newton-type methods for non-linear problems arising from the SUPG/PSPG solution of steady incompressible navier-stokes equations.* Journal of the Brazilian Society of Mechanical Sciences and Engineering, 2004. **26**(3): p. 330-339.

17. Ghia, U., K.N. Ghia, and C. Shin, *High-Re solutions for incompressible flow using the Navier-Stokes equations and a multigrid method.* Journal of computational physics, 1982. **48**(3): p. 387-411.

18. de Vahl Davis, G. and I. Jones, *Natural convection in a square cavity: a comparison exercise.* International Journal for numerical methods in fluids, 1983. **3**(3): p. 227-248.

19. de Vahl Davis, G., *Natural convection of air in a square cavity: a bench mark numerical solution.* International Journal for numerical methods in fluids, 1983. **3**(3): p. 249-264.

20. Vierendeels, J., B. Merci, and E. Dick, *Benchmark solutions for the natural convective heat transfer problem in a square cavity with large horizontal temperature differences.* International Journal of Numerical Methods for Heat & Fluid Flow, 2003. **13**(8): p. 1057-1078.

21. *Diffusion flame*. Available from: http://www.maidhof.com/glossary/glossary.html.